NOTE TO USERS

Page(s) not included in the original manuscript and are unavailable from the author or university. The manuscript was scanned as received.

58

This reproduction is the best copy available.

UMI®

DISSERTATION

CHARGE SEPARATION IN COVALENTLY BOUND AND SELF-ASSEMBLED DONOR CHROMOPHORE ACCEPTOR SYSTEMS

Submitted by

Matthew T. Rawls

Department of Chemistry

In partial fulfillment of the requirements

for the degree of Doctor of Philosophy

Colorado State University

Fort Collins, Colorado

Spring 2007

COLORADO STATE UNIVERSITY

January 23, 2007

WE HEREBY RECOMMEND THAT THE DISSERTATION PREPARED UNDER OUR SUPERVISION BY MATTHEW T. RAWLS ENTITLED **CHARGE SEPARATION IN COVALENTLY BOUND AND SELF-ASSEMBLED DONOR- CHROMOPHORE-ACCEPTOR SYSTEMS** BE ACCEPTED AS FULFILLING IN PART THE REQUIREMENTS FOR THE DEGREE OF DOCTOR OF PHILOSOPHY.

Committee on Graduate Work

PETER DORSEY

THOMAS MEERSMAN

TRAVIS BAILEY

ELLEN R FISHER

C. MICHAEL ELLIOTT

Advisor

Department Head

ABSTRACT OF DISSERTATION

CHARGE SEPARATION IN COVALENTLY BOUND AND SELF-ASSEMBLED DONOR CHROMOPHORE ACCEPTOR SYSTEMS

Donor-chromophore-acceptor (DCA) triads consisting of a central ruthenium polypyridyl complex chromophore with a covalently appended diquaternary bipyridine "diquat" acceptor and a phenothiazine donor form an interesting platform for study of fundamental photoinduced electron transfer processes. Upon photoexcitation of the chromophore, a series of electron transfer steps occurs which yields a long-lived charge separated state (CSS). Research into the electron transfer steps leading to CSS formation and decay in these triads has led to several interesting avenues for research.

First, in an effort to understand why these particular triads form, upon photoexcitation, charge separated states with such high quantum efficiency (nearly unity) an important discovery arose. The quantum efficiency for charge separation appears to be dependent upon an association interaction between the donor and the chromophore ligands which holds the donor in close electronic contact with the chromophore until the donor is oxidized. To study this association, covalently bound chromophore-acceptor species have been synthesized and the photoinduced electron transfer processes with a free donor have been studied. The D/C association appears to be sufficient for the formation of CSS. Further, this self-assembled system and related studies provides conclusive

evidence that high efficiency charge separation in bound triads results from this D/C association.

Covalently bound donor-acceptor species were synthesized in an attempt to extend the self assembly concept to a free chromophore system. A wide variety of DA species were studied, but ultimately triad-like behavior was not observed with free chromophore systems. Though attempts were made to control solvent effects, coulombic interactions, and DA flexibility, simple self assembled triad like behavior did not arise.

These complexes demonstrate a strong magnetic field effect (MFE): upon application of relatively small fields, the CSS lifetime increases by up to an order of magnitude. A model has been proposed to explain the MFE which is based on the formation of the CSS initially as a triplet. Application of a field induces Zeeman splitting of this triplet state and slows the CSS decay. DCA complexes have been synthesized with phenoxazine or phenoselenazine in place of the phenothiazine as donors. These donors provide a large variation of spin orbit coupling (SOC) of the heteroatom (O, S, Se). MFE results for these complexes with varying heteratom SOC provide some interesting details about this proposed MFE mechanism.

Matthew T. Rawls
Chemistry Department
Colorado State University
Fort Collins, CO 80523
Spring 2007

ACKNOWLEDGEMENTS

I first must thank the Chemistry Department of Colorado State University for providing such an excellent place to learn Chemistry. I have come a very long way in these years and greatly appreciate the education and experiences. Also, I have to thank my research advisor Mike Elliott, who taught me Chemistry ("Mike's Magic") and how to be tough. Colorado State University I must thank for providing such a fun and healthy community in which to live for 6 years. Finally, I must thank my wife Megan. You have been tough, resilient, supportive, sweet, and fun throughout the years.

TABLE OF CONTENTS

TABLE OF ABBREVIATIONS

ET	electron transfer
D	donor
C	chromophore
A	acceptor
DCA	donor-chromophore-acceptor triad
CA	bound chromophore-acceptor unit
DA	bound donor-acceptor unit
PXZ	azine type donor
MLCT	metal to ligand charge transfer
CSS	charge separated state
^{3}[CSS]	triplet charge separated state
Φ_{CSS}	quantum efficiency for charge separation
DQ	diquaternary electron acceptor
^{3}MLCT	triplet MLCT state
CT	charge transfer state
K_{eq}	complexation equilibrium constant
k_{bet}	back electron transfer rate
k_{cs}	charge separation rage
$T_{\pm}$, T_0	triplet substate
S	singlet
k_r	triad relaxation rate
τ_{slow}	slow component lifetime

^{3}CS	triplet charge separated state
MFE	magnetic field effect
esdi	electron spin dipolar interaction
ahfi	anisotropic hyperfine interaction
soc	spin orbit coupling
RP	radical pair
$B_{1/2}$	effective hyperfine field
k_s	singlet direct recombination rate constant
k_t	triplet direct recombination rate
k_{S,T_0}	rate of T_0 to S equilibration
ζ	spin orbit coupling constant
γ_e	gyromagnetic ratio
τ_c	orientational correlation time
ω_0	larmor frequency
T_1	longitudinal relaxation time
T_2	transversal relaxation time
g_{ii}	diagonal g-tensor
g_e	free electron g-factor
r_0	contact distance
D	diffusion coefficient
sri	spin rotational mechanism
gta	g-tensor anisotropy
μ	magnetic moment

CHAPTER 1

DISSERTATION INTRODUCTION

This dissertation chapter contains background into the importance of research into electron transfer in supermolecular triads and also frames the forthcoming chapters.

HIGHLY EFFICIENT CHARGE SEPARATING TRIADS

The study of photoinduced electron-transfer processes is of both practical and fundamental importance. Through decades of research, much effort has been focused on modeling and emulating the photoinduced charge separation reactions used by nature in photosynthesis. Such work adds to our fundamental understanding of photosynthesis while building a foundation for the creation of systems which can effectively harvest solar energy.[1-6]

Supramolecular photochemistry is one area which emerged from this field. In this form of electron-transfer research, the donor, acceptor and a photosensitizer are bound into a single supermolecule. It is thus possible to correlate electron-transfer (ET) data with knowledge of the spacing and orientation of the donor and acceptor species, while avoiding diffusional complications inherent in bimolecular studies. For these reasons supramolecular systems now play a major role in the study of photoinduced ET reactions.[6,7]

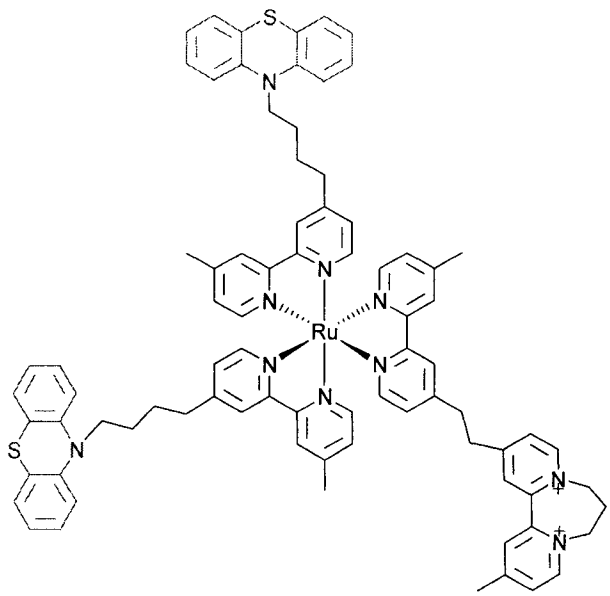

Figure 1.1 Representative Donor-Chromophore-Acceptor triad complex which undergoes efficient photoinduced charge separated state formation.

The complex shown in Figure 1.1 is an example of this type of supramolecular system. This DCA "triad" consists of an azine type (PXZ) (X = S in Figure 1.1) donor (D), a ruthenium polypyridyl complex chromophore (C), and a diquaternary bipyridine "diquat" acceptor (A). When this complex is irradiated with visible light, a metal-to-ligand charge transfer (MLCT) occurs in which an electron from a metal-based d-orbital is excited to a π^* orbital on one of the bipyridine rings. This state undergoes intersystem crossing to yield a triplet MLCT state.[8] Next, a series intramolecular electron-transfer steps occur which yield a charge separated state (CSS) where the acceptor is reduced, the donor is oxidized and the chromophore is in the ground state. The system is of particular interest because the quantum efficiency for formation of the CSS is very high near, unity.[9]

SELF-ASSEMBLED TRIADS

Extensive studies of these triads were undertaken previously in search of a better understanding of the electron-transfer steps leading to the formation of CSS as well as an explanation for the high quantum efficiency of this process. Studies which isolated the individual ET steps (chromophore to acceptor and donor to chromophore) provided sufficient information to construct a model of CSS formation.[10,11] The model shows that ultimately the overall quantum efficiency for CSS formation appears to be limited primarily by the donor's ability to intercept the recombination of the charge separated chromophore and acceptor. Preliminary studies of these triads led to a hypothesis regarding this unique efficiency: a ground state association between the donor and the chromophore is of critical importance in efficient charge separation in these triads. The donor is effectively "bound" in solution to the chromophore, and upon photoexcitation of the system is thus in position to quickly reduce the chromophore.

Chapter 3 of this dissertation examines in detail a series of experiments which definitively establish this association. Two bimolecular systems derived from the triad shown in Figure 1.1 are discussed. These systems consist of a chromophore bound to an acceptor in solution with a free donor. The association functions to assemble the two moieties into a triad-like species highly efficient at separating charge. An overwhelming selection of spectroscopic and logical evidence proves and details this association.

Chapter 4 of this dissertation presents a free chromophore study wherein the donor is bound to the acceptor and associates with a chromophore. This system ultimately proves to be very complex with distinctly non "triad-like" behavior. Several theories about this kinetic behavior are presented and tested to explain the complex results.

TRIAD SPIN CHEMISTRY

Spin chemistry is a growing area of research with very interesting current and potential applications. Spin chemistry is the study of the angular momentum or spin of electrons and nuclei and the effect of the fundamental restriction that reactants and products must have identical total electron spin for reaction to occur.[12-14] This rule plays a fundamental role throughout chemistry and suggests the importance of consideration of spin in many reactions. The large amount of recent literature, including several reviews and texts, attests to the current interest in spin chemistry.[13,15-17] Recent projects span from the fundamental physics of spin chemistry and the limitations which it mandates to the application of spin techniques as a tool to derive deeper understanding in a wide variety of biological and chemical systems.

Huping et. al. recently presented a study suggesting that nuclear spin plays a fundamental role in consciousness calling nuclear spins "mind-pixels".[18] In their study,

they suggest that the paramagnetic molecules O_2 and NO are pixel activating media. Spin also has been utilized to manipulate the kinetics of systems by providing a catalyst for spin equilibration. Spin catalysis research is a rapidly growing field with application in numerous areas. Buchachenko et. al. recently reported a review which summarizes many of the important projects in spin catalysis.[19] For instance, spin catalysis likely plays a critical role in the kinetics involved in the storage of energy by the photosynthetic reaction center.[20]

The DCA triad CSS is an excellent platform for spin chemical studies. The CSS is formed initially as an almost pure triplet while the ground state triad is a singlet; therefore recombination of the ^{3}[CSS] is formally spin forbidden. Triads are thus amenable to spin studies, as they must undergo a spin flip to a singlet state or experience spin orbit coupling before recombination to the ground state can occur.

Previous studies have shown that the triads, although they include the heavy central ruthenium atom, behave much like the classical model for biradical spin systems, two radicals bound through a flexible organic linker.[21] In such situations, processes such as hyperfine coupling, electron spin-spin coupling, and exchange interaction dominate the spin equilibration process. Application of a magnetic field slows the triplet to singlet equilibration due to Zeeman splitting, and thus provides a powerful technique for study of spin considerations.

Chapter 5 of this dissertation presents a detailed study of the magnetic field effect in these DCA triads to further understanding of the zero field electron transfer kinetics as well as the dominant forces leading to CSS recombination from fields of 0 to 3T.

Specifically, in all previous studies it was assumed that the previously mentioned processes which serve as routes for spin relaxation were dominant and there was little

contribution to spin equilibration from spin-orbit coupling.[22] Triads in which the sulfur in the phenothiazine is replaced with an oxygen atom (phenoxazine) or a selenium atom (phenoselenazine) can contribute to a deeper understanding of the kinetics of electron transfer and establish the importance of spin-orbit coupling in recombination of the CSS. These triads are particularly useful because they behave very similarly to the phenothiazine complexes in terms of redox properties and zero field behavior. The only relevant difference among these triads is the atomic number of the heteroatom and thus the expected spin-orbit coupling. Study of these systems provides an interesting route to further understand the kinetics of the system and, in particular, the importance of spin orbit-coupling in spin equilibration. Finally, spin catalysis of these triads is considered wherein low concentrations of paramagnetic quenchers radically affect the magnetic field effects in these triads.

REFERENCES

(1) Armaroli, N. *Photochem. Photobiol. Sci.* **2003**, *2*, 73.

(2) Kalyanasundaram, K. *Photochemistry of Polypyridine and Porphyrin Complexes*; Academic Press: San Diego, 1992.

(3) Scandola, F.; Chiorboli, C.; Indelli, M. T.; Rampi, M. T. Covalently Linked Systems Containing Metal Complexes. In *Biological and Artificial Supermolecular Systems*; Wiley: Weinheim, 2003; Vol. 3; pp 337.

(4) Schanze, K. S.; Walter, K. A. Photoinduced Electron Transfer in Metal-Organic Dyads. In *Molecular and Supermolecular Photochemistry: Organic and Inorganic Photochemistry*; Ramamurthy, V., Schanze, K. S., Eds.; Marcel Dekker: New York, 1998; Vol. 2; pp 75.

(5) Wasielewski, M. R. *Chem. Rev.* **1992**, *92*, 435.

(6) Ward, M. D. *Chem. Soc. Rev.* **1997**, *26*, 365.

(7) Balzani, V.; Scandola, F. *Supramolecular Photochemistry*; Ellis Horwood: Chichester, 1991.

(8) Demas, J. N.; Taylor, D. G. *Inorg. Chem.* **1979**, *18*, 3177.

(9) Danielson, E.; Elliott, C. M.; Merkert, J. W.; Meyer, T. J. *J. Am. Chem. Soc.* **1987**, *109*, 2519.

(10) Larson, S. L.; Cooley, L. F.; Elliott, C. M.; Kelley, D. F. *J. Am. Chem. Soc.* **1992**, *114*, 9504.

(11) Larson, S. L.; Elliott, C. M.; Kelley, D. F. *Inorg. Chem.* **1996**, *35*, 2070.

(12) Step, E. N.; Buchachenko, A. L.; Turro, N. J. *J. Am. Chem. Soc.* **1994**, *116*, 5462.

(13) Buchachenko, A. L. *Pure Appl. Chem.* **2000**, *72*, 2243.

(14) Hayashi, H. *J. Chin. Chem. Soc.* **2002**, *49*, 137.

(15) Step, E. N.; Buchachenko, A. L.; Turro, N. J. *J. Am. Chem. Soc.* **1994**, *116*, 5462.

(16) Mori, Y.; Sakaguchi, Y.; Hayashi, H. *J. Phys. Chem. A* **2000**, *104*, 4896.

(17) Levin, P. P.; Kuzmin, V. A. *Chem. Phys.* **1992**, *162*, 79.

(18) Hu, H.; Wu, M. *Medical Hypotheses* **2004**, *63*, 633.

(19) Buchachenko, A. L.; Berdinsky, V. L. *Chem. Rev.* **2002**, *102*, 603.

(20) Klevanic, A. *Biochim. Biuphys. Acta* **1996**, *1275*, 237.

(21) Zimmt, M. B.; Doubleday, C.; Turro, N. J. *J. Am. Chem. Soc.* **1986**, *108*, 3618.

(22) Klumpp, T.; Linsenmann, M.; Larson, S. L.; Limoges, B. R.; Buerssner, D.; Krissinel, E. B.; Elliott, C. M.; Steiner, U. E. *J. Am. Chem. Soc.* **1999**, *121*, 1076.

CHAPTER 2

EXPERIMENTAL METHODS

This dissertation chapter contains two main sections. First, the syntheses of all the materials used in this dissertation are described. Next the instrumental methods are described which allowed collection of all the data discussed in this dissertation. Cyclic voltammetry, fluorescence spectroscopy, spectroelectrochemistry, and magnetic field variable-transient absorption spectroscopy are described as well as sample preparations.

MATERIALS

2,2,6,6-Tetramethylpiperidinooxy (TEMPO). TEMPO (99%) was purchased from Aldrich and used without further purification.

10-Methylphenoxazine (Me-POZ). The synthesis and characterization of Me-POZ was reported elsewhere.[1]

10-Methylphenothiazine (Me-PTZ) Me-PTZ was obtained from Aldrich and recrytallized three times from 10:1 toluene-hexanes yielding a colorless crystalline solid.

10-Methylphenoselenazine (Me-PSZ) A procedure from the literature was modified as follows:[2] phenoselenazine[3] (0.140 g, 0.57 mmol) in a drybox under N_2 atmosphere was combined with lithium diisopropylamide (0.060 mg, 5.60 mmol) in THF. Trimethyloxonium tetrafluorobate (0.316 mg, 2.14 mmol) was added slowly and the solution was stirred for 1 hr. The solution was then quenched with methanol. Upon silica gel chromatography (20:1 methylene chloride-acetone), Me-PSZ (a white powder) was isolated. The compound was characterized with NMR, TLC and electrospray mass spectroscopy (M + H 261.0).

[Ru(1,10-phenanthroline)$_2$(4-(3-(1'-methyl-4,4'-bipyridinediium-1-yl)-propyl)-4'-methyl-2,2'-bipyridine)](PF$_6$)$_4$. Synthesis and characterization reported previously.[4]

[Ru(1,10-phenanthroline)$_2$(423-DQ)](PF$_6$)$_4$. A procedure from the literature was modified as follows:[5] Ru(1,10-phenanthroline)Cl_2[4] (0.022 g, 0.042 mmol) in a drybox under N_2 atmosphere was combined with (423-DQ)$(PF_6)_2$ (0.040 mg, 0.057 mmol) in ethylene glycol and heated to 120°C for 2 hr. The mixture was removed from the drybox, diluted with H_2O, and separated as PF_6^- salt using centrifugation; silica gel chromatography (eluent 40% H_2O-10% KNO_3 (aq satd)-50% acetonitrile (4:1:5(vol))

yielded the product as a dark solid. Light was rigorously excluded throughout the above procedure.[5] A combination of TLC, electrospray mass spectroscopy (M - PF_6^- 1305.17), and electrochemistry was used for determination of sample integrity.

10-(4-(4'-methyl-2,2'-bipyridin-4-yl)butyl)-10H-phenoxazine (44-POZ). A procedure from the literature was modified as follows:[5] in a drybox under N_2 atmosphere, phenoxazine (0.45 g, 2.46 mmol) was combined with NaH (0.0531 g, 1.48 mmol), a catalytic amount of NaI, and 4-(4-bromobutyl)-4'-methyl-2,2'-bipyidine (0.5002 g, 1.64 mmol) in THF (freshly distilled from Na/benzophenone).[5] The solution was then refluxed for 12 h, quenched with ethanol, then dried by rotary evaporation. Upon silica gel chromatography (20:1 methylene chloride-acetone), 44-POZ (a colorless oil) was isolated. The compound was characterized with NMR, TLC and electrospray mass spectroscopy (M + H 408.3).

10-(4-(4'-methyl-2,2'-bipyridin-4-yl)butyl)-10H-phenoselenazine (44-PSZ). The compound was prepared, isolated, and characterized by a method analogous to that of 44-POZ given above: phenoselenazine (0.2446 g, 9.93 mmol)[3]; NaH (0.0215 g, 8.96 mmol); 4-(4-bromobutyl)-4'-methyl-2,2'-bipyidine (0.202 g, 6.62 mmol); mass spectroscopy (M + 2H 472.2).[5]

1-methyl-12-(2-(4'-methyl-2,2'-bipyridin-4-yl)ethyl)-7,8-dihydro-6H-dipyrido[1,2-a:2',1'-c][1,4]diazepine-5,9-diium (423-DQ)$(PF_6)_2$. A procedure from the literature was modified as follows:[5] 1,2 Bis[4-(4-methyl-2,2'-bipyridyl)] ethane (0.70 g, 1.91 mmol) was dissolved in n-heptane with a large excess of diiodopropane (purified over alumina) and the solution was refluxed for 6 days. The crude product, (423-DQ)$(I)_2$, was isolated as a red solid, dissolved in water, and precipitated as the PF_6^- salt. Pure (423-DQ)$(PF_6)_2$

was isolated as a purple oil from this solid using Soxlet extraction with methanol. The product was characterized using TLC (eluent 40% H_2O-10% KNO_3 (aq satd)-50% acetonitrile (4:1:5(vol)) and electrospray mass spectroscopy (M + H 699.4).

[Ru(44-POZ)Cl_2]. A procedure from the literature was modified as follows:[5] in a drybox under N_2 atmosphere, [Ru(DMSO)$_4Cl_2$] (0.1947 g, 0.402 mmol) and LiCl (0.170 g, 4.01 mmol) were dissolved in DMF (dried over molecular sieves) and refluxed until an orange color appeared (30 min.); 44-POZ (0.327 g, 0.803 mmol) dissolved in minimum DMF was added over several minutes and the solution was refluxed for 90 min. After removing from the drybox, upon doubling the volume with H_2O, a purple solid precipitated which, upon silica gel chromatography (10:1 methylene chloride-methanol saturated with ammonia), yielded [Ru(44-POZ)Cl_2] as a purple oil. Light was rigorously excluded throughout the above procedure.[5]

[Ru(44-POZ)$_2$(423-DQ)](PF$_6$)$_4$. A procedure from the literature was modified as follows:[5] in a drybox under N_2 atmosphere [Ru(44-POZ)$_2Cl_2$] (0.061g, 0.062 mmol) was heated to 120°C in ethylene glycol for 30 min; (423-DQ)$(PF_6)_2$ (0.0561g, 0.080 mmol), dissolved in acetone, was added and the solution was heated for 30 min at 120°C. The mixture was removed from the drybox, diluted with H_2O, and separated as PF_6^- salt using centrifugation; silica gel chromatography (eluent 40% H_2O-10% KNO_3 (aq satd)-50% acetonitrile (4:1:5(vol)) yielded the product as a dark solid. Light was rigorously excluded throughout the above procedure.[5] A combination of TLC, electrospray mass spectroscopy (M + 1 1759), and electrochemistry was used for determination of sample integrity.

[Ru(44-PSZ)$_2$Cl$_2$]. The compound was prepared, isolated, and characterized by a method analogous to that of Ru(44-POZ)Cl$_2$ given above: [Ru(DMSO)$_4$Cl$_2$] (0.0824 g, 0.170 mmol); LiCl (0.150 g, 3.54 mmol); 44-PSZ (0.1683 g, 0.3579 mmol).

[Ru(44-PSZ)$_2$(423-DQ)](PF$_6$)$_4$. The compound was prepared, isolated, and characterized by a method analogous to that of [Ru(44-POZ)$_2$(423-DQ)](PF$_6$)$_4$ given above: [Ru(44-PSZ)$_2$Cl$_2$] (0.0796g, 0.0715 mmol); (423-DQ)(PF$_6$)$_2$ (0.06497g, 0.093 mmol); electrospray mass spectroscopy (M + 1 1885).

[Ru(44-PTZ)$_2$(423-DQ)](PF$_6$)$_4$. The preparation of this compound was reported previously.[5]

2-(7-(10H-phenothiazin-10-yl)heptyl)-12-methyl-7,8-dihydro-6H-dipyrido[1,2-a:2',1'-c][1,4]diazepine-5,9-diium (47-DQ-PTZ)(PF$_6$)$_2$. A procedure from the literature was modified as follows:[5] in a drybox under N_2 atmosphere, 4-methyl-4'-(7-(phenothiazino)heptyl)-2,2'-bipyridine (47-PTZ) (0.060 g, 0.129 mmol) [5] and 1,3-dibromopropane (0.38 g, 1.29 mmol) in acetonitrile was heated in acetonitrile for 12 hr. The solution was dried under vacuum, dissolved in H_2O, and separated as PF_6^- salt using centrifugation. The product (47-DQ-PTZ)(PF$_6$)$_2$ was isolated as a light purple oil (color due to an impurity that could not be removed). A combination of TLC, electrospray mass spectroscopy (M - PF_6^- 652.1), and electrochemistry was used for determination of sample integrity.

2-(4-(10H-phenoxazin-10-yl)butyl)-12-methyl-7,8-dihydro-6H-dipyrido[1,2-a:2',1'-c][1,4]diazepine-5,9-diium (44-DQ-POZ)(PF$_6$)$_2$. The compound was prepared, isolated, and characterized by a method analogous to that of (47-DQ-PTZ)(PF$_6$)$_2$ given above: 44-POZ (0.017 g, 0.042 mmol); 1,3 diiodopropane (0.123 g, 0.42 mmol). A

combination of TLC, electrospray mass spectroscopy (M - PF_6^- 594.6), and electrochemistry was used for determination of sample integrity.

Heptakis (2,3,6-tri-O-methyl) Beta Cyclodextrin. Sample obtained from Cyclodextrin Technologies Development, Inc.

[Ru(1,10-phenanthroline)$_2$(2,2'-bipyridine-4,4'-dicarboxylic acid)](PF$_6$)$_2$. A procedure from the literature was modified as follows:[5] in a drybox under N_2 atmosphere [Ru(1,10-phenanthroline)$_2$Cl$_2$] [5] (0.030g, 0.057 mmol) with 2,2'-bipyridine-4,4'-dicarboxylic acid (0.0183 g, 0.38 mmol) was heated to 120°C in ethylene glycol for 30 min. The mixture was removed from the drybox and dissolved in acetone. Silica gel chromatography (eluent 90% H_2O-10% NH_4OH (aq satd)(4:1(vol)) yielded the product an orange solid. A combination of TLC, electrospray mass spectroscopy (M - PF_6^- 850.93), and electrochemistry was used for determination of sample integrity.

2,2'-bipyridine-5,5'-diyldimethanesulfonic acid. A procedure from the literature was modified as follows:[6] 5,5'-bis(bromomethyl)-2,2'-bipyridine (1.00 g, 2.90 mmol) and tetraethylammonium bromide (50 g, 237 mmol) was heated in methanol. To this solution, a mixture of sodium sulfite (8.00 g, 63.54 mmol) dissolved in H_2O was added. The resulting solution was refluxed 24 hrs, cooled and the solid was removed. The product 2,2'-bipyridine-5,5'-diyldimethanesulfonic acid was precipitated by the addition of 2-propanol to the solution. A combination of NMR, electrospray and mass spectroscopy (M - Na^+ 365.07) was used for determination of sample integrity.

[Ru(1,10-phenanthroline)$_2$(2,2'-bipyridine-5,5'-diyldimethanesulfonate)]. A procedure from the literature was modified as follows:[6] in a drybox under N_2 atmosphere [Ru(1,10-phenanthroline)$_2$Cl$_2$] [5] (0.100g, 0.190 mmol) with 2,2'-bipyridine-5,5'-

diyldimethanesulfonic acid (0.146 g, 0.38 mmol) was refluxed in 2-propanol for 24 hrs. The mixture was removed from the drybox, dried under vacuum, dissolved in H_2O, and the insoluble portion removed. Silica gel chromatography (eluent 90% H_2O-10% NH_4OH (aq satd)(4:1(vol)) yielded the product as a dark solid. A combination of TLC, FAB mass spectroscopy (M + 1 805.5), and electrochemistry was used for determination of sample integrity.

[Ru(2,2'-bipyridine-4,4'-dicarboxylic acid)$_3$](TBA)$_4$. A procedure from the literature was modified as follows:[7] in a drybox under N_2 atmosphere ruthenium chloride (0.124g, 0.470 mmol) with 2,2'-bipyridine-4,4'-dicarboxylic acid (0.146 g, 0.38 mmol) was refluxed in anhydrous dimethylformamide for 24 hrs. The mixture was removed from the drybox, H_2O was added, and the resulting solution was refluxed for 2 hrs. The H_2O was removed under vacuum and upon cooling, the product precipitated as a dark solid. A combination of TLC, electrospray mass spectroscopy (M + 1 1554.0), and electrochemistry was used for determination of sample integrity.

PREPARATION OF SAMPLES FOR KINETIC STUDY

Samples for kinetic studies were initially prepared in cells as described previously using multiple freeze-pump-thaw cycles to remove dissolved oxygen.[8] Samples consisted of an approximately 2.5 x 10^{-5} M solution of the complex in the appropriate solvent or mixture (1,2 dichloroethane, dichloromethane, or acetonitrile). Once freeze-pump-thaw degassed, some samples were taken into a nitrogen filled drybox (below 1 ppm oxygen) and allowed to equilibrate with the box atmosphere with gentle agitation (30 min). Also,

some samples were prepared entirely in the box with solvents equilibrated with box atmosphere.

MEASUREMENTS

Cyclic Voltammetry (CV). A conventional 3-electrode electrochemical cell with a BAS 100B electrochemical analyzer was used for all CV measurements. 0.1 M tetra-n-butylammonium hexafluorophosphate ($TBAPF_6$) in acetonitrile was used as the electrolyte. A glassy carbon working electrode was used along with a platinum wire auxiliary electrode, and a saturated sodium calomel (SSCE) reference electrode. A scan rate of 200 mV/s was used for all measurements. All solutions were purged with argon prior to electrochemical experiments.

Spectroelectrochemistry. The optically transparent thin layer electrochemical cell (OTTLE) was adapted from the literature (see Figure 2.1).[9] The electrochemical cell consisted of an optically transparent gold minigrid working electrode (4.33×10^{-2} cm pathlength), a platinum wire auxiliary electrode, and a silver wire quasi-reference electrode. The electrolyte solution consisted of a 1 M tetraethylammonium perchlorate ($TEACIO_4$) solution in acetonitrile. Initially, the main cell chamber as well as the minigrid chamber were filled with electrolyte solution. Samples with concentrations of 10^{-3} M of the free donor (Me-POZ, Me-PTZ, or Me-PSZ) in electrolyte solution were injected into the optically transparent portion of the cell (excluding the electrolyte solution in the process) and a potential 100 mV positive of the first oxidation wave for the donor was applied. The cell was placed perpendicularly to the optical train of a Hewlett Packard 8452A UV-visible spectrometer and electronic spectra were taken at 1 s

intervals until the current passing through the cell dropped to a minimal level (usually around 60 s). Extinction coefficient spectra were calculated for the oxidized donors from the resulting data.

Emission Lifetime Measurements. Described previously.[4]

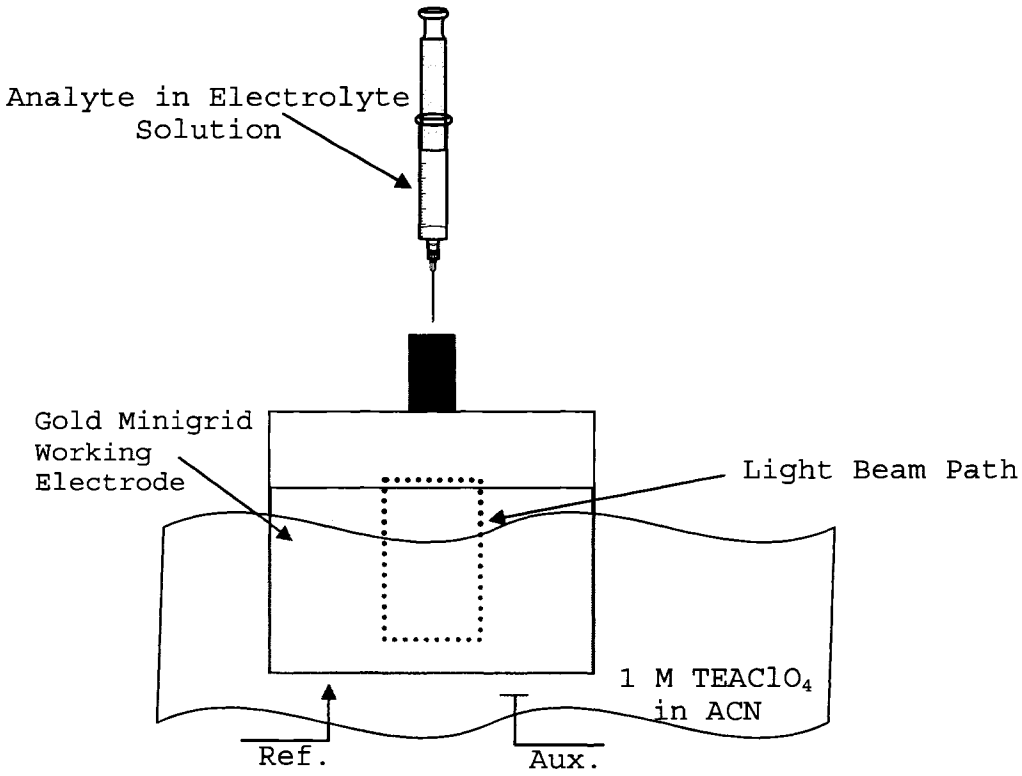

Figure 2.1 Optically transparent thin layer electrode setup (adapted from Ref. 7). This cell is placed in the beam path of a UVVisible spectrometer for data collection. The bulk electrolysis setting on a BAS100b electrochemical analyzer is used to electrolyze the analyte.

Solution Viscosity Determination. Solution viscosities were measured using Cannon-Ubbelohde type viscometers from Cannon Instrument Company.[4]

Nanosecond Laser Flash Photolysis. A typical transient spectrum was obtained as follows: The frequency-tripled beam of a Quanta-Ray Nd:YAG laser pumped a Spectra

Physics PDL-3 dye laser. Coumarin 450 laser dye was used with methanol which was operated at 450 nm. Dye laser power output was typically 85 mW at 30 Hz with a 5-7 ns pulse width. Alternately, an Opotek OPA was used to provide the 450 nm excitation beam at powers of 50-55 mW. The probe beam was provided by a homebuilt pulser powering a Xenon arc lamp (1 ms pulses). This probe beam was passed through the sample cell, and then focused onto the slit of a Jarrell Ash model 82-310 monochromator. A Hamamatsu R2496 photomultiplier tube measured the intensity of the probe beam and a Tektronix oscilloscope triggered by a Thorlabs DET210 photodiode was used to record and display the data. All data collection software was written by Jeremy Nelson on Labview 7.1. The experiment was run at 20 or 30 Hz and transient signals were averaged over 500 pulses. Magnetic field effect measurements were collected by the placement of the sample between the poles of a Walker Scientific Inc. HV4H electromagnet (Hewlett Packard 6574A power supply) and routing the optical train through the sample. The magnetic field was applied perpendicular to the optical path. Magnetic induction was measured with a Hall probe (F. W. Bell, model 5080).

Figure 2.1 Transient absorption instrument. Focusing lenses are shown in red and collimating lenses in blue for clarity. Pump beam is provided by either the OPO or the dye laser. The lens labeled "LF" (mounted on an adjustment track) denotes a lens to focus the highly divergent OPO pump beam prior to contacting the sample. The pump laser beam, through a photodiode, triggers scope data collection. When pulsed probe experiments are done, the pulser triggers the OPO laser system.

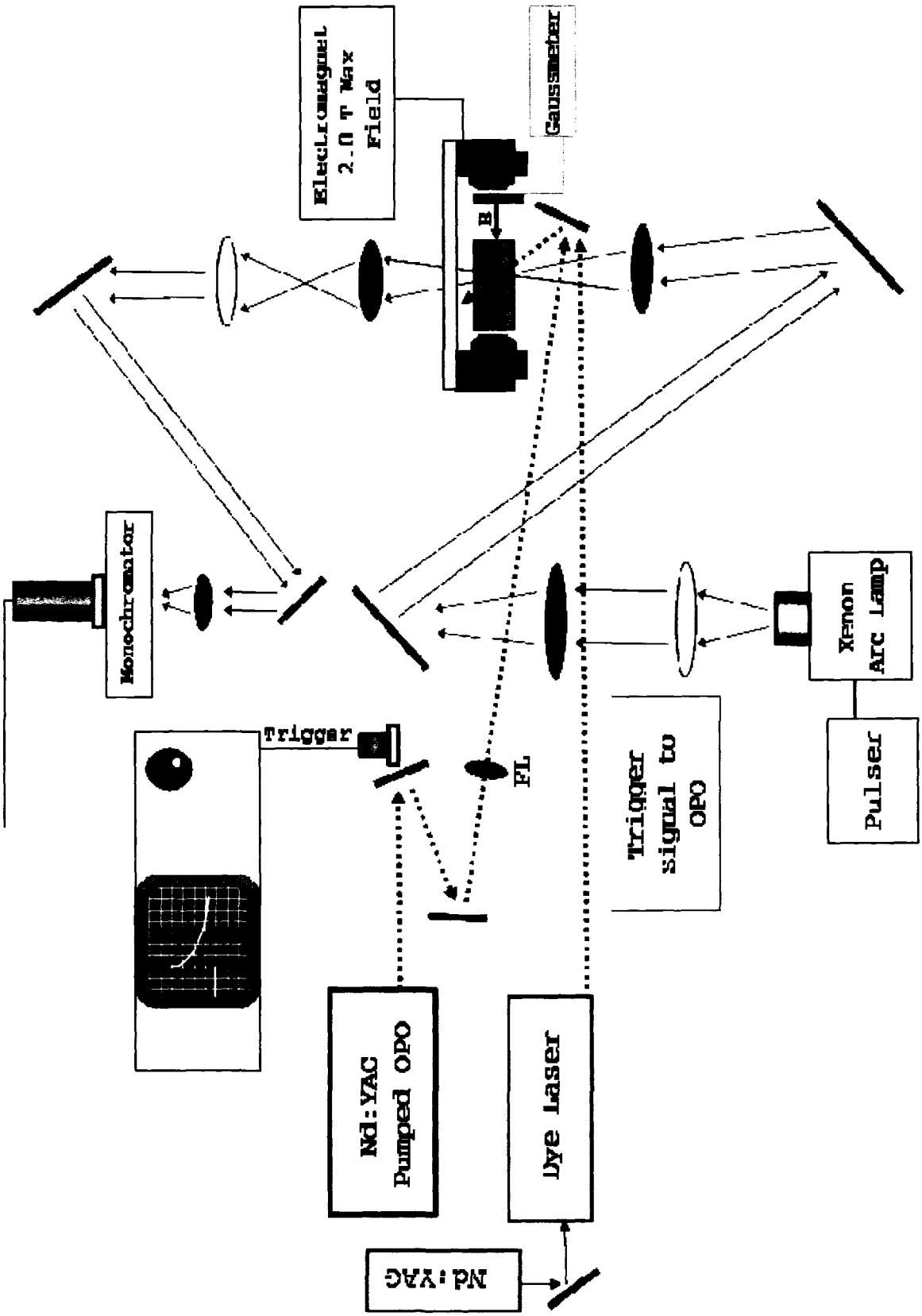

REFERENCES

(1) Weber, J. M. PhD Thesis, Colorado State University, 2007.

(2) Curphey, T. J. *Organic Syntheses* **1988**, *6*, 1019.

(3) Limoges, B. R. Dynamics of electron transfer reactions in ruthenium-based donor-chromophore-acceptor complexes involving phenothiazine-type donors, Colorado State University, 2001.

(4) Weber, J. H.; Rawls, M. T.; Mackenzie, V. J.; Limoges, B. R.; Elliott, C. M. *J. Am. Chem. Soc.* **2006**, *Web Release.*

(5) Larson, S. L.; Elliott, C. M.; Kelley, D. F. *J. Phys. Chem.* **1995**, *99*, 6530.

(6) Campa, C.; Camps, J.; Font, J.; DeMarch, P. *Anales De Quimica* **1987**, *84*, 128.

(7) Zhou, M.; Robertson, G. P.; Roovers, J. *Inorg. Chem.* **2005**, *44*, 8317.

(8) Danielson, E.; Elliott, C. M.; Merkert, J. W.; Meyer, T. J. *J. Am. Chem. Soc.* **1987**, *109*, 2519.

(9) Murray, R. W. H., W. R.; O'Dom, G. W. *Anal. Chem.* **1967**, *39*, 1666.

CHAPTER 3

HIGH ENERGY AND QUANTUM EFFICIENCY IN PHOTOINDUCED CHARGE SEPARATION

John M. Weber, Matthew T. Rawls, Valerie J. MacKenzie,

Bradford R. Limoges, and C. Michael Elliott

Published in the *Journal of the American Chemical Society*. Printed here with permission from the authors.

This dissertation chapter contains the results from an article published in the *Journal of the American Chemical Society* with a web release date of December 22, 2006. The manuscript was written primarily by John Weber and Mike Elliott with assistance from Matthew Rawls. The chapter describes the experimental evidence for explanation of the uniquely high quantum efficiency of charge separation in DCA triads consisting of a central trisbipyridineruthenium(II) chromphore, with an appended azine type donor and a diquat type acceptor. An association between the donor and the bipyridine rings of the chromophore places the donor in favorable electronic contact with the chromophore allowing for rapid oxidation (and thus charge separation) upon reduction of the acceptor. John Weber collected the primary data. Matthew Rawls contributed experiments which provided conclusive evidence of this donor chromophore association. These experiments included 2D ROESY NMR studies, association studies utilizing a C-A analogue to the primary species reported, and study of solvent effects in the association.

ABSTRACT

Supramolecular triad assemblies consisting of a central trisbipyridineruthenium(II) chromophore (C^{2+}), with one or more appended phenothiazine electron donors (D) and a diquat-type electron acceptor (A^{2+}) have been shown to form long-lived photoinduced charge separated states (CSS) with unusually and consistently high quantum efficiency. Up to now, there has been no understanding for why these large efficiencies (often close to unity) are achieved across this entire class of triads when other, seemingly similar systems are often much less efficient. In the present study, using a bimolecular system consisting of a chromophore-acceptor diad (C^{2+}-A^{2+}) and an N-methylphenothiazine donor, we demonstrate that a ground-state association exists between the RuL_3^{2+} and the phenothiazine prior to photoexcitation. It is this association process that is responsible for the efficient CSS formation in the bimolecular system, and by inference, also must be an essential factor in the fully intramolecular process occurring with the D-C^{2+}-A^{2+} triad analogs.

3.1 INTRODUCTION

In photosynthetic reaction centers, nature has designed a molecular apparatus capable of separating charge with unsurpassed efficiency. In bacterial systems, where we have good structural data, the process initiates when a photon is absorbed by the so-called "special pair" of chlorophylls.[1,2] Within a few picoseconds, the resulting excited state transfers an electron with unity efficiency to an adjacent pheophytin electron acceptor, reducing it and leaving a hole on the special pair.[3] It is at this stage where arguably the most remarkable step in the entire photosynthetic process occurs. The photoinjected electron on the pheophytin has two choices. It can recombine with the hole on the special pair or it can transfer to an adjacent quinone molecule which serves as a secondary electron acceptor. What makes this second step so surprising is that essentially 100% of the time the electron transfers to the quinone and does not recombine with the hole on the special pair, despite the much larger thermodynamic driving force for the latter process and roughly similar electron transfer distances. Subsequently, the electron continues to cascade down the series of electron acceptors until eventually it and the hole are "harvested" as chemical energy.

Over the last several decades various groups, including our own, have attempted to provide functional mimics of the first several steps in this photosynthetic process.[4-9] A common approach is to synthesize supramolecular assemblies which contain various functional analogs (which may or may not also be structural analogs) of the photosynthetic reaction center: for example, a light absorbing chromophore (C) covalently linked to an electron acceptor (A) and/or an electron donor (D). Efficiently mimicking the first step in the photosynthetic process is not difficult. There have been many systems reported over the years in which a photoexcited chromophore, attached to

an acceptor (or a donor), undergoes electron transfer quenching with essentially 100% efficiency. The tricky bit is efficiently affecting the second electron transfer which actually separates the charge. Here, success with synthetic mimics has been much less common because of the inherent competition between the productive, second charge separation step and the parasitic back electron transfer, wherein the latter usually wins. For example, it is uncommon for such systems to form multi-step charge separated states (CSS) with quantum efficiencies, Φ_{CSS}, greater than ca. 25-30% and frequently it is much lower. There are few examples outside of the systems exemplified by the structure in Figure 3.1 (vide infra) where Φ_{CSS} is very large (e.g., >90%) but these systems are exceptions rather than the rule.[10]

A significant portion of our efforts in this area has focused on so-called "triad" assemblies incorporating an electron acceptor (A), an electron donor (D) and a light absorbing chromophore (C) represented by the structure shown in Figure 3.1. The components of these triads typically consist of a central trisbipyridine ruthenium(II) chromophore ($RuL_3^{2+} = C^{2+}$) covalently linked to one or more phenothiazine donors (PTZ = D) and to an N,N'-diquaternary-2,2'-bipyridinium electron acceptor ($DQ^{2+} = A^{2+}$).[11-14] The linkages between the chromophore and the D and A^{2+} moieties are typically polymethylene chains emanating from the periphery of bipyridine ligands. Thus, the saturated alkyl chains bridging the molecular components are both nominally electrically insulating and flexible. The molecule shown in Figure 3.1 is one example of roughly 50 similar triad assemblies which we have prepared and studied.[11-14]

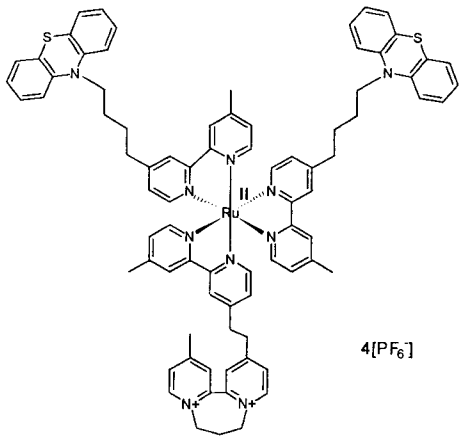

Figure 3.1 Representative Donor-Chromophore-Acceptor triad complex which undergoes efficient photoinduced charge separated state formation.

Considering the many types of light-induced charge-separation systems that exist, there is no *a priori* reason one should expect triads exemplified by Figure 3.1 to be uniformly efficient at charge separation; yet, they are. Typically, all $D\text{-}C^{2+}\text{-}A^{2+}$ systems of this family undergo photoinduced CSS formation with very high quantum efficiencies, *often approaching unity.*[15,16] Additionally, counter to what Marcus Theory predicts, there seems to be little correlation between the thermodynamic driving force for the various electron transfer steps and Φ_{CSS}. To illustrate this point, consider the $D\text{-}C^{2+}\text{-}A^{2+}$ triad shown in Figure 3.1 but with two methylenes in the chain connecting the quaternary nitrogens of the acceptor (rather than three). The photoinduced CSS formed from this triad stores ca. 1.13 eV of energy— about 56% of the ^{3}MLCT energy and 42% of the incident photon energy at λ_{max} of the chromophore absorption (460 nm). Altering the diquat acceptor such that a four carbon chain links the two quaternary nitrogens, increases the energy stored in the CSS to 1.47 eV or 72% ^{3}MLCT energy and 55% of the incident photon energy at λ_{max}, yet both systems have essentially the same Φ_{CSS} (close to unity). For comparison, the group at the Center for Study of Early Events in Photosynthesis at

Arizona State has studied D-C-A triads containing carotenoid donors, porphyrin chromophores, and C_{60} acceptors. Within this family of triads, Φ_{CSS} can be changed from 100% to 22% by merely altering the type of substituents on the porphyrin chromophore periphery without even affecting the amount of stored energy.[10,17]

The purpose of this paper is to develop an explanation for why the particular assemblies exemplified in Figure 3.1 are so uniformly efficient at forming CSS while other putatively similar photoinduced charge separation systems are not. Before embarking on the discussion of the present results, it is necessary to review a few important general facts established in previous studies about this family of triad assemblies. The excited state form of the chromophore is a triplet metal-to-ligand charge-transfer excited state (^{3}MLCT) that is highly luminescent in the absence of any attached acceptors or donors. The solution emission lifetime, τ_{em}, is ca. 600 to 900 ns dependant upon the solvent. Diad assemblies of both C^{2+}-A^{2+} and C^{2+}-D have been prepared and their emission lifetimes examined in order to establish the respective quenching rates. As the driving force is changed and numbers of methylenes in the chain linking C^{2+} and A^{2+} are varied from 2 to 6, the oxidative electron transfer quenching rates for C^{2+}-A^{2+} diads vary from about 1 x 10^{10} to 1 x 10^7 s^{-1}.[12,14,18-20] In contrast, as the numbers of methylenes in the chain linking C^{2+} and D is varied from 1 to 9, the reductive quenching rates for C^{2+}-D vary only from ca. 5 x 10^6 to 1 x 10^6 s^{-1}.[13,21] Thus, the slowest oxidative quenching is at least 2 times faster than the fastest reductive quenching. More importantly, when the emission decay rate of *any* D-C^{2+}-A^{2+} triad is compared with that of the corresponding C^{2+}-A^{2+} diad (i.e., with the same A^{2+}-containing ligand), the *relative rates* never differ by more than a factor of two even though the absolute decay rates change by over a factor of ca. 10^3 (over the entire collection of compounds). The conclusion that must be drawn from these data is

that the initial quenching event in all D-C^{2+}-A^{2+} triads of this family is *always* oxidative quenching and D is, at this point, not involved:

$$D\text{-}C^{2+*}\text{-}A^{2+} \rightarrow D\text{-}C^{3+}\text{-}A^{+\bullet}$$

Another relevant fact from these earlier studies is that, in the time-resolved absorption spectra of the C^{2+}-A^{2+} diads, there is never any detectable amount of $A^{+\bullet}$ present.[12] One must conclude then, that the back electron transfer rate for

$$C^{3+}\text{-}A^{+\bullet} \rightarrow C^{2+}\text{-}A^{2+}$$

must be significantly faster than the oxidative quenching rate.

At this juncture, the stage has been set to propose two alternate hypotheses for the origin of the consistently large Φ_{CSS} values of these triads:

1. The rate of intramolecular electron transfer between D and C^{3+} is inherently and significantly faster than between C^{3+} and $A^{+\bullet}$ and there is nothing else unusual about these triads.
2. The rate of intramolecular electron transfer between D and C^{3+} is abnormally fast as a result of some type of ground-state association involving D prior to photoexcitation.

In order to test these hypotheses it is necessary to determine the effect on Φ_{CSS} of varying the relative concentrations of D and C. Obviously, this cannot be done in an entirely intramolecular system. Thus, in what follows, results are presented for the CSS process in a bi-molecular system consisting of an N-MePTZ donor, D, and a C^{2+}-A^{2+} diad. Figure 3.2 shows the C^{2+}-A^{2+} moiety, **VI**, chosen for the present study. The C^{2+} and A^{2+} components differ somewhat from those comprising the D-C^{2+}-A^{2+} assemblies represented in Figure 3.1. First, the electron acceptor is a "paraquat-type" moiety rather than a "diquat" (i.e., it is based on a N,N'-dialkyl-4,4'-bipyridinium instead of an N,N'-

dialkyl-2,2'-bipyridinium).[22] Second, the two "remote" ligands on the ruthenium (i.e., the ones not having an appended paraquat) are 1,10-phenanthroline rather than 2,2'-bipyridine. Phenanthroline was chosen over bipyridine for reasons that will be considered later but, suffice it so say that, from the ruthenium's perspective, the electronic difference between phenanthroline and bipyridine are fairly minor (i.e., $Ru(bpy)_3^{2+}$ and $Ru(phen)_3^{2+}$ have very similar visible spectra and redox properties).[23] Regardless of the exact identity of the acceptor (i.e., whether diquat or paraquat), the first electron-transfer event following photo-excitation is oxidative quenching.[14,19,20] Paraquat was chosen as the acceptor based on the recombination kinetics of this initial electron-transfer quenching product (vide infra).[18,22]

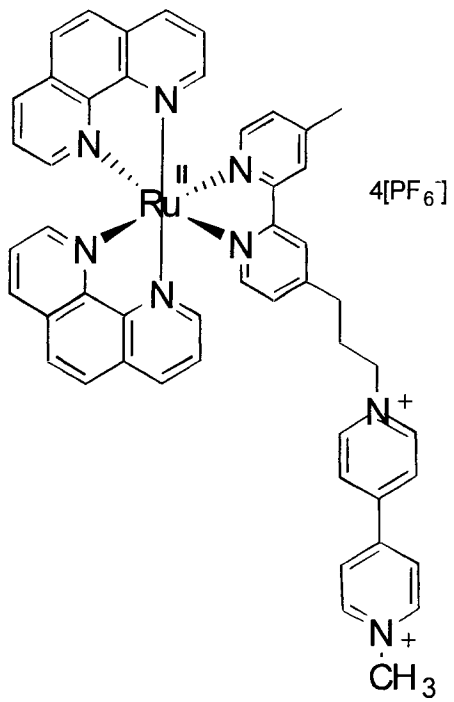

Figure 3.2 The C^{2+}-A^{2+} diad, **VI**, used in bimolecular quenching experiments with N-MePTZ donor.

The choice of donor is straightforward. The redox potentials of N-alkylphenothiazines are essentially insensitive to the identity of the alkyl group. A methyl group is the least sterically demanding, so N-methylphenothiazine (N-MePTZ) was employed as the donor.

MePTZ to obtain each concentration desired was weighed into vials and 3 mL of stock solution of **VI** added to each vial. Samples were then transferred to an optical cell constructed with a side-arm for freeze-pump-thaw (FPT) degassing, a teflon valve, and a fitting for attachment to a vacuum line. Solution in the cell was transferred to the sidearm and frozen in liquid nitrogen. Each sample was FPT degassed several times until there was no evidence of outgassing upon thawing.

3.2 RESULTS AND DISCUSSION

The first goal in this study is to establish which of the two hypotheses best explains the observed CSS formation in D-C^{2+}-A^{2+} assemblies. In the form of a Jablonsky diagram, Scheme 3.1 allows simultaneous examination of both of the limiting mechanistic possibilities.

Scheme 3.1 Jablonsky energy level diagram for collisional (left-hand branch) and pre-association mechanisms (right-hand branch) for CSS formation in C^{2+}-A^{2+}/D bimolecular system.

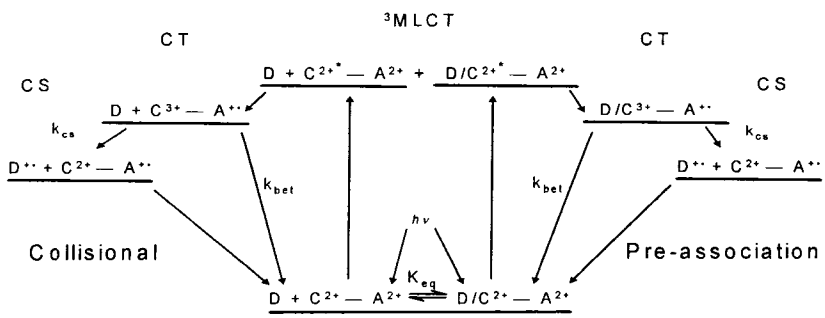

The bottom center of the Scheme 3.1 depicts a ground-state association equilibrium between the donor, D, and the C^{2+}-A^{2+} diad. For the sake of discussion, this association is represented in the Scheme as if it were occurring between D and C^{2+}; however, the nature of any association has yet to be established and this issue will be revisited subsequently. In considering the two limiting cases represented by the left- and right-hand branches of Scheme 3.1, we assume that the CSS exclusively results through either a diffusional mechanism or a preassociation – not both.[17]

Transient spectroscopy was utilized to monitor the absorbance (397 nm) of the reduced viologen radical ($A^{+\bullet}$) formed upon photoexcitation (450 nm) of a C^{2+}-A^{2+} diad as a function of [N-MePTZ]. First, in the absence of N-MePTZ there is no signal for reduced viologen. Thus, it can be assumed that the only viologen radical observed comes from CSS production. In other words, it is only when the donor reduces the oxidized chromophore prior to geminate recombination that the CSS (and thus reduced viologen) is observed. The lifetime of the bimolecular CSS is on the order of tens of microseconds. *Therefore, the change in absorbance at $t \rightarrow 0$ (i.e., ΔA°_{397}) is directly proportional to the amount of CSS initially formed.*

The results obtained for CSS formation in acetonitrile and dichloromethane solvents are shown in Figure 3.3A and 3.3B, respectively, along with fits of the data to equation 3 (vide infra). While the range of [D] available in acetonitrile only permits about 40% of the predicted (from equation 3) maximum ΔA°_{397} (and, thus the maximum [CSS]) to be accessed, the quality of the fit is very good. The value of R^2 is 0.9996 which gives us considerable confidence that the data in Figure 3.3A truly follows the functional form expressed in equation 3 (vide infra). In dichloromethane it is possible to reach D concentrations yielding ΔA°_{397} values much closer to the maximum predicted from

equation 3. As with acetonitrile, the fit at lower [D] to equation 3 is excellent but above ca. 20 mM there is some scatter.[24] However, if only the data below 20 mM is used in the fit to equation 3, almost exactly the same values of *a* and *b* result (i.e., the fit constants) as when the entire data set is used.

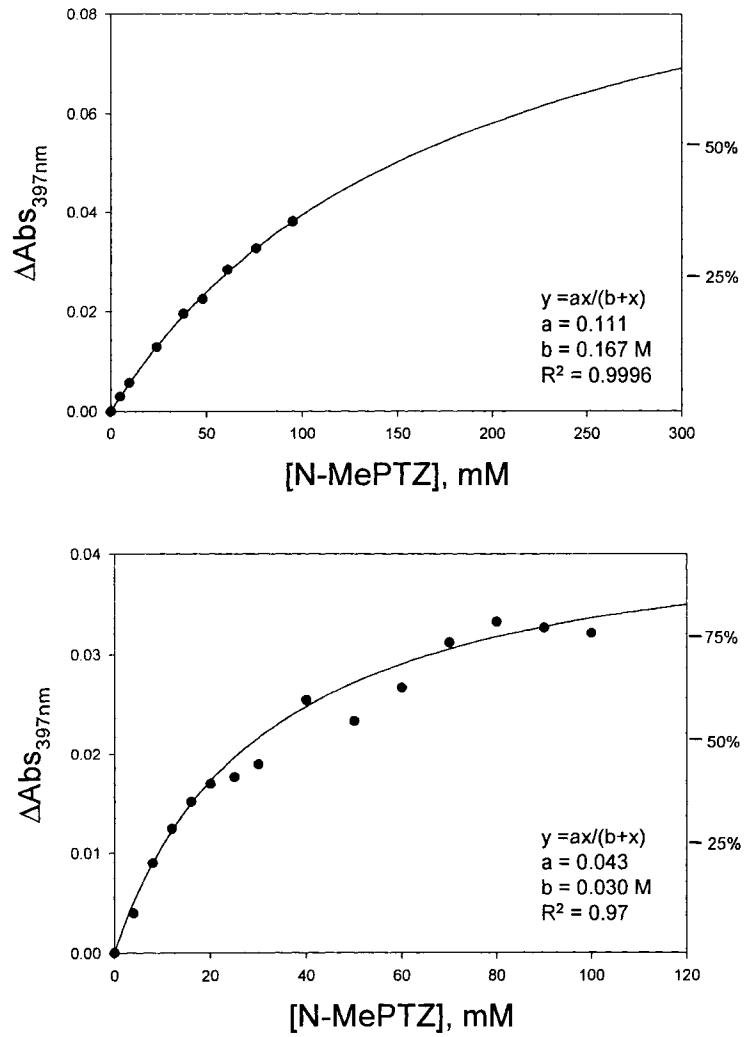

Figure 3.3 ΔA°_{397} (proportional to the amount of charge separated state initially formed) plotted vs. [N-MePTZ] in acetonitrile (3A – upper) and dichloromethane (3B – lower) solvents. The right-hand y-axis is the amount of CSS formed expressed as a percentage of CSS_{max} as predicted from equation 3 (see text for explanation).

To further probe the role of solvent, $\Delta A°_{397}$ was measured at a fixed [D] in binary mixtures of dichloromethane and acetonitrile and those results are presented in Figure 3.4. The relative amount of each solvent was varied from neat acetonitrile to neat dichloromethane. The concentration of N-MePTZ (20 mM) was chosen to give a large relative difference in $\Delta A°_{397}$ for the pure solvents but also such that enough CSS is produced in each solvent to be easily measured. Starting with neat acetonitrile, the amount of CSS formed remains roughly constant with increasing dichloromethane until the solvent is ca. 40% dichloromethane. Above that concentration, $\Delta A°_{397}$ increases roughly linearly up to the value obtained for pure dichloromethane. The D/C association likely results from a π-π stacking interaction (vide infra). Smith et al showed using complexation of pyrene and cyclophanes that the association stability varies linearly with solvent polarity.[24,25] Clearly simple macroscopic solvent considerations do not fully explain the charge separation efficiency in this bimolecular system: molecular level processes must be considered as well.

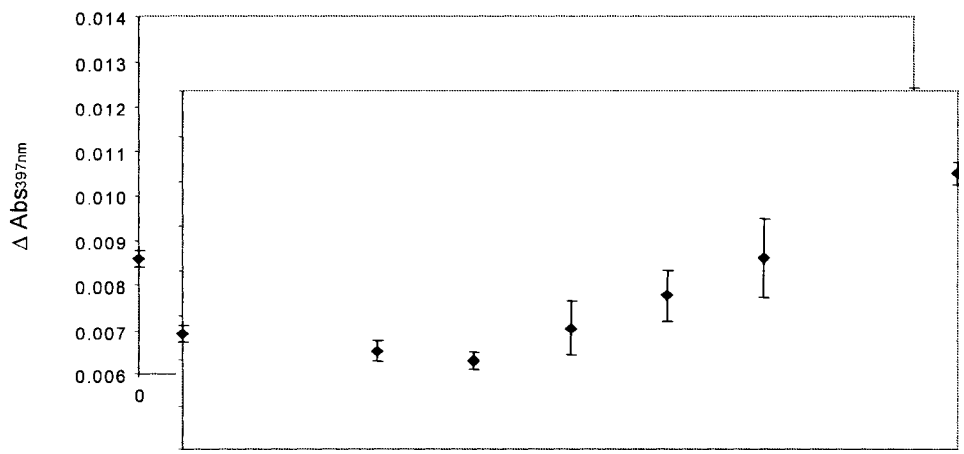

Figure 3.4 $\Delta A°_{397}$ in the presence of 20 mM N-MePTZ plotted vs. % dichloromethane in a binary mixture of dichloromethane and acetonitrile.

In a mechanism involving only bimolecular diffusional encounters between the N-MePTZ donor and C^{3+}-$A^{+\bullet}$ (the left-hand side of Scheme 3.1), the resulting relationship connecting [CSS] and [D] takes the form:

$$\frac{[CSS]_0}{[CA]_i} = \frac{(k_{cs}/k_{bet})[D]}{1+(k_{cs}/k_{bet})[D]} \qquad (1)$$

where $[CA]_i$ is the total concentration of the C^{2+}-A^{2+} diad, $[CSS]_0$ is the concentration of CSS at t = 0, k_{cs} is the bimolecular rate constant for forming the charge separated state and k_{bet} is the rate of geminate recombination between C^{3+}-$A^{+\bullet}$ (see Scheme 3.1).

If, on the other hand, ground-state association between D and C^{2+}-A^{2+} were the sole mechanism responsible for CSS formation (the right-hand side of Scheme 3.1), the following relationship results:

$$\frac{[CSS]_0}{[CA]_i} = \frac{(k_{cs}/k_{bet})}{1+(k_{cs}/k_{bet})} \bullet \frac{K_{eq}[D]}{1+K_{eq}[D]} \qquad (2)$$

where K_{eq} is the complexation equilibrium constant. Again, in deriving equation 2 it is assumed that an equilibrium association between D and C^{2+}-A^{2+} is established prior to excitation and that CSS is only formed from that part of the total population of C^{2+}-A^{2+} that is associated with D in the ground state. Additionally, k_{bet} and k_{cs} are, respectively, first order rate constants of geminate recombination and charge separation relevant to the associated complex. In this instance k_{bet} may or may not be the same as k_{bet} in the absence of D/C^{2+}-A^{2+} association (i.e. as in equation 1).

In either of the above scenarios, the governing relation between $[CSS]_0$ and [D] has the same functional (i.e. mathematical) form. Also, since $[CSS]_0$ is directly proportional to $\Delta A°_{397}$, both expressions can be written in the general form:

$$\Delta A°_{397} = a([D]/(b + [D])) \qquad (3)$$

Thus, the only differentiating factors in the mathematical relations governing the two limiting mechanisms are the meaning of the constants. In both cases the constant *a* depends on, among other things, experimental parameters such as the laser power and overlap of the pump and probe beams. For the sake of the work presented here, *a* can be considered to be an arbitrary constant in both models. In contrast, *b* is independent of similar experimental parameters (as long as they are constant). In the case of a simple bimolecular collisional reaction:

$$b = k_{bet}/k_{cs} \qquad (4)$$

In the case of an equilibrium preassociation:

$$b = K_{eq}^{-1} \qquad (5)$$

Mallouk et al. previously reported values for both k_{et} and k_{bet} obtained in acetonitrile for a C^{2+}-A^{2+} complex very similar to **VI.**[26] Values of the forward electron-transfer rate constant, k_{et}, for Mallouk's complex and for **VI** (in dichloromethane) are similar (1.9×10^9 and 8.2×10^{10} s^{-1}, respectively). It is reasonable to assume, therefore, that Mallouk's

et al value of k_{bet} (6.5×10^9 s^{-1}) is a fair lower-limit estimate for the analogous process in **VI**. Assuming the bimolecular collisional mechanism and using Mallouk's value for k_{bet} and the value of *b* obtained from the fit to equation 3, a lower limit of 3.9×10^{10} $M^{-1}s^{-1}$ is obtained for k_{cs}. Using the standard relation,[27]

$$k_{diff} = \frac{8RT}{3\eta} \qquad (6)$$

an estimate for the diffusion-controlled limiting rate constant of CSS formation in acetonitrile is calculated to be 2×10^{10} $M^{-1}s^{-1}$, where η is the viscosity of acetonitrile at room temperature. The lower limit for k_{cs} obtained from the fit to equation 3 is thus greater than the estimated diffusion controlled rate constant by a factor of ca. ×2. The same calculations performed on the dichloromethane data yield a lower-limit value for k_{cs} of 2.1×10^{11} $M^{-1}s^{-1}$ and an estimated diffusion-controlled rate constant is 1.7×10^{10} $M^{-1}s^{-1}$-i.e., k_{cs} is too large by an order of magnitude. Both calculations depend on the assumption that Mallouk et al.'s value is a reasonable lower-limit estimate for k_{bet}.[28-30] The observations that: (1) Irrespective of solvent, we were unable to observe any photo-reduced acceptor with **VI** in the absence of N-MePTZ and (2) Back electron-transfer rates for related compounds are typically not strongly solvent dependent are facts fully consistent with a $k_{bet} > 6.5 \times 10^9$ s^{-1} for **VI.**

The results that the values of k_{cs} exceed the diffusion controlled limit in both solvents is strongly suggestive that the mechanism of CSS formation is not diffusional; however, a much stronger argument can be made by examining the dependence of Φ_{CSS} on solution viscosity. A series of stock solutions containing ca. 10^{-5}M C^{2+}-A^{2+} complex (**VI**) and 50

mM N-MePTZ were prepared in dichloromethane solvent. To these solutions 0-80 mg/mL of polystyrene was added to increase solution viscosities. A corresponding weight of toluene was also added such that the (polystyrene + toluene):solvent ratio was held constant. The viscosity of each solution was measured five times and the averages ranged from 0.46cP to 12.1cP. Figure 3.5 shows the dependence of $\Delta A°_{397}$ on viscosity.

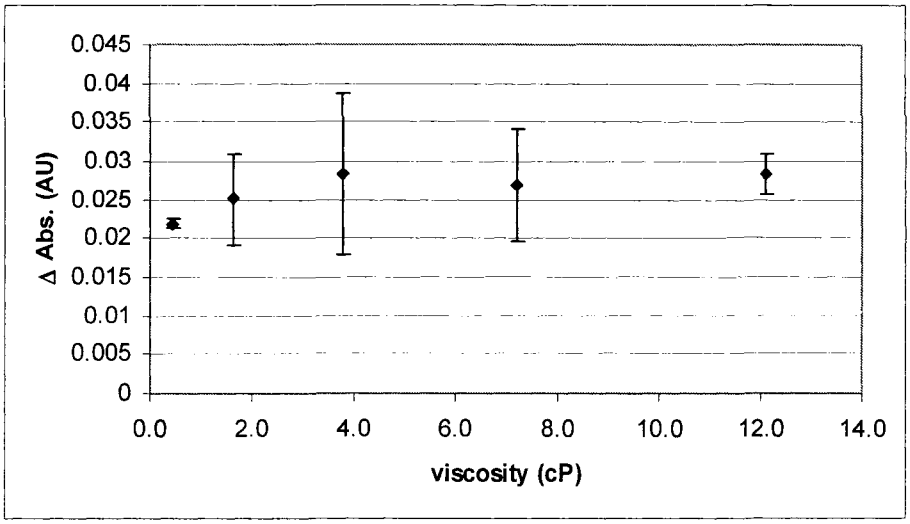

Figure 3.5 $\Delta A°_{397}$ (proportional to the amount of charge separated state initially formed) in the presence of 50 mM N-MePTZ plotted vs. solution viscosity. The error bars represent one standard deviation.

These data demonstrate conclusively that the amount of $[CSS]_0$ formed is independent of solution viscosity. Clearly, a ca. 25-fold increase in viscosity with *no change* in $[CSS]_0$ effectively rules out any CSS-formation mechanism whereby simple collisional encounters between D and C^{3+}-$A^{+\bullet}$ are involved (i.e., Hypothesis 1). If the process is not collisional, then the only reasonable possibility remaining is the mechanism represented in the right hand side of Scheme 3.1 and by Hypothesis 2. However, none of the results considered thus far addresses the nature of the ground state pre-association. To shed light on this issue, other data must be considered.

In looking into the nature of the association, it is helpful at this point to construct two additional hypotheses:

2a. The association between D and C^{2+}-A^{2+} leading to CSS formation, is between D and C^{2+} (D/C^{2+})—most likely π-π van der Waals in nature.

2b. The association between D and C^{2+}-A^{2+} leading to CSS formation is between D and A^{2+} (D/A^{2+})—possibly both charge-transfer and π-π van der Waals in nature.

Distinguishing between these hypotheses has proven more challenging than simply demonstrating the participation of the pre-association in CSS formation. While there is literature precedent for both D/A^{2+} and D/C-type associations (at least in loosely related systems),[31,32] there is no single piece of data which unambiguously demonstrates the nature of the association—rather consideration of a collection of data from several experiments is necessary to develop a case. First, spectral evidence for any association between the two pairs of moieties (i.e., between D/A^{2+} and D/C^{2+}) was examined. Neither D nor A^{2+} absorb light in the visible but both absorb strongly in the UV. If any degree of interaction between these species were occurring in solution some perturbation in UV spectra of the two moieties should be evident—especially if there is any charge-transfer nature to that interaction. Figure 3.6 shows that the absorption bands of the donor and acceptor are unperturbed by mixing the solutions. This is most clearly demonstrated by the fact that the spectrum resulting from the mathematical sum of the individual components exactly overlays the spectrum obtained from mixing the donor and acceptor solutions together (within experimental error).

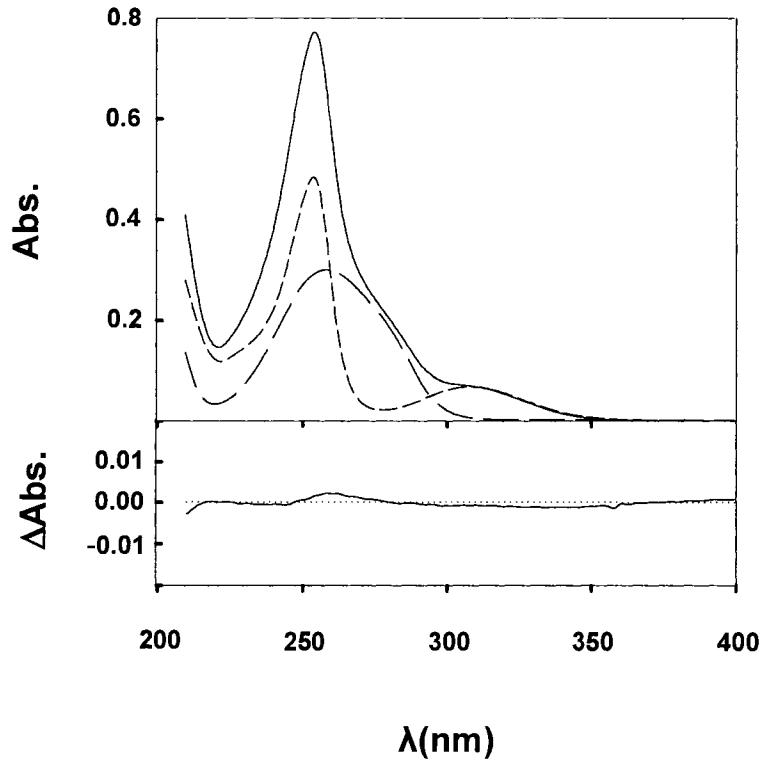

Figure 3.6 Visible spectra in acetonitrile of a 1.5 mM solution of N-MePTZ (long-dashed curve), 1.5 mM solution of methyl viologen (short-dashed curve) and a solution that is 1.5 mM in both N-MePTZ and methyl viologen (solid curve). Superimposed on the solid spectrum is the sum of the two dashed spectra (i.e., the spectra of the isolated components). The lower part of the figure is the difference spectrum obtained by subtracting each spectrum of the individual components from the spectrum of the mixture.

In contrast to the data in Figure 3.6, there is a small but clear perturbation in the visible spectrum of combined solutions of D and C^{2+}. Attempts to quantify the intermolecular interaction via titration are complicated by overlap from the intense MLCT transitions and the weak nature of the optical signal resulting from the D/C^{2+} interaction; nevertheless, the qualitative effect of added N-MePTZ on the MLCT band of **VII** can be clearly seen in the spectra of Figure 3.7. Similar evidence of a D/C^{2+} interaction comes from comparisons between spectra from $D\text{-}C^{2+}$ diads, $D\text{-}C^{2+}\text{-}A^{2+}$ triads and isolated C^{2+},

D and A^{2+} moieties. We have noted in earlier publications that whenever a complex has incorporated one or more D-containing ligands, it is never possible to exactly simulate the spectrum by summing weighted spectra of the respective C^{2+}, D and A^{2+} components.[13,21] Difference spectra from those attempts look qualitatively similar to those in Figure 3.7.[33]

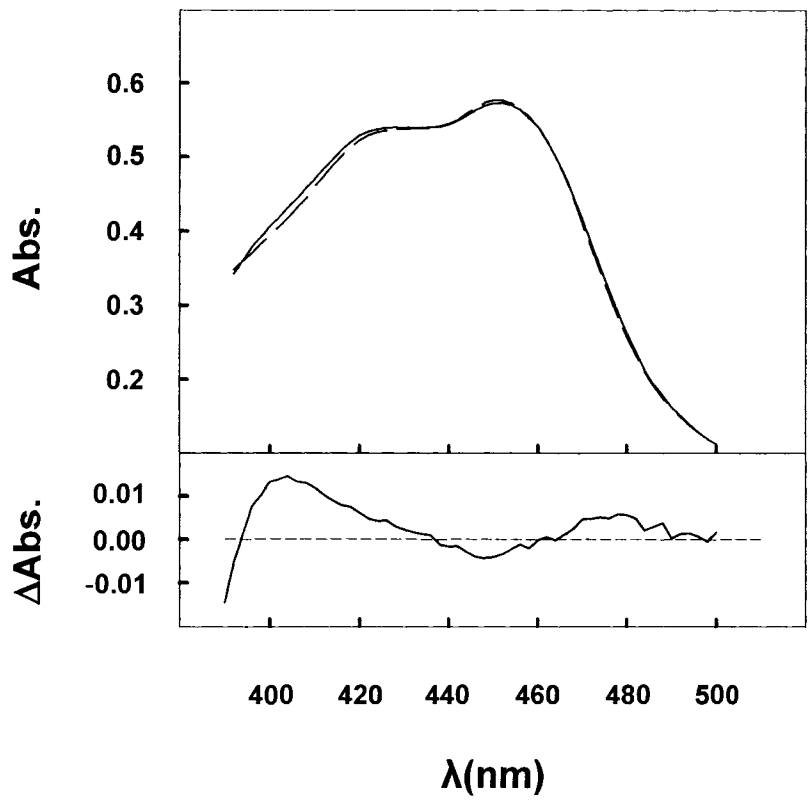

Figure 3.7 Visible spectra of a ca. 3×10^{-5} M solution of **VII** in dichloromethane (solid curve) and the same solution containing 50 mM N-MePTZ (dashed curve). The dashed curve was corrected for any small absorption of N-MePTZ by subtracting the spectrum of a 50 mM N-MePTZ solution in dichloromethane. The lower part of the figure is the difference spectrum obtained by subtraction of the dashed spectrum from the solid spectrum.

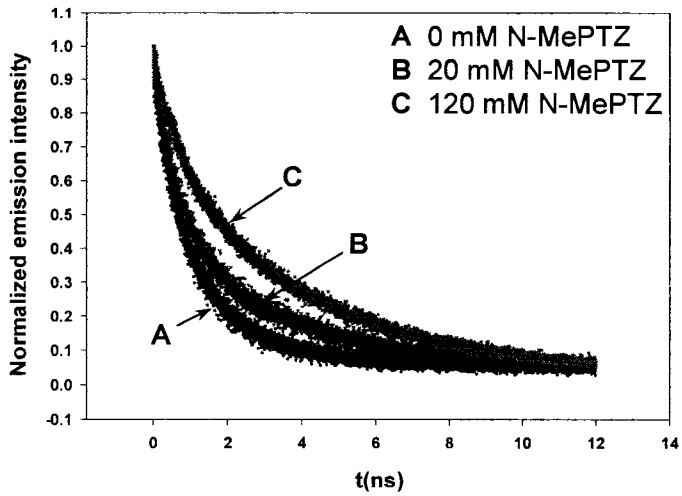

Figure 3.8 Time-resolved emission decays for a ca. 1×10^{-5} M solution of **VI** in oxygen-free dichloromethane: **A**, [N-MePTZ.] = 0.0 mM; **B**, [N-MePTZ.] = 20.0 mM; **C**, [N-MePTZ.] = 120.0 mM.

Time-resolved emission spectra of C^{2+}-A^{2+} **VI** as a function of added N-MePTZ also assist in understanding the nature of the association between D and C^{2+}-A^{2+}. Figure 3.8 shows the emission decay of a ca. 1 x 10^{-5} M dichloromethane solution of **VI** in the presence, of 0, 20 and 120 mM N-MePTZ, respectively. In the absence of any D, the lifetime of the emission is determined entirely by the oxidative quenching process. Obvious from the figure, however, is that addition of N-MePTZ *increases* the average emission lifetime of C^{2+*}-A^{2+}. From biexponential fits, curves B and C in Figure 3.8 each consist of the same two lifetime components—i.e., 3.8 ± 0.2 ns and 0.72 ± 0.03 ns. While the lifetimes are within experimental error the same, the relative contributions of each are different. When the data in Figures 3.8 is compared with that in Figure 3.3B, an interesting and relevant correlation emerges. As stated previously, the right hand Y-axis of Figures 3.3A&B represent the fraction of CSS formed relative to the theoretical maximum CSS. That axis also represents the fraction of the total C^{2+}-A^{2+} which is tied

up as D/C^{2+}-A^{2+}. Expressed as percentages, at 20 and 120 mM N-MePTZ, respectively, 40% and 80% of the C^{2+}-A^{2+} is associated with D. From the fits of the data in Figure 3.7, the slow component contributes 45% and 70% to the total emission at 20 and 120 mM N-MePTZ, respectively. The correlation suggests that the slow component of the emission decay arises from the fraction of the C^{2+}-A^{2+} population associated with D. Since conformational flexibility of the C^{2+}-A^{2+} linkage appears to be required for the initial oxidative quenching,[18] were D associated with A^{2+} (rather than C^{2+}), much larger changes in emission lifetime should result than are observed. The difference in hydrodynamic radii between A^{2+} and D/A^{2+} should be large and should produce large changes in the quenching rate. In contrast, an association between C^{2+} and D might sterically restrict some encounters between A^{2+} and C^{2+} but only along a limited fraction of possible approach trajectories resulting in a more modest change in emission lifetime (as is observed).

Finally, if the association of D and C^{2+}-A^{2+} were between D and A^{2+}, the formation constant, K_{eq}, should be quite sensitive to the structure and redox potential of the acceptor. A titration with N-MePTZ in dichloromethane was carried out on an analog of **IV** in which only the acceptor ligand was changed--specifically, the paraquat was replaced with the same diquat ligand as shown in Figure 3.1. Within experimental error, the resulting titration is *identical* to that in Figure 3.3B. The solid curve is NOT a fit to the data points in Figure 3.9, rather it is the calculated line generated using the fit parameters obtained from the data in Figure 3.3B. It is difficult, indeed, to rationalize how a K_{eq} for association between D and A^{2+} could be the same given such dramatic differences in A^{2+} structure (i.e., rigidly twisted vs. freely rotating around the π-π bond), especially in light of the strong solvent dependence demonstrated in Figures 3.3A&B.

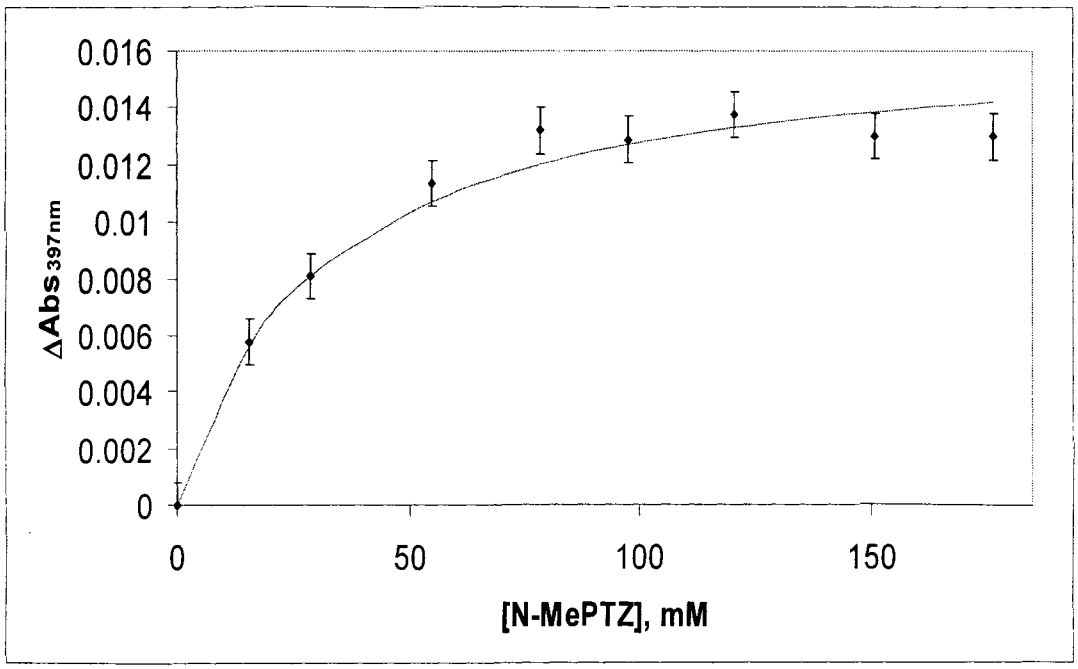

Figure 3.9 $\Delta A°_{397}$ for a CA with diquat acceptor in the presence of N-MePTZ in dichloromethane. The line was generated using the parameters from the CA viologen fit (from Figure 3.3B).

To summarize, it seems quite clear from these collective results that CSS formation is dependent on a ground-state preassociation of the donor with the chromophore. Were there a significant charge-transfer component to this association process, differences is redox potentials would predict that a D/A^{2+} association should have a significantly more favorable enthalpy than would a D/C^{2+} association. If, on the other hand, the association is driven predominantly by van der Waals interactions and entropy, there is no a priori reason why one pair-wise association should be favored over the other. The very minor changes in the absorption spectrum (Figure 3.7) and in time-resolved emission spectrum (Figure 3.8) produced by bimolecular association of N-MePTZ and **IV**, and the similarly small absorption and time-resolved emission differences between C^{2+}-A^{2+} diads and D-C^{2+}-A^{2+} triads,[12-14] all suggest that there is not a large enthalpic contribution for either the

inter- or intramolecular association. The equilibrium may, therefore, be largely driven by entropy, but that is yet to be determined.

Finally, the question must be addressed of how the results from the bimolecular system actually informs about behavior in triad assemblies. First, consideration of molecular models demonstrates that intramolecular D/C^{2+} associations are stericaly possible without significant strain energy. In the triad systems, the effective local concentration of D in the vicinity of the C^{2+} is much higher than can be achieved in the bimolecular system. This inherent concentration bias is the reason for using phenanthroline ligands, with their extended π-systems, in **IV** rather than bipyridines. The argument that an analogous intramolecular D/C^{2+} associations occurs in the triad assemblies is further supported the fact that difference spectra between C^{2+}-A^{2+} diads and D-C^{2+}-A^{2+} triads are qualitatively similar to the difference spectrum in Figure 3.7. Lastly, D-C^{2+}-A^{2+} triads incorporating phenoxazine (POZ) rather than phenothiazine donors, form photoinduced CSS with equivalently large Φ_{CSS} values.

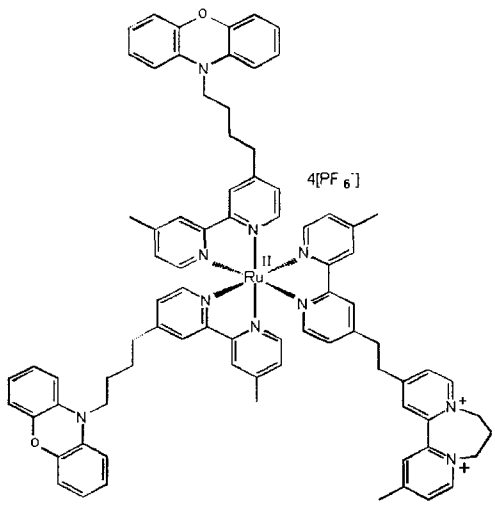

Figure 3.10 Donor-chromophore-acceptor triad with phenoxazine donors.

Direct spectroscopic observation of the D/C interaction came in the form of 2D NMR spectroscopy. ROESY NMR spectroscopy utilizes a pulse sequence which measures spin-spin cross relaxation of NMR active nuclei in close spatial proximity. ROE signals are very sensitive to the through space distance separating the two interacting nuclei ($1/r^6$). Figure 3.10 shows a POZ analog of the triad shown in Figure 3.1. The 1D ^1H NMR spectrum of the triad along with peak assignments is shown in Figure 3.11. Two-dimensional ^1H-^1H ROESY NMR experiments were performed on this triad and the resulting spectrum is shown in Figure 3.11. The figure is plotted with chemical shift on each axis and a 1D ^1H NMR trace is included in each legend. ROESY spectra can be complicated containing signals not necessarily indicative of ROE contact such as instrumental artifacts and TOCSY breakthrough: these features must be considered in examination of the spectrum (Dr. Chris Rithner of Colorado State University assisted in this spectral interpretation). Of interest here are the off diagonal signals (cross peaks) due to ROE contact. Referring first to the 1D spectrum, peaks between 6 and 7 chemical shift arise purely from donor protons, while the singlet at chemical shift 2.6 arises purely from the methyl protons on the chromophoric bipyridine. Interaction of these regions in a 2D spectrum indicates ROE contact (association) between the donor protons (labeled POZ in Figure 3.11) and the bipyridine protons (labeled BPY in Figure 3.11). Cross peaks are clearly seen in this region of the ROE spectrum. Next consider the region of 4 to 5 chemical shift (acceptor) and 6 to 7 (donor). Crosspeaks in this region would suggest interaction of the donor and the acceptor. Very little signal is seen in this region: in fact, very little correlations arise (significant within the limit of signal-to-noise) involving the diquat acceptor protons except those with itself and with its linker methylene protons.

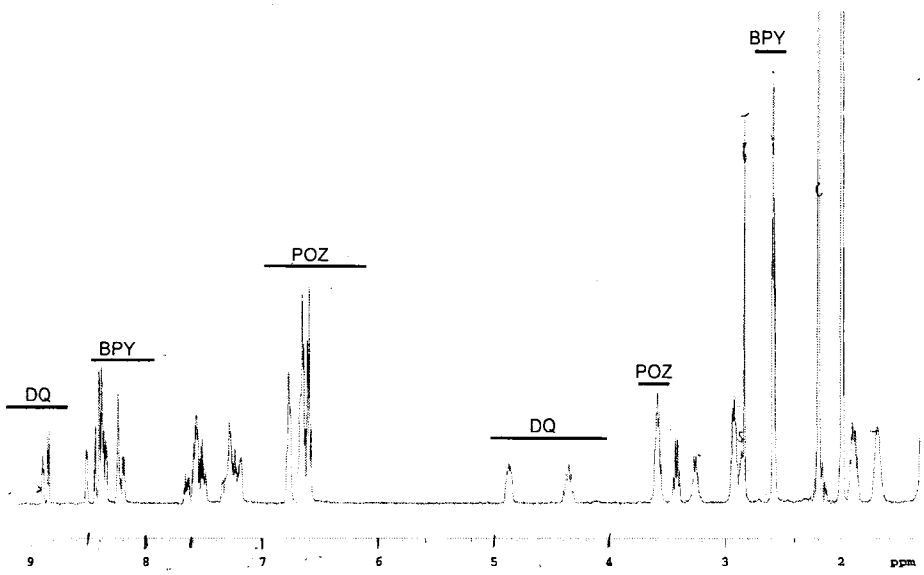

Figure 3.11 1D ^{1}H NMR spectrum of covalently bound donor-chromophore-acceptor triad (Figure 3.10) in deuterated acetonitrile.

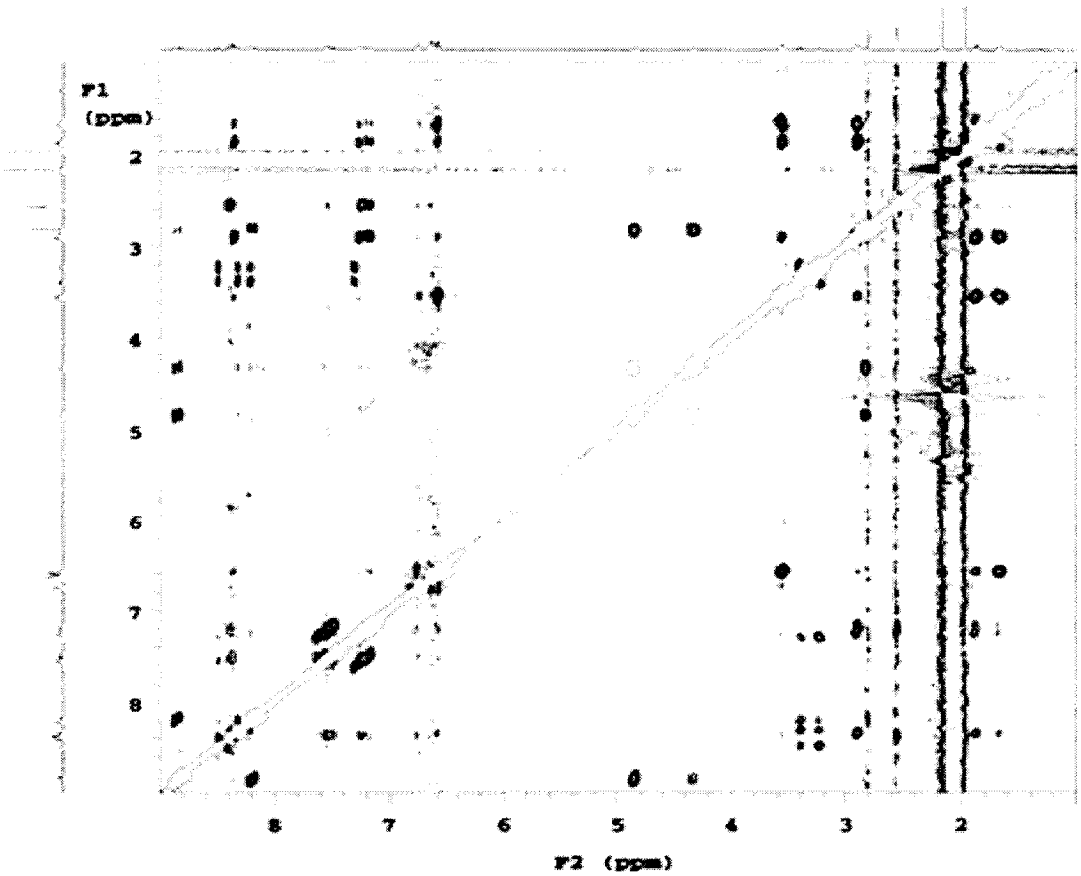

Figure 3.12 2D ROESY NMR spectrum of covalently bound donor-chromophore-acceptor triad (Figure 3.10) in deuterated acetonitrile. ^{1}H NMR spectra are also including along each axis.

Scheme 3.2 A depiction of the phenothiazine electron donor moiety associating with the local bipyridine ligand in a triad assembly such as in Figure 3.1.

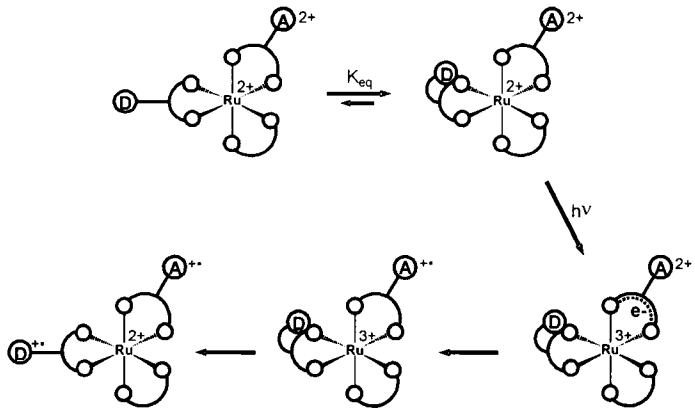

3.3 CONCLUSION

Scheme 3.2 represents, in cartoon form, how the D/C^{2+} association plays the critical role in intramolecular CSS formation for triads such as in Figure 3.1. This mechanism provides a plausible explanation for the large CSS-formation quantum efficiencies observed uniformly across this class of triads; but most importantly, it provides insight into a general means whereby systems might be designed to give efficient photoinduced charge separation *without automatically sacrificing the quantity of energy stored in the CSS*. Typically, the electronic coupling between donor and acceptor orbitals does not change dramatically upon electron transfer; consequently, an efficient forward electron-transfer usually means an efficient recombination. Therefore, with a multi-step photoinduced charge separation system, increasing Φ_{CSS} often comes with a concomitant cost in stored energy. For $D\text{-}C^{2+}\text{-}A^{2+}$ triads like in Figures 3.1 and 3.10, the flexible linkage allows D/C^{2+} to associate prior to any electron transfer, thus enhancing the D/C^{2+} orbital coupling, and to turn off the enhanced coupling by disassociation once the donor

is oxidized. Consequently, Φ_{CSS} is largely independent of driving force, and thus, of the energy stored in the CSS.

Considered in light of the present results, these specific triad assemblies provide the first example of which we are aware where a change in orbital coupling of this magnitude is induced by an intramolecular electron transfer—a change large enough to swamp the thermodynamic factors which usually control the charge-separation kinetics. This suggests that related self-assembly processes could be intentionally designed and exploited to effect efficient CSS formation. Of particular importance is, in principle, that efficient photoinduced charge separation via such a mechanism should be possible without the loss in stored energy that most often accompanies efforts to use driving-force manipulations to improve CSS formation quantum efficiencies.

REFERENCES

(1) Deisenhofer, J.; Michel, H. *Annual Review of Cell Biology* **1991**, *7*, 1.

(2) Deisenhofer, J.; Michel, H. *Annual Review of Biophysics and Biophysical Chemistry* **1991**, *20*, 247.

(3) Greenfield, S. R.; Wasielewski, M. R. *Photosynthesis Research* **1996**, *48*, 83.

(4) Kalyanasundaram, K. *Photochemistry of Polypyridine and Porphyrin Complexes*; Academic Press: San Diego, 1992.

(5) Schanze, K. S.; Walters, K. A. Photoinduced Electron Transfer in Metal-Organic Dyads. In *Organic and Inorganic Photochemistry*; Ramamurthy, V., Schanze, K. S., Eds.; Marcel Dekker: New York, 1998; Vol. 2; pp 75.

(6) Armaroli, N. *Photochem. Photobiol. Sci.* **2003**, *2*, 73.

(7) Scandola, F.; Chiorboli, C.; Indelli, M. T.; Rampi, M. T. Covalently Linked Systems Containing Metal Complexes. In *Biological and Artificial Supermolecular Systems*; Wiley: Weinheim, 2003; Vol. 3; pp 337.

(8) Gust, D.; Moore, T. A.; Moore, A. L. *Electron Transfer in Chemistry* **2001**, *3*, 272.

(9) Gust, D.; Moore, T. A. *Porphyrin Handbook* **2000**, *8*, 153.

(10) Bahr, J. L.; Kuciauskas, D.; Liddell, P. A.; Moore, A. L.; Moore, T. A.; Gust, D. *Photochem.and Photobio.* **2000**, *72*, 598.

(11) Danielson, E.; Elliott, C. M.; Merkert, J. W.; Meyer, T. J. *J. Am. Chem. Soc.* **1987**, *109*, 2519.

(12) Cooley, L. F.; Larson, S. L.; Elliott, C. M.; Kelley, D. F. *J. Phys. Chem.* **1991**, *95*, 10694.

(13) Larson, S. L. Ph. D Dissertation, Colorado State University, 1994.

(14) Larson, S. L.; Elliott, C. M.; Kelley, D. F. *J. Phys. Chem.* **1995**, *99*, 6530.

(15) Klumpp, T.; Linsenmann, M.; Larson, S. L.; Limoges, B. R.; Buerssner, D.; Krissinel, E. B.; Elliott, C. M.; Steiner, U. E. *J. Am. Chem. Soc.* **1999**, *121*, 4092.

(16) Klumpp, T.; Linsenmann, M.; Larson, S. L.; Limoges, B. R.; Buerssner, D.; Krissinel, E. B.; Elliott, C. M.; Steiner, U. E. *J. Am. Chem. Soc.* **1999**, *121*, 1076.

(17) Kodis, G.; Liddell, P. A.; Moore, A. L.; Moore, T. A.; Gust, D. *J. Phys.Org.Chem.* **2004**, *17*, 724.

(18) Schmehl, R. H.; Ryu, C. K.; Elliott, C. M.; Headford, C. L. E.; Ferrere, S. *Adv. Chem. Ser.* **1990**, *226*, 211.

(19) Cooley, L. F.; Headford, C. E. L.; Elliott, C. M.; Kelley, D. F. *J. Am. Chem. Soc.* **1988**, *1122*, 6673.

(20) Ryu, C. K.; Wang, R.; Schmehl, R. H.; Ferrere, S.; Ludwikow, M.; Merkert, J. W.; Headford, C. E. L.; Elliott, C. M. *J. Am. Chem. Soc.* **1992**, *114*, 430.

(21) Larson, S. L.; Elliott, C. M.; Kelley, D. F. *Inorg. Chem.* **1996**, *35*, 2070.

(22) Yonemoto, E. H.; Riley, R. L.; Kim, Y. I.; Atherton, S. J.; Schmehl, R. H.; Mallouk, T. E. *J. Am. Chem. Soc.* **1992**, *114*, 8081.

(23) Balzani, V.; Juris, A.; Barigelletti, F.; Campagna, S.; Belser, P.; Von Zelewsky, A. *Coord. Chem. Rev.* **1988**, *84*, 84.

(24) Zuccarello, F.; Raudino, A.; Buemi, G.; Rigano, C. *Bull. Chem. Soc. Jpn.* **1983**, *56*, 1839.

(25) Hunter, C. A.; Lawson, K. R.; Perkins, J.; Urch, C. J. *J. Chem. Soc., Perkins Trans. 2* **2001**, 651.

(26) Yonemoto, E. H.; Saupe, G. B.; Schmehl, R. H.; Hubig, S. M.; Riley, R. L.; Iverson, B. L.; Mallouk, T. E. *J. Am. Chem. Soc.* **1994**, *116*, 4786.

(27) Atkins, P. W. *Physical Chemistry*, 5th ed.; W.H. Freeman and Co.: New York, 1994.

(28) Ohno, T.; Yoshimura, A.; Prasad, D. R.; Hoffman, M. Z. *J. Phys. Chem.* **1991**, *95*, 4723.

(29) Sun, H.; Hoffman, M. Z. *J. Photochem. Photobiol. A* **1994**, *84*, 97.

(30) Linsenmann, M. Ph. D. Dissertation, Universtiy of Konstanz, 1997.

(31) Deronzier, A.; Essakalli, M. *J. Phys. Chem.* **1991**, *95*, 1737.

(32) McClenaghan, N. D.; Loiseau, F.; Puntoriero, F.; Serroni, S.; Campagna, S. *Chem Comm.* **2001**, 2634.

(33) Limoges, B. Ph. D. Dissertation, Colorado State University, 2001.

CHAPTER 4

CHARGE SEPARATION IN A SELF-ASSEMBLED FREE CHROMOPHORE TRIAD SYSTEM

Chapter 3 outlined the donor to chromophore association (D/C) responsible for the high quantum efficiency of charge separation in certain DCA systems. This dissertation chapter will describe the use of this association to assemble a free chromophore and a bound donor-acceptor unit into a functional triad-like unit. All synthesis, data collection, manipulation, and manuscript preparation was completed by Matthew Rawls.

4.1 INTRODUCTION

Previous chapters have detailed the study of electron transfer kinetics in supermolecular donor chromophore acceptor triads systems. It can, however, be very difficult to covalently bind complex photochemical components into supermolecules. This limits the application of supramolecular studies to fairly simple systems. Self-assembly is one strategy which researchers often use to overcome this synthetic limitation. Non-covalent "bonds" are used to self-assemble complex systems into functional supermolecules.[1] Hydrogen bonding, hydrophobic interactions, and ion pairing have been used successfully in this capacity.[2]

Research described in Chapter 3 on the triad shown in Figure 3.1 suggests the possible addition of the D/C association (azine donor to chromophoric polypyridyl ring) to this list of self-assembly interactions. Chapter 3 provides evidence that this D/C interaction is sufficient to function as a self-assembly mechanism. A free donor, N-methylphenothiazine, was placed in solution with a covalently bound CA complex. The system showed a higher quantum efficiency for CSS formation than would be allowed by diffusional processes suggesting that the D/C interaction was sufficiently strong to hold the donor in a functional supramolecular moiety prior to photoexcitation.

The next logical step in the progression is to self-assemble a free chromophore along with covalently bound donor-acceptor into a triad-like unit. This chapter deals with the results of various attempts to demonstrate triad-like behavior with what will be referred to as a "free chromophore" system. Figure 4.1 shows the basic system which will be considered, a donor (phenoxazine, phenothiazine, or phenoselenazine) bound through a variable length polymethylene chain to a diquat type acceptor in solution with a ruthenium trisbipyridyl type chromophore complex. Triad-like behavior will be defined

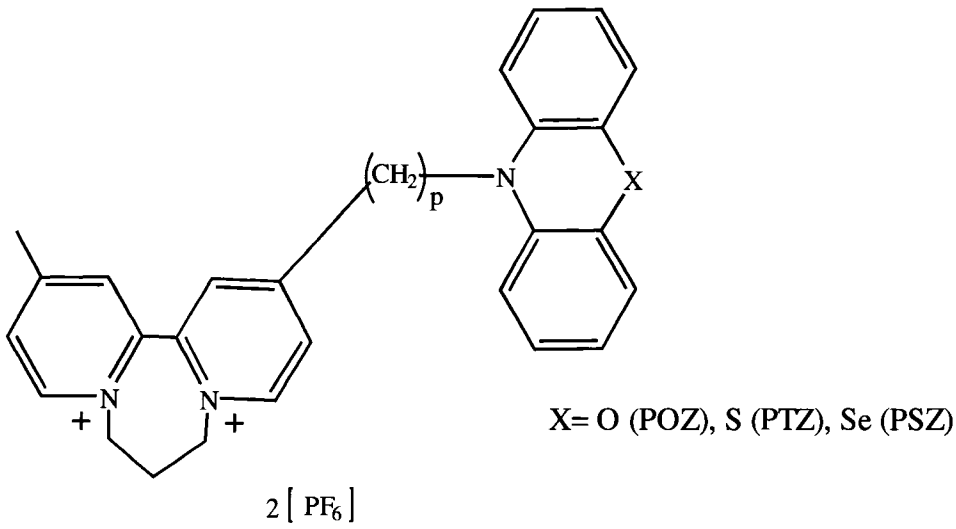

Figure 4.1 (p-DQ-PXZ)$(PF_6)_2$

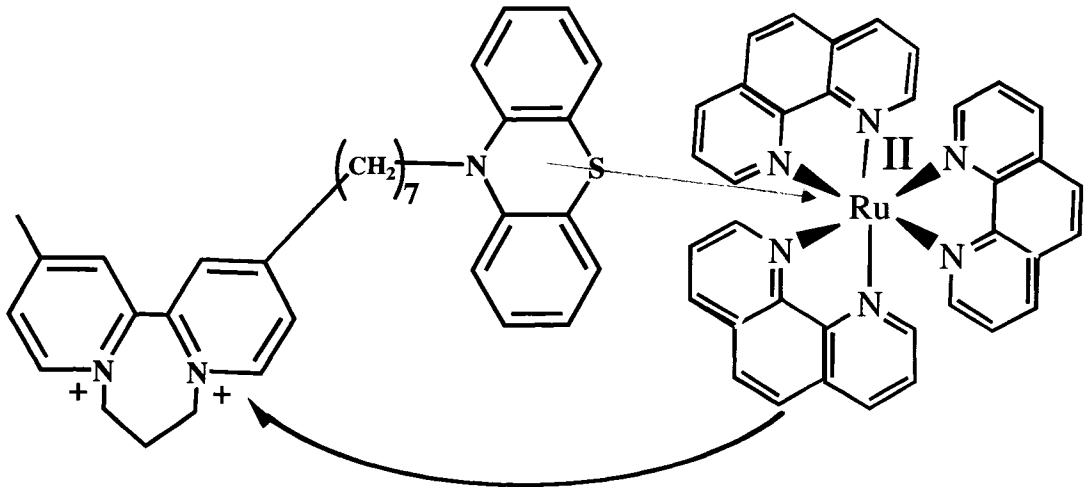

Figure 4.2 Triad-like charge separation in a free chromophore self-assembled triad.

(Figure 4.2) as a D-A species associating with a chromophore and upon photoexcitation of the chromophore, the donor is oxidized and the acceptor is reduced resulting in intramolecular charge separation. Simple diffusional quenching of excited chromophores will also occur and must be considered in the interpretation of data. Study of this system

should reveal further information regarding the nature of the D/C association, as well as ultimately demonstrate the applicability of this particular association interaction for more general application.

Chapter 5 describes the extreme effect that application of a magnetic field can have on the charge separated state recombination kinetics in covalently bound DCA triads. Detailed research is presented which outlines the mechanism explaining this magnetic field effect. In theory, a self-assembled "free-chromophore" system has similar spin characteristics to that of the covalently bound system. It is thus possible that the recombination of CSS in free chromophore systems might show a magnetic field effect. In a fashion analogous to that of Chapter 5, various donor-acceptor species were synthesized varying only in the spin orbit coupling of the donor heteroatom (X = O, S, Se) to facilitate a similar theoretical approach.

4.2 RESULTS

As discussed in previous chapters, the oxidized donor and reduced acceptor both have strong transient absorption peaks, 515 nm and 388 nm respectively.[3,4] It is therefore possible using transient absorption spectroscopy to measure the presence of oxidized donor and/or reduced acceptor. A time resolved transient absorption spectrum is given in Figure 4.3 for the chromophore alone in solution, upon photoexcitation by 450 nm laser light. Each spectral line corresponds to a different CCD camera delay upon photoexcitation of the chromophore.[5-7] Regardless of the relative concentrations of DA units and chromophore, results from previous studies of the association formation constant show there will always be unassociated chromophores which are excited upon pump beam excitation. This means that the spectral features seen in Figure 4.3

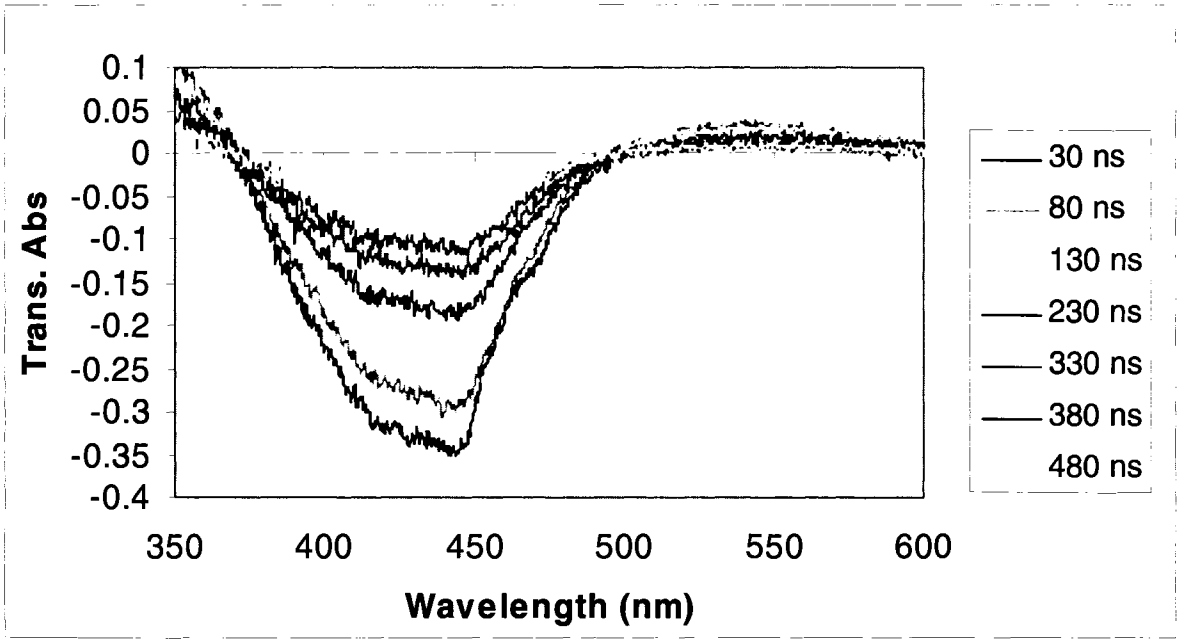

Figure 4.3 Transient absorption spectrum for Ru(1,10-phenanthroline)$_3$(PF_6)$_2$. Each spectral line corresponds to a delay for collection of the spectrum upon photoexcitation.

will overlay all data for these systems. The important regions of the spectrum to observe are those which are used to probe the reduced acceptor and oxidized donor. At 388 nm the chromophore shows a strong bleach which lasts several hundred nanoseconds. At 515 nm, the chromophore only exhibits a slight transient absorption.

Figure 4.4 shows the results of a transient absorption study of a 3 mM solution of the species 7-DQ-PTZ (a diquat acceptor bound through a 7 carbon methylene chain to a PTZ acceptor) in acetonitrile with 10^{-5} M Ru(1-10 phenanthroline)$_3$(PF_6)$_2$ chromophore. The measurement is analogous to that of Figure 4.3. This figure clearly shows several features. The strong unquenched chromophore bleach is evident along with formation of oxidized donor and reduced acceptor. Figure 4.5 shows the kinetic data at the specific probe wavelength of 388 nm (reduced acceptor) upon photoexcitation (t = 0). Figure 4.6 shows the analogous data at 515 nm (oxidized donor).

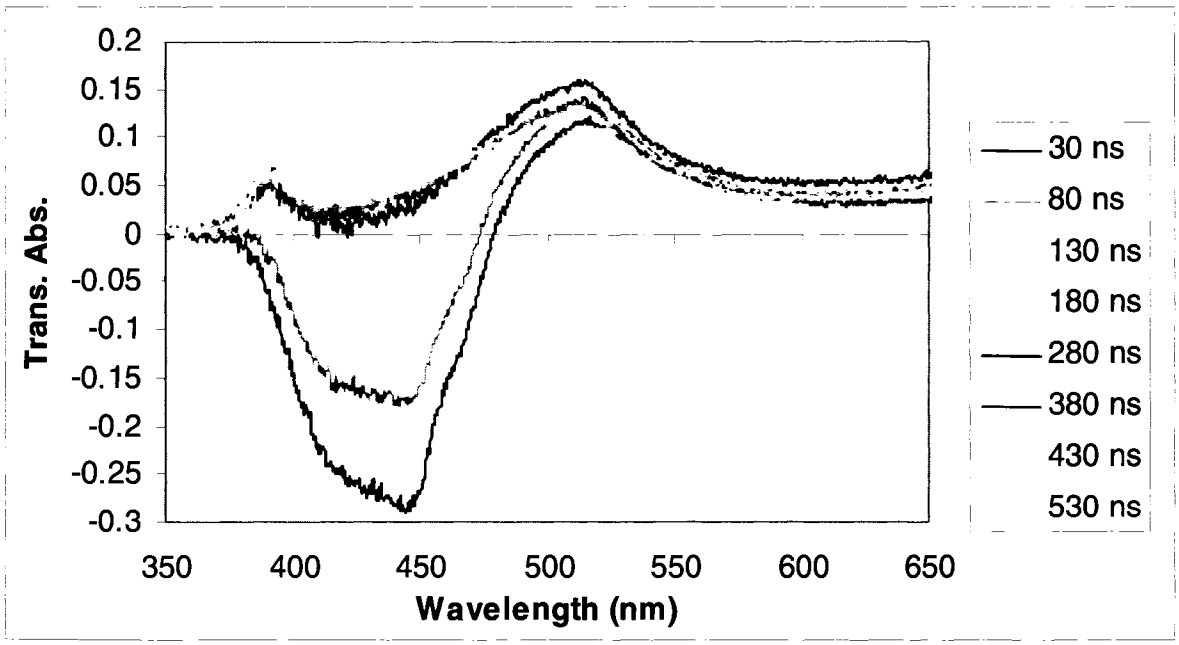

Figure 4.4 Transient absorption spectrum for 7-DQ-PTZ .

These two spectra while demonstrating the presence of both oxidized donor and reduced acceptor, also highlight the complexity of this system. Kinetic data at 388 nm shows recovery from the unquenched chromophore bleach leading to a very long (hundreds of microseconds) reduced acceptor presence. The spectrum at probe wavelength of 515 nm shows a slight "instantaneous" (on the time scale of this nanosecond resolution instrument) signal which is likely due to unquenched chromophore transient absorption. Next, a slower rise in transient absorption occurs due to formation of oxidized donor: the transient absorption peaks at approximately 200 ns and finally undergoes a long multicomponent decay. This spectrum shows the presence of oxidized donor over many microseconds. A substantial amount of literature reports on the kinetic behavior of charge separated across flexibly linked biradicals.[8,9] This literature generally predicts that intramolecular charge separation on a flexibly linked biradical moiety, regardless of the

nature of the linker or any spin restrictions, recombines more quickly than the long time component seen in Figures 4.5 and 4.6. Thus, the long component at 515 nm can be ascribed to diffusional reductive quenching of the excited state chromophore by the donor portion of the DA. The long component at 388 nm corresponds to diffusional interaction and reduction of the acceptor portion of a DA by a chromophore which has been quenched already by a donor (on a different DA molecule). The result of these diffusional processes is not intramolecular charge separation and is not of interest here. The interesting aspect of these results is triad-like, intramolecular charge separation. Thus, for the remainder of this chapter, the focus will be on the observation of triad-like charge separation. Various studies will be presented which utilize manipulation of experimental parameters to emphasize intramolecular charge separation over diffusional quenching.

4.3 DONOR ACCEPTOR INTERACTIONS

A complication in the synthesis of the DA species must be mentioned which may provide a clue to the kinetic results seen thus far. Over 20 donor-acceptor species were synthesized with variation in azine donor (POZ, PTZ, and PSZ), linker chain length, and counterion. Also, several synthetic routes were utilized to obtain many of these species. Extremely thorough purification efforts were made including adsorbent chromatography, recrystallization, size exclusion chromatography, thin layer chromatography, ion chromatography and numerous other techniques. Nonetheless, no donor-acceptor species was ever created without some colored "impurity" which varied from yellow to purple. Careful characterization was done as well to identify the impurity. NMR was initially utilized with further verification from electrospray mass spectroscopy and

electrochemical measurements. Figure 4.7 shows an electrospray mass spectrum for the 7-DQ-PTZ DA unit. The peaks at mass-to-charge ratios of 652.0 and 253.5 correspond to the expected m/z ratios for this compound (M – (PF_6) and M – 2(PF_6)). Electrospray can only provide verification of the presence of the desired species: it cannot show previously unidentified impurities. Cyclic voltammetry, shown in Figure 4.8, was used to identify any electrochemically active impurities. A scan rate of 100 mV/s was used along with standard electrochemical procedures (as discussed in Chapter 2). Three reversible electrochemical waves can be seen in the resulting voltammogram. These can be assigned to the expected electrochemical processes for the compound based on literature values for the free and isolated components.[10] Comparable results were obtained for the other DA compounds and no extra peaks were ever observed. While it is possible that this color could be eliminated with appropriate synthetic technique, it is probable that the color does not come from an impurity. Upon consideration of these species (an electron donor attached to an electron acceptor), it is possible that the color arises from an intramolecular charge transfer interaction between the donor and the acceptor. Several features of these DA molecules suggest this interaction might exist. For instance, DA compounds varying only in the donor species (POZ, PTZ, PSZ) were synthesized in identical fashion. The only difference in these species is a variation in redox potentials between the donors. As might be expected, these species vary significantly in color.

Data from Chapter 3 of this dissertation complicates this conclusion. In Chapter 3, discussion of a bimolecular system consisting of a free donor and a covalently bound chromophore-acceptor unit showed using 2D ROESY NMR clear interaction of the donor with the chromophore but not with the acceptor. Unfortunately, analogous NMR experiments in the free chromophore system have yet to be done.

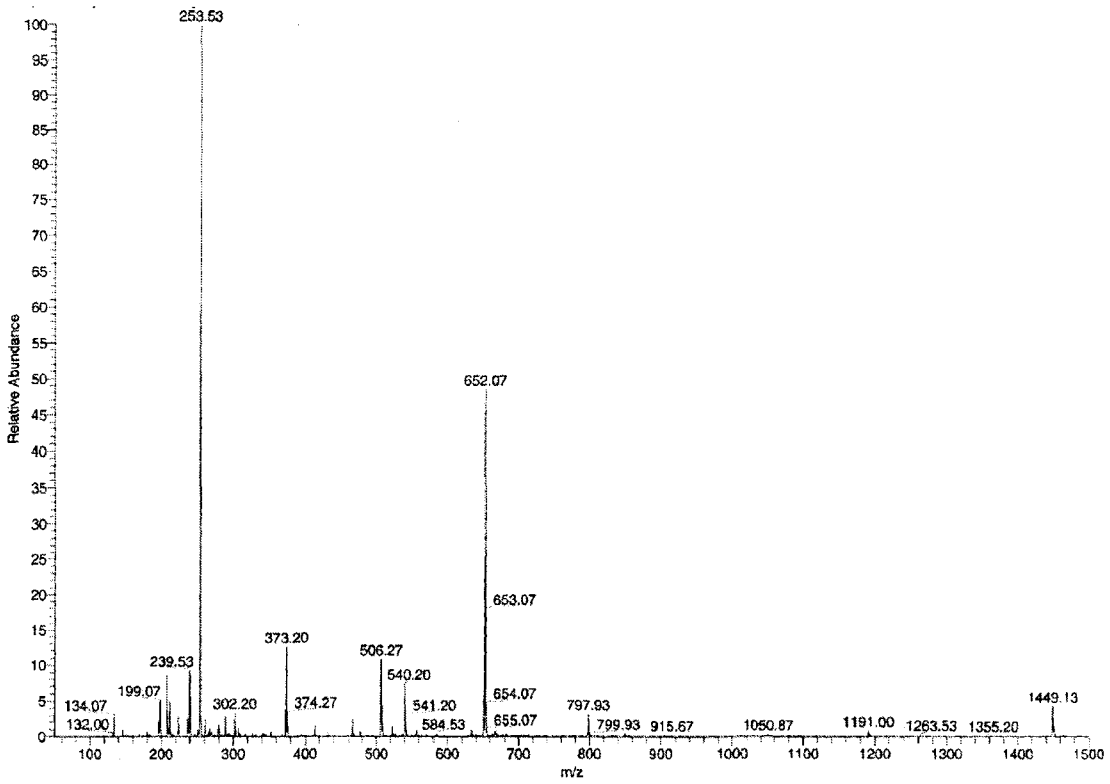

Figure 4.7 Electrospray ionization mass spectrum of (7-DQ-PTZ)$(PF_6)_2$.

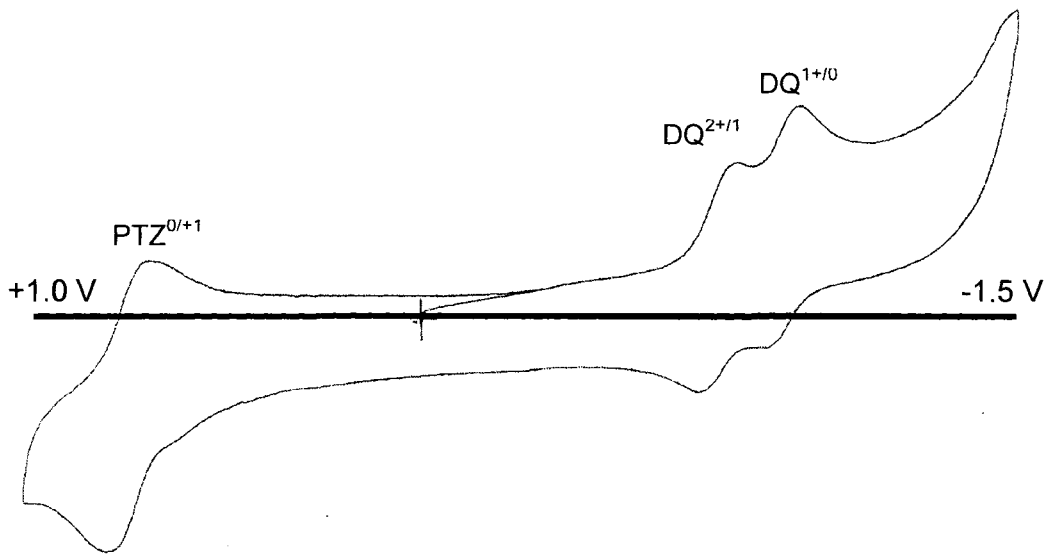

Figure 4.8 Cyclic voltammogram of (7-DQ-PTZ)$(PF_6)_2$ in 0.1 M $TBAPF_6$ solution of CH_3CN with WE=glassy carbon, RE=SSCE, CE=Pt coil and scan rate of 100 mV/s.

If it is assumed that some charge transfer interaction occurs between the donor and the acceptor in DA species, it is possible to speculate as to the effect on the charge separation kinetics. A charge transfer interaction could mean that the donor and acceptor are not extended in solution but instead may bend the linker chain and lie close together. Also, clearly the donor and acceptor would be closely coupled electronically. In this situation, the kinetics of charge separation would likely vary from that of the covalently bound triad situation. For instance, if the donor, acceptor, and chromophore were all in very close proximity and closely coupled, the charge separation and recombination might occur too quickly to be measured by a nanosecond laser instrument. The DA units preassociated (associated upon photoexcitation) with chromophores would undergo charge separation and recombination prior to observation using the nanosecond laser system. Further, even if a charge transfer interaction is not the cause of the color, interaction of the donor and the acceptor separated only by the flexible linker chain could allow this fast kinetic situation to exist.

Obviously, a measurement with higher time resolution might provide this information; however, an experiment was done to attempt to simply avoid any donor to acceptor interaction (charge transfer and otherwise). Hiroaki Yonemura et al reported a study on a very similar system to those currently under consideration.[11] The system, shown in Figure 4.9, consisted of a bound viologen type acceptor (see Chapter 3 for details) linked through a polymethylene chain to a PTZ donor. Direct excitation of the PTZ moiety was used to transfer an electron to the acceptor. In these systems, charge separation was only seen when certain cyclodextrin species were present in the solution. The function of the cyclodextrin, a cylindrical sugar (see Figure 4.10) was to encase the DA unit and act as a spacer to obstruct donor to acceptor interaction.

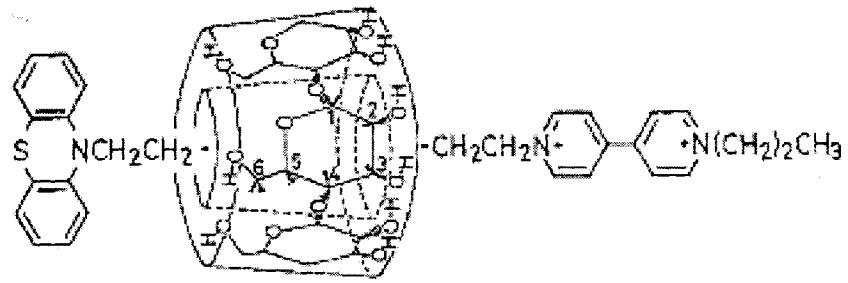

Figure 4.9 Cyclodextrin encapsulated PTZ bound to viologen acceptor.[11]

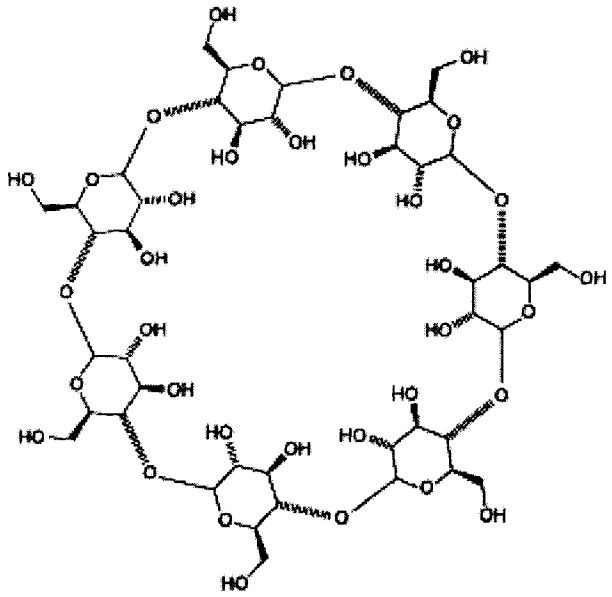

Figure 4.10 β-cyclodextrin.[12]

Figure 4.10 shows a simple β-cyclodextrin.[12] Heptakis (2,3,6-tri-O-methyl) beta cyclodextrin results from substitution of a methyl group at the 2, 3, and 6 hydroxy positions (conversion of all hydroxy groups into methoxy groups). This cyclodextrin was selected for application in free chromophore studies due to its high solubility in organic solvents. Extensive NMR studies are typically required to conclusively show that a

species has threaded into a cyclodextrin pore. While these studies were not undertaken, literature reports of very similar systems suggest that threading is likely.[13]

Experiments were done to study any effect the presence of this cyclodextrin had on charge separation in the 7-DQ-PTZ with chromophore system. When the cyclodextrin was added to a solution of DA (a large variety of solvents and solvent mixtures were studied) no effect was seen in the UVVis. This suggests that if the color is due to a CT interaction, the cyclodextrin does not break the interaction. The possibility remains that the cyclodextrin still could function to separate the donor and acceptor physically to allow triad-like charge separation. The data in Figure 4.10 is a plot of the transient absorption signal of the same system as that of Figure 4.2 with and without cyclodextrin. As is immediately apparent, there is no effect measurable on this time scale due to the addition of cyclodextrin.

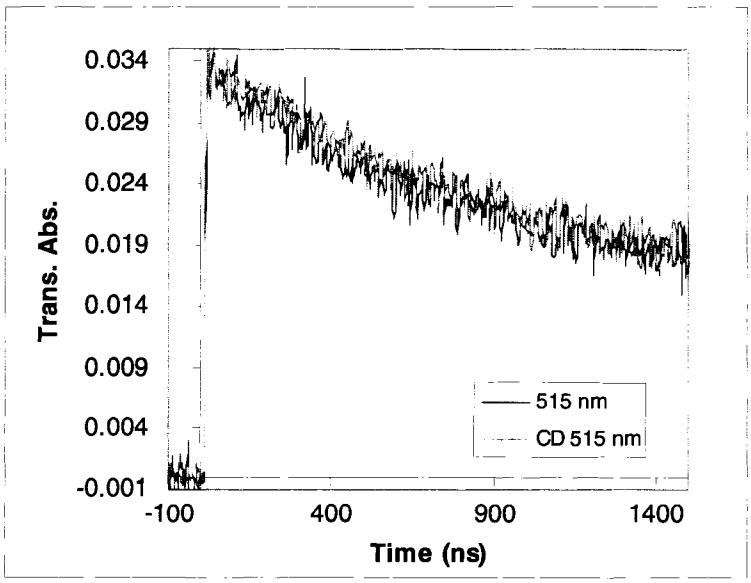

Figure 4.10 7-DQ-PTZ with Ru(1,10-phenanthroline)$_3$(PF_6)$_2$. A probe wavelength of 515 nm was used with a 450 nm pump beam. The trace labeled CD shows the effect of the addition of β-cyclodextrin to the sample.

4.4 MIXED SOLVENT SYSTEM

The free donor experiment discussed in Chapter 3 which proved the D/C preassociation interaction in triads, also showed that this interaction is substantially weaker in acetonitrile solvent than in methylene chloride. However, the DA compounds as hexafluorophosphate salts are virtually insoluble in methylene chloride but soluble in 10% acetonitrile in methylene chloride. As seen in Figure 3.4 at this concentration of acetonitrile, the charge separation efficiency of the free donor system is the same as in pure methylene chloride. A large number of samples of various DA species were tested utilizing this 10% acetonitrile solution. For a given DA species, very little variation was seen when mixed solvents were used.

4.5 COULOMBIC INTERACTIONS

Coulombic interactions could play a large role in self assembled-free chromophore systems. The chromophore carries a 2+ charge while the acceptor "diquat" end of the DA unit also carries a 2+ charge. Thus, coulombic interactions inevitably cause repulsion countering the D/C association interaction. In an effort to minimize this repulsion, the complex shown in Figure 4.11 was synthesized. This complex with a 2- charge on the disulfonic acid bipyridine ligand is Zwitterionic. The complex however behaves electrochemically and optically very similarly to the Ru(1,10-phenanthroline)$_3$(PF_6)$_2$ chromophore studied in previous examples. While emission quenching studies showed this complex more rapidly quenched by the DA than the cationic chromophores, the transient absorption spectra looked very similar to the Ru(phenanthroline)$_3$(PF_6)$_2$ situation. Ultimately, the results with this chromophore did not provide additional evidence of triad like charge separation.

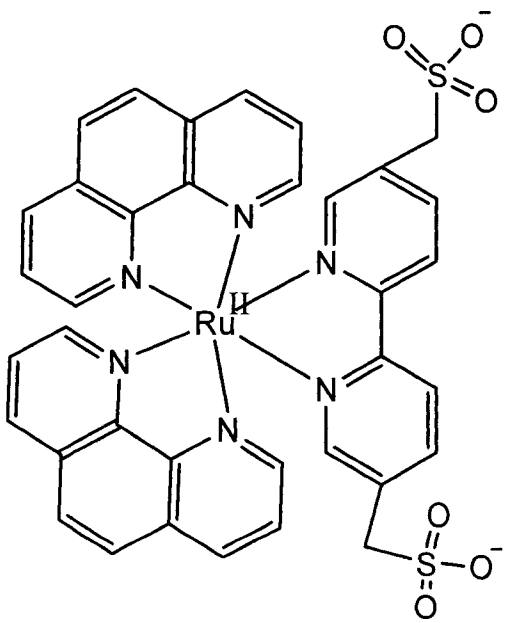

Figure 4.11 Zwitterionic chromophore.

4.6 MAGNETIC FIELD EFFECTS

As was stated previously, in self-assembled free chromophore triads, intramolecular charge separation should yield a spin situation analogous to that in a covalently bound triad: triplet spin correlation of the radicals (refer to Scheme 5.1 for details). Diffusional quenching would yield uncorrelated spins and therefore little magnetic field effect (MFE). Thus, the presence of a strong MFE could provide evidence of intramolecular charge separation.

A number of magnetic field controlled experiments were done on a variety of DA with chromophore samples. Figures 4.12 and 4.13 show the results of a MFE study of the 7-DQ-PTZ DA with Ru(1,10-phenanthroline)$_3$(PF_6)$_2$. The results show little if any magnetic field effect (small variations can be seen but were not sufficient to permit studies analogous to that of Chapter 5). Experiments were done with other DA species

POZ and PSZ substituted donors and similar results were always seen. The lack of MFE suggests that little of the signal seen is due to triad-like charge separation.

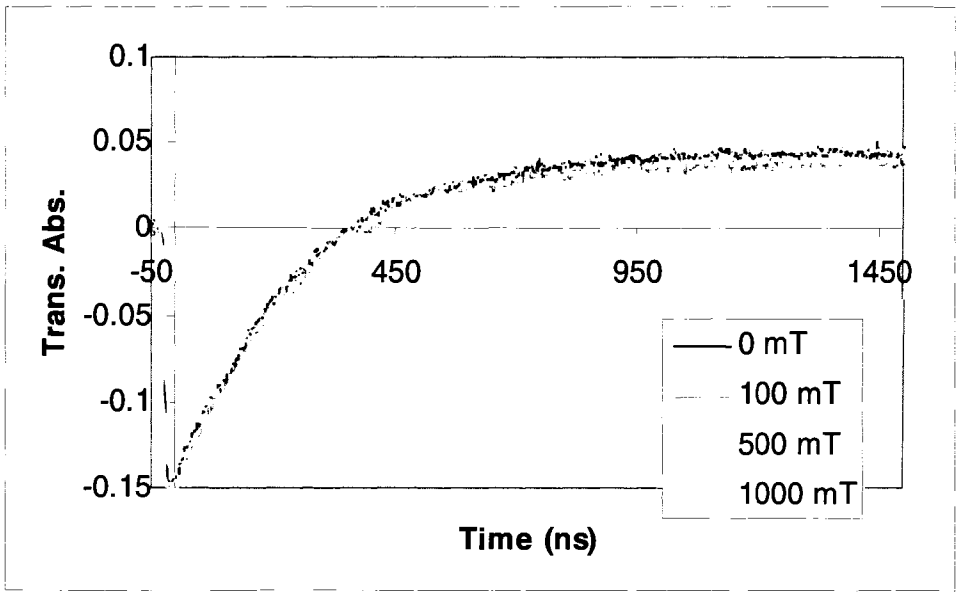

Figure 4.12 7-DQ-PTZ with Ru(1,10-phenanthroline)$_3$(PF_6)$_2$ magnetic field effect study with 388 nm probe and 450 nm pump.

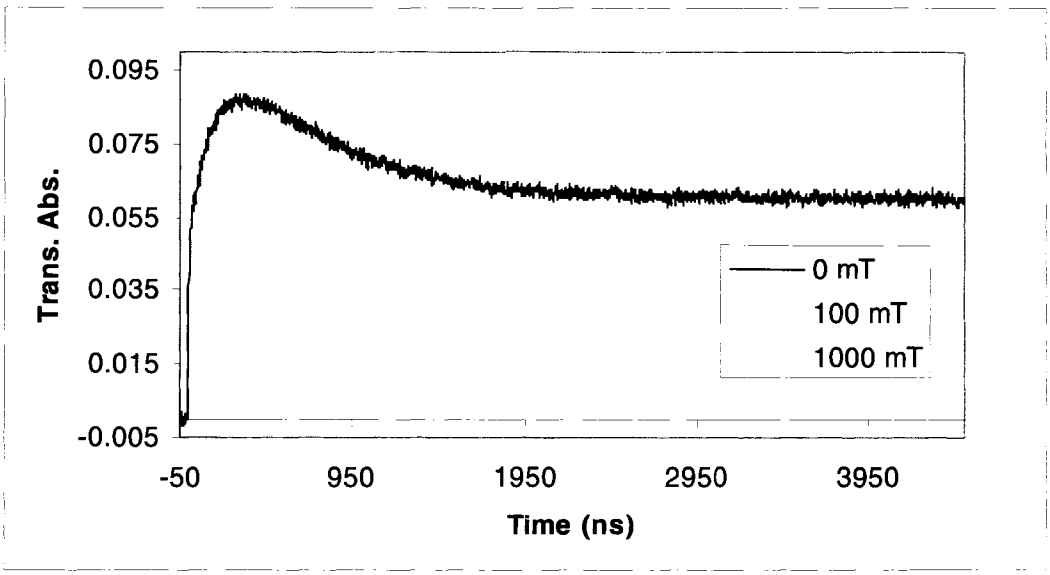

Figure 4.13 7-DQ-PTZ with Ru(1,10-phenanthroline)$_3$(PF_6)$_2$ magnetic field effect study with 515 nm probe and 450 nm pump.

4.7 CONCLUSIONS AND FUTURE WORK

This chapter detailed extensive efforts to demonstrate charge separation in a self-assemble free chromophore system. Ultimately, many more experiments were undertaken in addition to those reported. In all cases the kinetic results were very similar to those described here. There is simply no clear and conclusive evidence of triad-like charge separation in any system studied. To this point, all experiments focused on emphasizing triad-like kinetics of diffusional quenching have proven unsuccessful. The obvious step must be moving to a higher resolution, picosecond, transient absorption measurement. If triad-like behavior does occur on a significant level, it must occur too rapidly to measure in the nanosecond time scale.

REFERENCES

(1) Lehn, J. M. *Supramolecular Chemistry*; VCH: Weinheim, 1995.

(2) Ward, M. D. *Chem. Soc. Rev.* **1997**, *26*, 365.

(3) Klumpp, T.; Linsenmann, M.; Larson, S. L.; Limoges, B. R.; Buerssner, D.; Krissinel, E. B.; Elliott, C. M.; Steiner, U. E. *J. Am. Chem. Soc.* **1999**, *121*, 1076.

(4) Danielson, E.; Elliott, C. M.; Merkert, J. W.; Meyer, T. J. *J. Am. Chem. Soc.* **1987**, *109*, 2519.

(5) Linsenmann, M. Doctoral Thesis, University of Konstanz, 1997.

(6) Fodor, L.; Ulveczki, A.; Horvath, A.; Steiner, U. E. *Inorg. Chem. Acta* **2002**, *338*, 133.

(7) Woll, D., University of Konstanz, 2006.

(8) Zimmt, M. B.; Doubleday, C.; Turro, N. J. *J. Am. Chem. Soc.* **1986**, *108*, 3618.

(9) Doubleday, C.; Turro, N. J.; Wang, J. *Acc. Chem. Res.* **1989**, *22*, 199.

(10) Elliott, C. M.; Freitag, R. A.; Blaney, D. D. *J. Am. Chem. Soc.* **1985**, *107*, 4647.

(11) Yonemura, H.; Nakamura, H.; Matsuo, T. *Chem. Phys.* **1992**, *162*, 69.

(12) Hapiot, F.; Tilloy, S.; Monflier, E. *Chem. Rev.* **2006**, *106*, 767.

(13) Otagiri, M.; Uekama, K.; Ikeeda, K. *Chem. Pharm. Bull.* **1975**, *23*, 188.

CHAPTER 5

SPIN CHEMICAL CONTROL OF PHOTOINDUCED ELECTRON-TRANSFER PROCESSES IN RUTHENIUM(II)-TRISBIPYRIDINE-BASED SUPRAMOLECULAR TRIADS: 2. THE EFFECT OF OXYGEN, SULFUR, AND SELENIUM AS HETEROATOM IN THE AZINE DONOR

Matthew T. Rawls, Georg Kollmannsberger, C. Michael Elliott, Ulrich E. Steiner

Submitted for publication in *The Journal of Physical Chemistry A* January 10, 2007. Printed here with permission from the authors.

This dissertation chapter describes an interesting magnetic field effect which occurs upon photoexcitation of DCA triads. Upon application of a field, the recombination lifetimes increase many fold. Matthew Rawls was the primary researcher, synthesizing all species studied and collecting all the data. Ulrich Steiner of the University of Konstanz provided assistance with the theoretical interpretation and manuscript preparation. The manuscript was written by Matthew Rawls, Mike Elliott, and Ulrich Steiner.

ABSTRACT

Nanosecond time-resolved absorption studies in a magnetic field ranging from zero to 2.0 T have been performed on a series of covalently linked donor-Ru(bipyridine)$_3$-acceptor complexes (D-C^{2+}-A^{2+}). In these complexes, the electron acceptor (A) is an *N,N'*-diquaternary-2,2'-bipyridinium moiety, linked to a bipyridine by a (-CH_2-)$_2$ chain and the electron donor (D) is a phenazine moiety PXZ linked to a bipyridine by a (-CH_2-)$_4$ chain. In the PXZ moiety the heteroatom (X = O (oxygen), T (sulfur) and S (selenium)) is systematically varied to study spin-orbit coupling effects. On the nanosecond time scale, the first detectable photoinduced electron-transfer product after exciting the chromophore C^{2+} is the charge-separated (CS) state, D^+-C^{2+}-A^+, where an electron of the PXZ moiety, D, has been transferred to the diquat moiety, A^{2+}. In zero field, the lifetime of the CS state is about 150 ns for all three compounds. As the field is increased, the decay becomes biexponential. For DCA-POZ and –PTZ, the slow decay component τ_{slow} increases strongly with increasing field, reaching a saturation value of around 2000 ns above 600 mT. For DCA-PSZ, the increase of τ_{slow} is much weaker. It reaches a maximum of about 330 ns at 350 mT and then gently decreases again, down to 250 ns at 2000 mT. The kinetics can be quantitatively modelled by the radical pair relaxation mechanism, assuming creation of the CS state with pure triplet spin correlation (^{3}CS), fast, field-independent equilibration between the T_0 and S spin sublevels, and field-dependent relaxation with a relaxation rate constant k_r between $T_\pm$ and T_0,S. Recombination to the singlet ground state is allowed only from the ^{1}CS spin level, spin-forbidden recombination from ^{3}CS seems negligible even for DCA-PSZ. The field dependence of k_r has been decomposed into the contributions of various relaxation

mechanisms. For all compounds, the electron spin dipolar coupling relaxation mechanism dominates the field dependence of τ_{slow} at fields up to about 100 mT. Spin relaxation due to the g-tensor anisotropy relaxation mechanism accounts for the field dependence of τ_{slow} for DCA-PSZ at high fields. For the underlying stochastic process, a very short correlation time of 2 ps has to be assumed, which is tentatively assigned to a flapping motion of the central, nonplanar ring in PSZ. Magnetic field independent contributions to k_r are about 4.5×10^5 s^{-1} for DCA-POZ and –PTZ and 3.5×10^6 s^{-1} for DCA-PSZ. While the former is probably due to a vibrational mechanism, the latter can be quantitatively accounted for by the spin-rotational mechanism. Relative to the contributions of the other relaxation mechanisms, those of the anisotropic hyperfine interaction relaxation mechanism are of minor importance. It has been confirmed by paramagnetic quenching experiments of the magnetic field effects with TEMPO that all magnetic field dependences observed with the present DCA-PSZ systems are indeed due to the magnetic field dependence of spin relaxation. It has been shown that the quenching is due to Heisenberg spin exchange between TEMPO and the CS state of DCA-PSZ. A rate constant of 2×10^9 $M^{-1}s^{-1}$ has been determined for this process.

5.1 INTRODUCTION

Donor-chromophore-acceptor (DCA) triad systems (vide infra) are a class of supramolecular assemblies that have played an important role in deepening the understanding of photoinitiated electron transfer processes. These systems are utilized as analogues of natural photosynthesis where nature converts solar energy to chemical energy. Such systems have been studied for many years yielding much information relevant to natural photosynthesis as well as providing insights into possible applications of synthetic photosynthesis mimics in photochemical cells.[1-7] Our group studies complexes exemplified by the triad in Figure 5.1.[8-11] These supramolecular assemblies consist of a central trisbipyridine ruthenium chromophore covalently linked through variable length polymethylene chains to a "diquat" electron acceptor and a pair of azine-type electron donors.[12] These triads have proven to be a very fruitful platform for study of photoinduced electron transfer processes and charge separation. Specific details about the various triads can be found in the literature, but a brief description of the processes of interest is necessary here before considering the present study. In these triads, a photon of around 450 nm will directly excite a metal-to-ligand charge transfer transition (MLCT) in the chromophore. The initial singlet MLCT state (^{1}MLCT) undergoes rapid intersystem crossing (< 1 ps) to the triplet MLCT state (^{3}MLCT). Within a few nanoseconds, a series of electron transfers occur initiating from the ^{3}MLCT and yielding a charge separated state (CS) wherein the acceptor is reduced, the chromophore is in its original ground state and one donor is oxidized. Interestingly, in the case where donors are phenothiazine (i.e., X = S; PTZ), the radical cation pair which constitutes the CS is formed with almost pure triplet spin correlation.[8] Depending on the structural details of

the particular triad complex, this ^{3}CS recombines to the ground state with a lifetime in the range of 100-300 ns.[8]

Spin chemical studies of these triads have proven to be a valuable tool for developing a more sophisticated understanding of the complexities of the CS formation and recombination to the ground state.[8] Since direct recombination of the ^{3}CS to the singlet ground state is formally a spin forbidden process, magnetic field effect (MFE) studies of CS formation and recombination have proven of critical importance to the understanding of this spin the model we have successfully employed to explain the spin chemical behavior of the triad CS is the *relaxation mechanism* of Hayashi and Nagakura.[13]

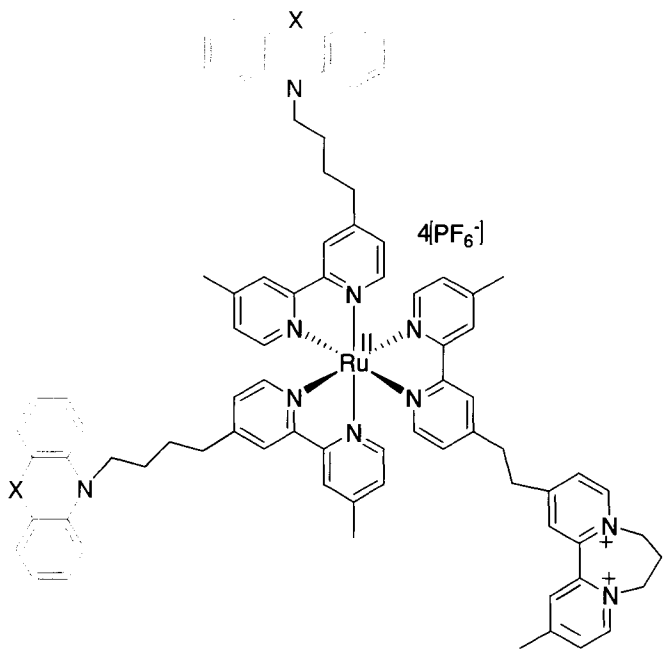

Figure 5.1 Donor-Chromophore-Acceptor (DCA) triad (X = O, S, or Se).

Scheme 5.1 shows the processes operative in ^{3}CS recombination. As ^{3}CS and ^{1}CS states are essentially degenerate at zero applied magnetic field (vide infra), isotropic hyperfine interaction provides a mechanism for coupling and thus mixing ^{3}CS and ^{1}CS states. In

the absence of any applied field ^{3}CS/^{1}CS spin equilibration is rapid relative to recombination via the spin-allowed path k_s (which is the only kinetically important route to recombination in zero applied field) resulting in a nearly monoexponential decay of ^{3}CS back to ground state.[8] Upon application of a magnetic field, the triplet state experiences Zeeman splitting, as shown in Scheme 5.1, wherein the T_0 state energy is unchanged and the energies of T_+ and T_- states move as indicated. At relatively small fields, the difference in energies of T_- and T_+ states and those of ^{1}CS and T_0 states becomes significant relative to the hyperfine coupling energy thus resulting in a slowing of the rate of their conversion to the ^{1}CS state. Stated another way, the coherent isotropic hyperfine coupling is suppressed resulting in inefficient mixing of the S and T_+ and T_- states. Thus, strongly biexponential kinetics develop characterized by a "fast" field-independent component due to T_0 recombination and a "slow" field-dependent component corresponding to recombination of the T_- and T_+ states. As the applied field is increased from zero to 3 T, kinetics of the "slow" component of the CS decay, and thus the mechanism responsible for it, undergoes a transition. At low fields, isotropic hyperfine coupling is still operative in mixing states and allowing recombination, albeit progressively less efficiently as the field is increased. At medium fields, a number of other processes start to become potentially important. These are incoherent processes such as anisotropic hyperfine interaction (*ahfi*), g-tensor anisotropy (*gta*), spin rotational coupling (*src*), and electron spin-spin dipolar interaction (*esdi*). Also, direct spin-orbit coupling (*soc*) assisted spin-forbidden recombination k_T to the singlet ground state could contribute.[8]

Our previous MFE study yielded much kinetic detail about formation and recombination of ^{3}CS in one class of triad molecules; however, there remain a number of unanswered questions. We were unable to establish which incoherent process or processes dominated recombination at intermediate-to-high magnetic fields. We established that at moderate fields it was likely the *esdi* or *ahfi* mechanisms were dominant, but we were unable to distinguish between the two. Also, we assumed direct spin forbidden recombination was contributing. This assumption, while reasonable, was not unambiguously verified. Further inquiry is necessary to clearly distinguish among the operative recombination processes across the medium to high field region.

Scheme 5.1

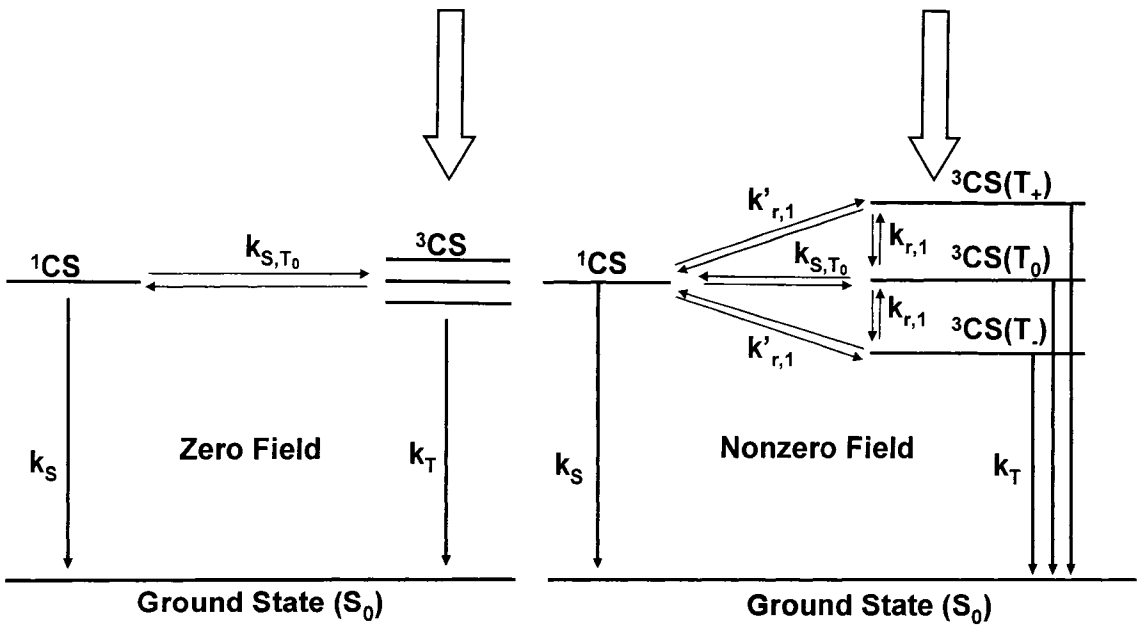

To this end, we have synthesized an expanded series of triad complexes in an attempt to answer some of the questions remaining from our earlier studies. We chose one triad from the previous study, namely the triad DCA-PTZ shown in Figure 5.1 where X = S,

and modified it by changing the chalcogen heteroatom in the donor. A series of three triads results in which only the donor heteroatom differs, where X = oxygen (DCA-POZ), sulfur (DCA-PTZ), or selenium (DCA-PSZ). These complexes are useful for spin study as they provide a variation of one order of magnitude of donor heteroatom *soc* while remaining very similar in redox properties and essentially isostructural. Variation of *soc* of this magnitude is expected to dramatically affect processes dominant in recombination at higher fields, specifically direct spin forbidden recombination, *gta*, and *src*.[14]

Finally, several unexpected findings arose in the course of this study that provide a powerful route for strengthening the model. An extreme sensitivity of the MFE of these complexes to paramagnetic spin catalysts (such as molecular oxygen and TEMPO) was observed. Studies have shown that the effect of spin catalysts on the MFE of diradical pairs can provide a means to distinguish the dominant recombination process.[15] Also, the high field behavior of recombination of the DCA-PSZ complex requires a broadening of the model, as none of the previously discussed mechanisms can explain the magnetic field dependence at fields above 100 mT.

5.2 RESULTS

Prior to photoexcitation, only the chromophore moiety of DCA triads exhibits any significant visible absorbance above ca. 375 nm. In contrast, each oxidized donor and the reduced acceptor have various strong absorption bands across the visible spectral region. Figure 5.2 shows spectra of oxidized donors Me-POZ$^{+\bullet}$, Me-PTZ$^{+\bullet}$, and Me-PSZ$^{+\bullet}$, obtained using an optically transparent thin layer electrode spectroelectrochemical cell. Each donor exhibits a strong increase in absorbance around 520 nm upon oxidation.

Upon reduction, the acceptor moiety also develops a number of absorption bands, the strongest appearing at 388 nm.[8,16] In our earlier study with DCA-PTZ, we showed that the transient absorption spectrum of the CS could be faithfully reproduced by summing equally weighted individual spectra of $Me\text{-}PTZ^{+\bullet}$ and $DQ^{+\bullet}$.[8,16] Therefore, transient absorption measurements at either 388 or 520 nm should show identical CS decay rates as is indeed observed. Decay profiles for the CS of DCA-POZ and DCA-PSZ are shown in Figures 5.3a and 5.4a respectively. As expected from previous nanosecond and picosecond

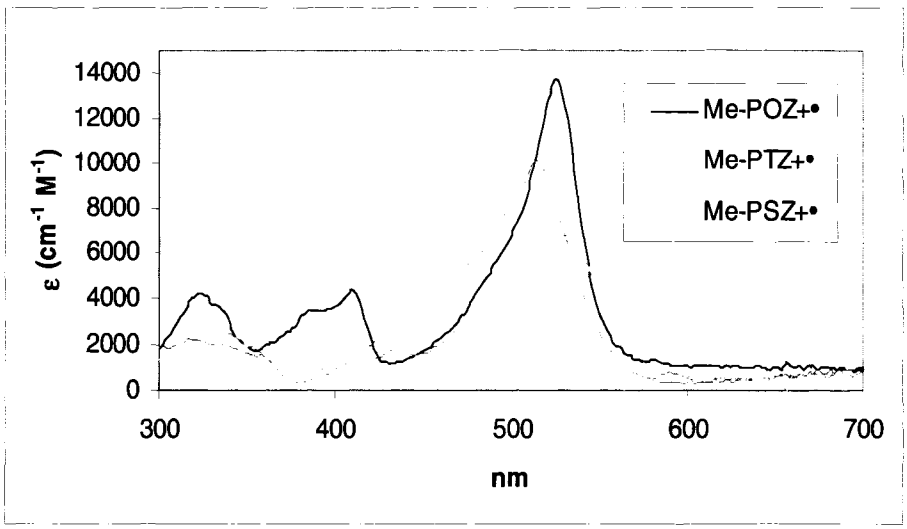

Figure 5.2 Extinction coefficient spectra for the radical cation of each donor. At the maximum absorbance near 520 nm the respective values of ε obtained are: 14,360 ± 1,800 (Me-POZ); 10,008 ± 315 (Me-PTZ); 7531 ± 582 (Me-PSZ).

studies, all decays show "instantaneous" formation of the CS upon laser excitation (i.e., well within the 6 ns FWHM laser pulse).[8] The zero field decay for each of the complexes deviates slightly from monoexponential behavior due to the presence of several geometric isomers of each triad.[17] With increasing magnetic field, all three complexes undergo qualitatively similar changes in CS decay. Between 0 and ca. 500 mT, decays

become distinctly biexponential. In this field regime, the rate of the major component progressively decreases with increased field and the rate of the minor component remains unchanged. DCA-POZ and DCA-PTZ triads show almost identical MFEs with increasing field up to a saturation limit of about 500 mT (Figure 5.5). The DCA-PSZ, on the other hand, shows qualitatively similar behavior except that the rate constant of the slow component is an order of magnitude larger (Figure 5.6). Also, the time constant of the slow component reaches a minimum at ca. 500 mT and shows a definite decrease with increasing field up to at least 3000 mT. In our earlier study of DCA-PTZ and other PTZ containing triads, we were able to show that the amount of CS initially formed upon photo-excitation has a subtle field dependence above 500 mT (i.e., <10% decrease between 500 and 3000 mT).[8] We presume that similar changes may exist with DCA-POZ and DCA-PSZ; however, because of issues in the present studies with long-term power stability of the dye laser, we were unable to experimentally verify this assumption.

Finally, in the course of these studies, we observed that the MFEs for all of these compounds are extremely sensitive to trace O_2 — so much so, that we were unable to obtain quantitatively reproducible CS decay rates when we attempted to remove dissolved O_2 by multiple freeze-pump-thaw cycles on a Schlenk line. Only when sample cells were loaded in a N_2 inert atmosphere box having an O_2 concentration of <1 ppm, were we able to obtain consistently reproducible rates.[18] The observation of this extreme O_2 sensitivity led us to study the effects of a spin catalyst, specifically TEMPO, on the MFE for the DCA-PSZ triad. Figure 5.7 shows plots of τ_{slow} as a function of field at a series of TEMPO concentrations. As this data shows, at about 3 mM TEMPO the MFE on this triad is essentially obliterated.

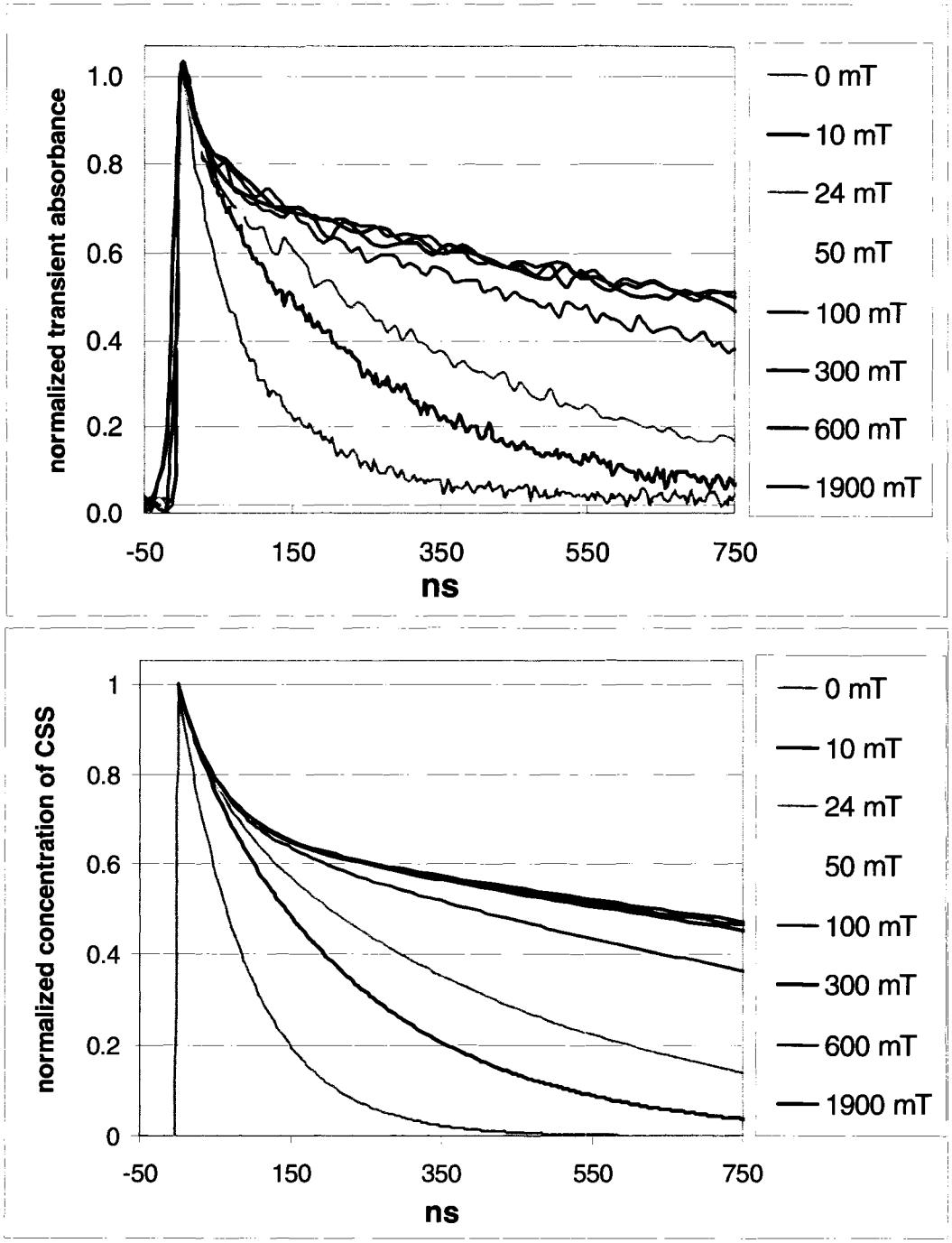

Figure 5.3 Transient decays for CS of DCA-POZ. Upper panel experimental curves. Lower panel simulation using the relaxation scheme with parameters: $k_S = 3.5 \times 10^7\ s^{-1}$, $k_T = 0$, $k_{r,10} = 6.4 \times 10^6\ s^{-1}$, $k_{r,25} = 2.8 \times 10^6\ s^{-1}$, $k_{r,50} = 1.5 \times 10^6\ s^{-1}$, $k_{r,100} = 9.3 \times 10^5\ s^{-1}$, $k_{r,300} = 5.7 \times 10^5\ s^{-1}$, $k_{r,600} = 5.4 \times 10^5\ s^{-1}$, $k_{r,1900} = 5.1 \times 10^5\ s^{-1}$. (For zero field a monoexponential with $k = 1.1 \times 10^7\ s^{-1}$ is shown).

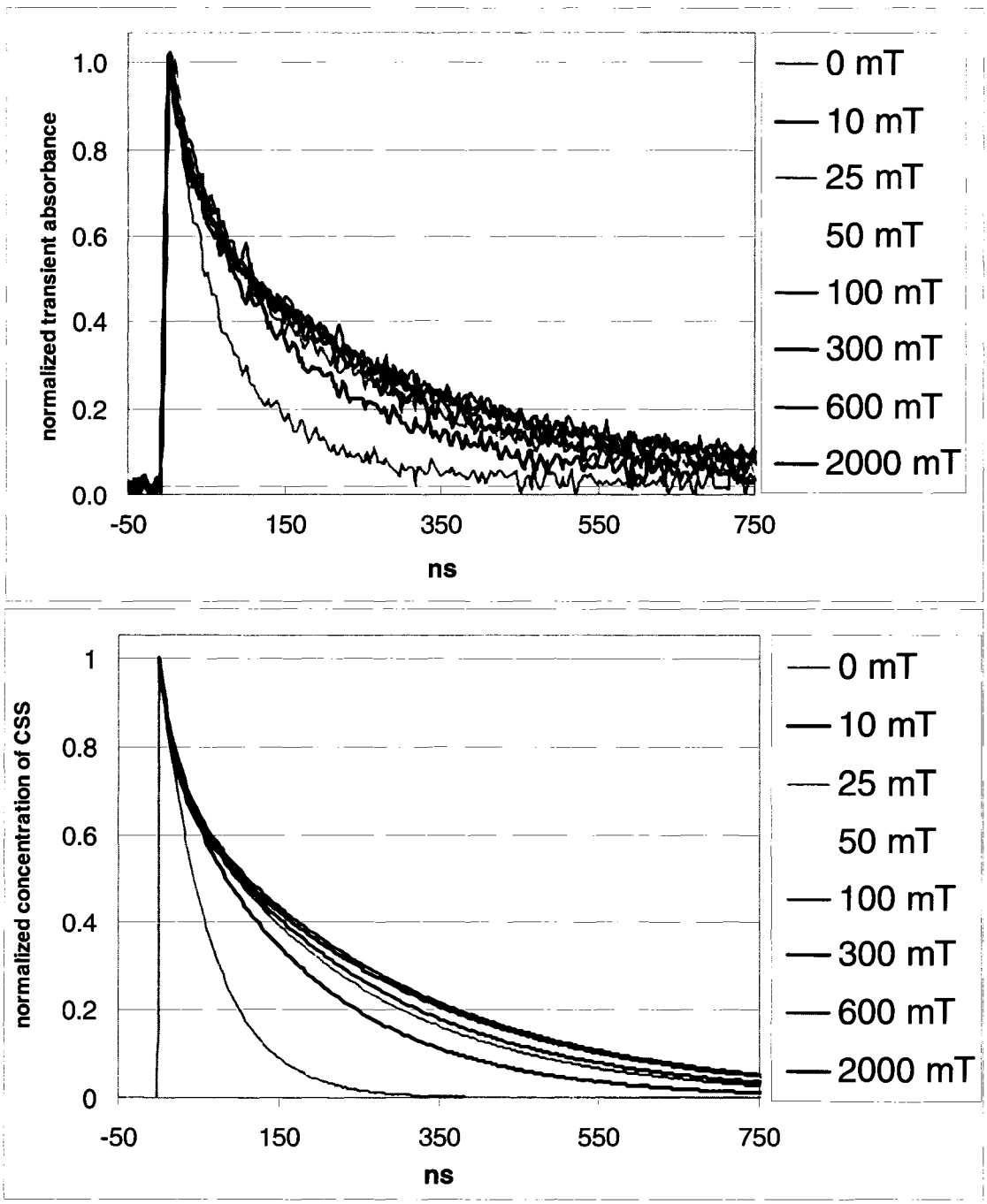

Figure 5.4 Transient decays for CS of DCA-PSZ. Upper panel experimental curves. Lower panel simulation using the relaxation scheme with parameters: $k_s = 7.6 \times 10^7$ s^{-1}, $k_T = 1.0 \times 10^6$ s^{-1}, $k_{r,0} = 5.00 \times 10^7$ s^{-1}, $k_{r,10} = 5.39 \times 10^6$ s^{-1}, $k_{r,,25} = 3.83 \times 10^6$ s^{-1}, $k_{r,50} = 3.00 \times 10^6$ s^{-1}, $k_{r,100} = 2.72 \times 10^6$ s^{-1}, $k_{r,300} = 2.71 \times 10^6$ s^{-1}, $k_{r,600} = 2.71 \times 10^6$ s^{-1}, $k_{r,2000} = 3.42 \times 10^6$ s^{-1}.

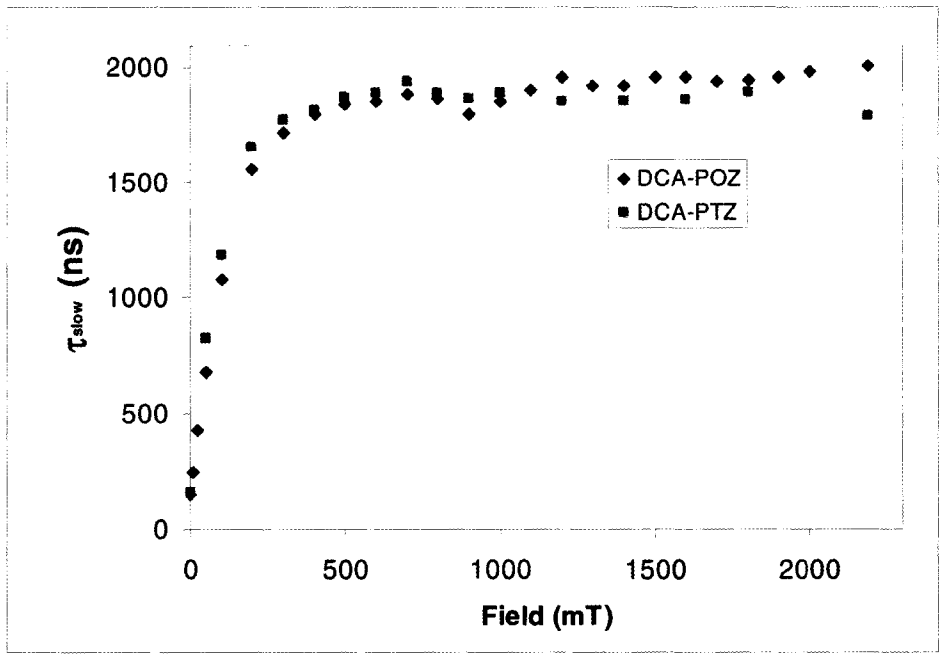

Figure 5.5 τ_{slow} vs B for DCA-PTZ and DCA-POZ.

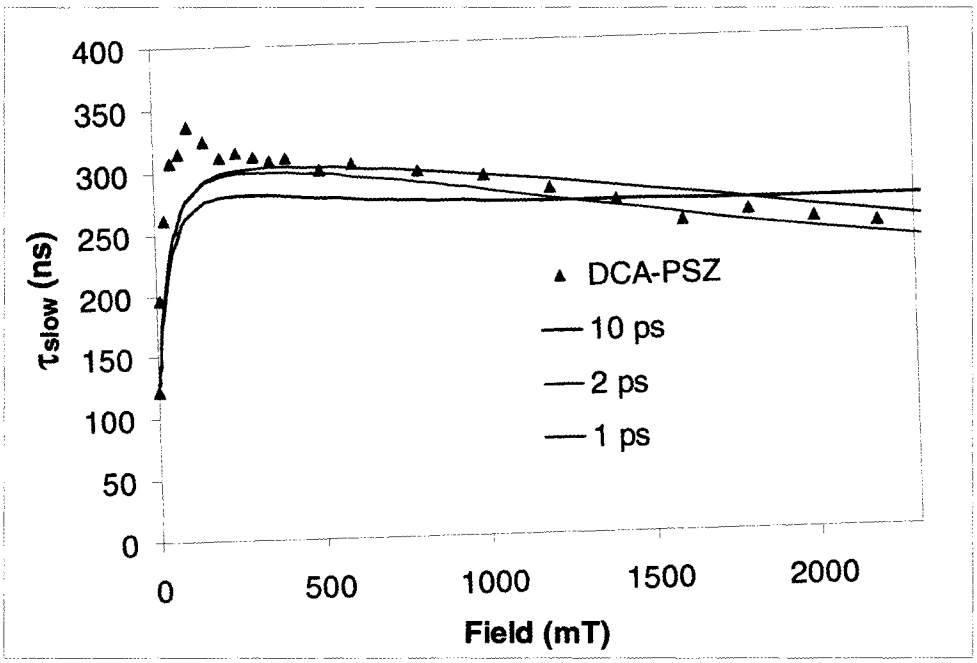

Figure 5.6 τ_{slow} vs. B for DCA-PSZ. The solid lines correspond to theoretical predictions according to the *gta* mechanism and adopting values of 10 ps, 2 ps and 1 ps for the orientational correlation time as indicated. For the calculation of the theoretical curves cf. Discussion.

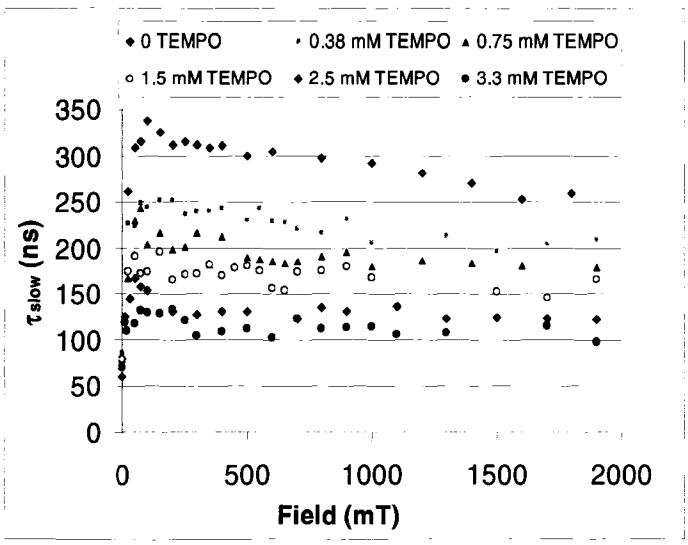

Figure 5.7 Tempo effect on τ_{slow} for DCA-PSZ.

5.3 DISCUSSION

The kinetic analysis of the observed magnetic-field dependence of the recombination kinetics of the CS state must be based on a detailed spin substate dependent reaction scheme as depicted in Scheme 5.1. As has been previously shown,[8] in magnetic fields below 1 T it can be assumed that the CS state originates with almost pure triplet spin. The CS state represents a radical pair (RP) with an average separation of more than 10 Å, so that exchange interaction is negligible for most conformations of the chains linking the radical moieties to the bipyridine ligands. Therefore, in zero magnetic field all the spin substates are degenerate and the three triplet substates are kinetically equivalent. For the radical species we are dealing with here, the most effective mechanism for triplet-singlet transitions in the CS state is due to isotropic hyperfine interaction causing a coherent triplet-singlet mixing process at a rate that can be estimated by the semiclassical effective hyperfine field $B_{1/2}$ defined as:[19,20]

$$B_{1/2} = \left(3 \sum_i a_i^2 I_i (I_i + 1) \right)^{1/2} \qquad (1)$$

where a_i and I_i are the isotropic hyperfine coupling constant and nuclear spin quantum number of a nucleus and the index i runs over all magnetic nuclei of the RP. For the CS state with PTZ, a value of 2.82 mT is obtained. Since the hyperfine coupling constants for the radicals of POZ and PSZ are very similar to that of PTZ (cf. Table 5.1), the $B_{1/2}$ value is essentially the same for the three systems. It corresponds to a time constant of about 2 ns, i.e. a very short time scale in relation to the time scale of the observed kinetics. So, in zero field, established spin equilibrium between all spin sublevels can be assumed. As the field is increased above the value of $B_{1/2}$ the Zeeman splitting of T_+ and T. exceeds the typical hyperfine coupling and the coherent spin transitions between $T_\pm$ and T_0, S are quenched, whereas the coherent transitions between T_0 and S are not affected. On a longer time scale, transitions between $T_\pm$ and T_0, S are brought about in an incoherent fashion through the individual longitudinal (T_1) spin relaxation of the radical spins or through their combined $T_\pm \rightarrow T_0$ relaxation caused by dipolar electron spin-spin interaction. The rates of these processes are magnetic field dependent at least to some degree, so that a magnetic field effect on the overall recombination kinetics of the CS state results.

It is appropriate to describe the kinetics in terms of coupled rate equations for relaxation and reaction as originally suggested by Hayashi and Nagakura[13] and also employed in our previous investigation.[8] The rate constants assigned in Scheme 5.1 are the following: k_S and k_T denote the rate constants of direct recombination of the singlet and triplet substates of CS, respectively. For the singlet state ^{1}CS, this process is spin

allowed and therefore much faster than for the triplet substates ^{3}CS. In the latter case spin conversion must go along with the backward transfer of the electron, which is only possible under special conditions with enhanced spin-orbit coupling. The rate constants $k_{r,1}$ and $k_{r,1}'$ characterize the relaxation transitions $T_{\pm} \rightarrow T_0$ and $T_{\pm} \rightarrow S$, respectively. The effective sum of all processes contributing to the establishment of the $T_0 \rightarrow S$ equilibrium is denoted by k_{S,T_0}. It is assumed that $k_{S,T_0} >> k_S, k_T$, so that this equilibrium is maintained during all stages of the recombination of CS. For this reason the rate constants $k_{r,1}$ and $k_{r,1}'$ can be combined and only their sum $k_r \equiv k_{r,1} + k_{r,1}'$ enters the kinetic result.

Assuming initial population of the ^{3}CS states only, the decay kinetics of CS is described by[8]

$$[CS] = [CS]_0 \left(c_a e^{-k_a t} + c_b d^{-k_b t} \right) \qquad (2a)$$

The corresponding equation holds for the transient absorbance A if [CS] is replaced by A:

$$A = A_0 \left(c_a e^{-k_a t} + c_b d^{-k_b t} \right) \qquad (2b)$$

with

$$c_a + c_b = 1 \qquad (3)$$

$$c_a = \frac{1}{2} + \frac{3k_r + (k_S - k_T)/4}{6\sqrt{k_r^2 + (k_S - k_T)^2/16}} \qquad (4)$$

$$k_a = k_r + \frac{1}{4}k_S + \frac{3}{4}k_T - \sqrt{k_r^2 + (k_S - k_T)^2/16} \qquad (5)$$

$$k_b = k_r + \frac{1}{4}k_S + \frac{3}{4}k_T + \sqrt{k_r^2 + (k_S - k_T)^2/16} \qquad (6)$$

Equation (2b) represents a biexponential decay function with 4 independent parameters, viz. A_o, c_a, k_a, k_b. Variations of A_o are due to variations in the laser intensity

and can be eliminated by normalization of the signal curves. The remaining three degrees of freedom can be represented by the rate constants k_S, k_T, k_r. Of these, only k_r is expected to be magnetic field dependent. Thus, in fitting a set of normalized kinetic traces for a certain sample for varying magnetic fields, k_S and k_T should be kept fixed as global parameters and only k_r is free for fitting the complete decay curve. This is a strong criterion for the validity of the kinetic model. As is shown in Figures 5.3 and 5.4 the procedure describes the complete behaviour of the observed decay curves very well.

According to Scheme 5.1, there are two channels, the "k_r-channel" and the "k_T-channel", through which ^{3}CS can recombine. Although k_r and k_T do not enter the equations (4-6) in an equivalent manner (for the phenomenological parameters of the biexponential), their influence becomes essentially indistinguishable if only kinetic reasoning is invoked. If $k_S >> k_r$, k_T then $k_a \rightarrow (k_r+k_T)$. For $k_S \approx 5 \times 10^7$ s^{-1} as is the typical order of magnitude for the systems under consideration this is not exact and one has to resort to the general equation

$$k_r = \frac{(k_S - k_T)^2/16 - \left(\frac{1}{4}(k_S + 3k_T) - k_a\right)^2}{2\left(\frac{1}{4}(k_S + 3k_T) - k_a\right)} \quad (7)$$

to obtain kinetically equivalent pairs of k_r and k_T for a certain value of k_a.[21] The relation between equivalent pairs of k_r and k_T for fixed values of k_a is shown in Figure 5.8 which will be used when criteria limiting the sensible range of values of either k_r or k_T are at hand.

The rate constant k_r may be generally decomposed into a magnetic-field dependent contribution $k_{r,B}$ and a magnetic-field independent contribution $k_{r,c}$, viz.

$$k_r(B) = k_{r,B}(B) + k_{r,c} \quad (8)$$

Through its magnetic field dependence, $k_{r,B}(B)$ can be separated from $k_{r,c}$. So the problem of separating k_r and k_T is reduced to a separation of $k_{r,c}$ and k_T, i.e. to the situation prevailing at high fields.

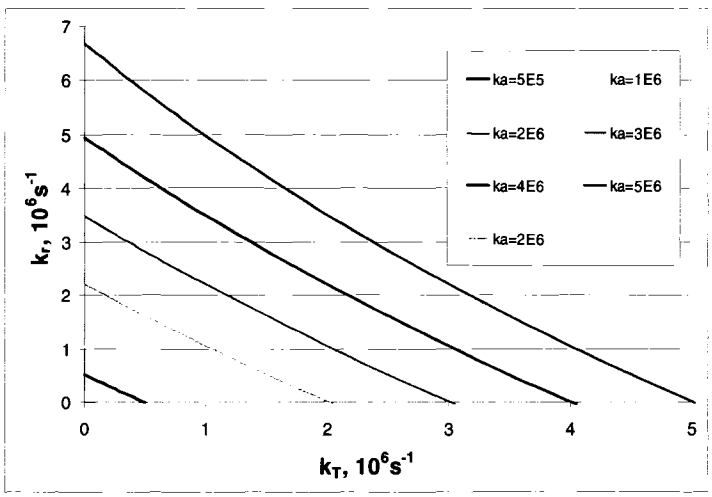

Figure 5.8 Representation of k_r and k_T pairs that are compatible with the same value of k_a ($k_S = 5 \times 10^7$ s^{-1}) and yield exactly the same quality of the kinetic fit.

The magnetic field dependence of the k_r-values for DCA-POZ and DCA-PSZ obtained from fitting the decay curves by assuming specific values for k_T are shown in Figure 5.9. No data points for DCA-PTZ are shown here because they are actually very close to the results for DCA-POZ. As becomes clear from Figure 5.9, the results for k_r depend to a significant extent on the assumed value of k_T. The quality of the fits is independent of the value assumed for k_T and thus does not provide a criterion for narrowing the bounds of this parameter. There are, however, other criteria at hand. As the value of k_T is increased, the value of k_r decreases. Obviously, for DCA-POZ the relative change of k_r with k_T is small for large values of k_r (low fields) and large for small values of k_r (high fields). As

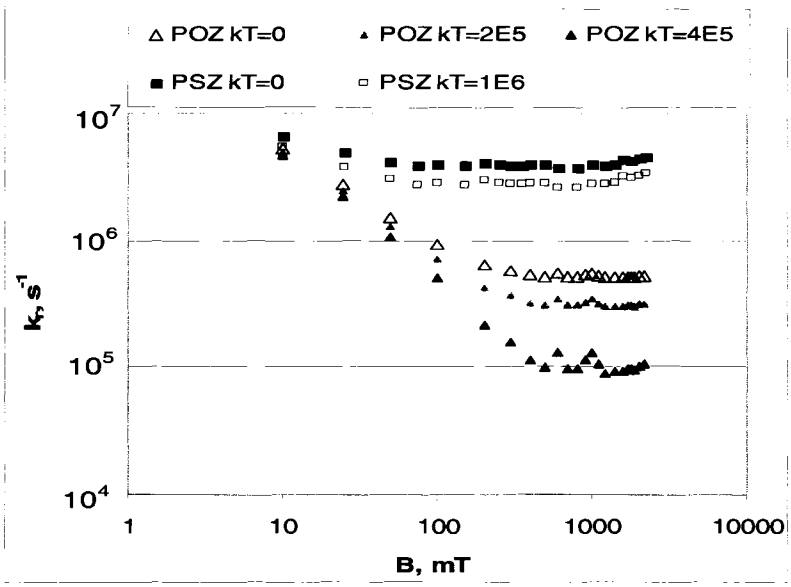

Figure 5.9 Magnetic field dependence of k_r as obtained from fitting the signal decays for DCA-POZ and DCA-PSZ (cf. Figures 5.3 and 5.4) for different values of k_T.

can be seen in Figure 5.9, the low field values of k_r for DCA-PSZ drop below the k_r values for DCA-POZ if $k_T > 10^6$ s^{-1} is assumed for DCA-PSZ. Such a result is not sensible, however, since spin relaxation in PSZ must be faster than for POZ, as is qualitatively borne out by the EPR linewidths of the cation radicals (cf. Table 5.1) and as to be expected from the increased spin-orbit coupling of selenium with respect to oxygen. Thus, $k_T = 10^6$ s^{-1} seems to represent an upper bound for DCA-PSZ. However, this limit can still be lowered. If we assume that all relaxation mechanisms operating in the DQ-POZ radical pair are also effective in the DQ-PSZ pair and we add to the experimental k_r-values of the former the field independent contribution (3.8×10^6 s^{-1}) of the latter, then the resulting values exceed the k_r-values for DQ-PSZ obtained under the assumption $k_T = 10^6$ s^{-1}. Actually, in the case of DQ-PSZ the possible contribution of k_T must be within the experimental accuracy limit.

The relative strength of spin-orbit coupling in oxygen and selenium provides an argument for an upper bound of k_T for POZ. The process to which k_T refers, i.e. direct recombination of the ^{3}CS state to the singlet ground state requires a spin flip during electron transfer. By the way they can be influenced by heavy atom substituents, such processes have been shown to be controlled by spin-orbit coupling.[22] A proportionality of the rate constant to the square of the atomic spin-orbit coupling constant has been observed. Considering that the atomic spin-orbit coupling constants of selenium and oxygen are in the ratio of 1990:158 = 12.6, the k_T value for PSZ is expected to be about 150 larger than for POZ. Thus the upper bound of k_T for POZ would be established at about 10^4 s^{-1}. Such a small value of k_T is indistinguishable from $k_T = 0$ in the k_r curves obtained from the kinetic fits and one can realistically assume that k_T is negligible for POZ and hence also for PTZ since the experimental results for it are almost indistinguishable from those for POZ.

That *soc* in the donor radical is in fact governed by the heteroatom center is also supported by the observed g-values of the Me-PXZ cation radicals. It has been established[24] that the deviation of the g-factor from the value g_e of the free electron (g-g_e) is proportional to the spin-orbit coupling constant ζ if spin-orbit coupling at one particular atomic center is responsible for this deviation. The values of (g-g_e) for Me-POZ, Me-PTZ, Me-PSZ were found in the ratio 0.59 : 1 : 4.5 (cf. Table 5.1) which is in reasonable agreement with the atomic spin-orbit coupling constants of O, S, Se (158:396:1990 = 0.4 : 1 : 5.0).[25,26]

Table 5.1 EPR Parameters[a] of Me-PXZ cation radicals[23]

	Me-POZ	Me-PTZ	Me-PSZ
a(1N)	9.18	7.56	6.82
a(3H)	9.07	7.22	7.30
a(2H)	2.99	2.17	2.13
a(2H)	1.49	0.96	0.92
a(2H)	0.56	0.75	0.77
a(2H)	0.57	0.31	0.43
a(^{77}Se)[b]			23.5
g	2.0040	2.0052	2.0153
Line width	0.30	0.30	0.55

[a]) Hyperfine couplings and line widths in Gauss. [b]) natural abundance of 7.6%.

Theoretical estimation of various contributions to k_r.

The contributions to the relaxation rate constant k_r to be explicitly considered are listed in Table 5.2. Expressions accounting for the contribution of *anisotropic hyperfine coupling* to k_r have been given by Hayashi and Nagakura[13] for model radical pairs with

Table 5.2 Contributions to the relaxation rate constant k_r

mechanism	rate constant
anisotropic hyperfine interaction (*ahfi*)	$k_{r,a}$
g-tensor anisotropy (*gta*)	$k_{r,g}$
combined action of *ahfi* and *gta*	$k_{r,ag}$
spin-rotational interaction	$k_{r,sri}$
electron spin dipolar interaction	k_{esdi}

one proton spin on each radical. In our systems the radicals carry one (PXZ radical cation) or two (diquat cation radical) ^{14}N spins with $I_N = 1$. The anisotropic hyperfine interaction in these radicals is by far dominated by these nuclei. Therefore we derived appropriate expressions accounting for this situation. Starting from the general equation for a radical pair with two nuclear spins of $I = 1$ in one radical, i.e. the diquat cation radical:

$$k_{r,a} = \frac{4}{9}\frac{\gamma_e^2\tau_c}{\left(1+\omega_0^2\tau_c^2\right)}\sum_{k,l,m,n}\overline{\left|\langle T_+,k,l\,|\,\mathbf{S}_1\left(\mathbf{t}_{N1}\mathbf{I}_{N1}+\mathbf{t}_{N2}\mathbf{I}_{N2}\right)|\,T_o,m,n\rangle\right|^2} \qquad (9)$$

where the indices k, l, m and n run over the (1, 0, -1) hyperfine states of the two nitrogen nuclei, we arrive at

$$k_{r,a} = \frac{383}{405}(\Delta A)^2\frac{\gamma_e^2\tau_c}{1+\omega_0^2\tau_c^2} \qquad (10)$$

In equation (9) a factor of 2 is included, taking into account that the transitions between T_+ (or T_-) and T_o as well as S contribute to k_r and that their probabilities are equal. In equation (10), γ_e denotes the gyromagnetic ratio of the electron, τ_c the orientational correlation time and ω_0 the angular Larmor frequency. The symbols $\mathbf{S}_1, \mathbf{I}_{N1}, \mathbf{I}_{N2}$ denote the vector operators of electron spin and nuclear spins, respectively, on the diquat radical; $\mathbf{t}_{N1}$ and $\mathbf{t}_{N2}$ are the anisotropic hyperfine tensors of the two nitrogen nuclei. We assume axial symmetry and hence may neglect that their main axes x and y are rotated with respect to each other around the common z-axis, the one perpendicular to the aromatic plane. Thus

$$\mathbf{t}_{N1} = \mathbf{t}_{N2},\ t_{N,xx} = t_{N,yy} = A_\perp,\ t_{N,zz} = A_\parallel \qquad (11)$$

For axially symmetric tensors a single quantity ΔA defined as

$$\Delta A \equiv A_{\|} - A_{\perp} \quad (12)$$

is sufficient to define the anisotropy.

For the *combined action of anisotropic hyperfine coupling and g-tensor anisotropy* as taking place in the PXZ cation radical, we take into account the anisotropic hyperfine coupling of one nitrogen nucleus. The analogue of equation (9) is:

$$k_{r,ag} = \frac{4}{3}\frac{\gamma_e^2 \tau_c}{(1+\omega_0^2\tau_c^2)} \sum_{k,l} \overline{\left|\langle T_+, k \,|\, \mathbf{S}_1 (\mathbf{t}_N \mathbf{I}_N + \mathbf{g'}\mathbf{B}_0 / g_e) \,|\, T_o, l \rangle\right|^2} \quad (13)$$

The symbol $\mathbf{g'}$ denotes the anisotropic part of the g-tensor. We assume that it is axially symmetric and that its main axis coincides with the axis of the anisotropic hyperfine tensor $\mathbf{t}_N$. As for the anisotropic hyperfine tensor, the effect of the axially symmetric anisotropic g-tensor can be expressed by a single quantity:

$$\Delta g' = \Delta g \equiv g_{\|} - g_{\perp} \quad (14)$$

It should be noted that the effects of *ahfi* and *gta* are not simply additive: there is an interference term. Evaluating the matrix elements in equation (13) we obtain:

$$k_{r,ag} = \frac{4}{27}(\Delta A)^2 \frac{\gamma_e^2 \tau_c}{1+\omega_0^2\tau_c^2} - \frac{1}{90}(\Delta g\, \Delta A)\frac{\gamma_e \omega_0 \tau_c}{1+\omega_0^2\tau_c^2} + \frac{1}{60}(\Delta g)^2 \frac{\omega_0^2 \tau_c}{1+\omega_0^2\tau_c^2} \quad (15)$$

An expression for the longitudinal and transversal relaxation times T_1 and T_2 of a radical due to *spin-rotational relaxation* has been derived by Atkins and Kivelson.[27,28] If one radical in the radical pair relaxes due to spin rotational interaction, the contribution to k_r in the radical pair is given by:

$$k_{r,sri} = \frac{1}{2T_{1,sri}} = \frac{1}{2T_{2,sri}} = \frac{1}{18}\frac{\overline{\delta g^2}}{\tau_c} \quad (16)$$

where $\overline{\delta g^2}$ is given by

$$\overline{\delta g^2} = \sum_{i=x,y,z} (g_{ii} - g_e)^2 \quad (17)$$

with g_{ii} the main values of the diagonal g-tensor and g_e the g-factor of the free electron. Assuming the g-tensor to be axially symmetric, and spin-orbit coupling effects at the heavy atom center in the aromatic ring to contribute only to the components in the ring plane, we have

$$g_{\parallel} = g_e \text{ and } g_{\perp} = (3g - g_e)/2 \qquad (18)$$

where g is the isotropic average of the g-factor. Hence

$$\overline{\delta g^2} = \frac{9}{2}(g - g_e)^2 \qquad (19)$$

The role of *electron spin dipolar interaction* on electron spin relaxation in the confined space of a micellar supercage, where the stochastic modulation of the interaction is due to the translational diffusion of the two radicals in the micelle, has been quantitatively analyzed by Steiner and Wu[29] using Monte Carlo simulations. If r_0 denotes the contact distance of the two radicals and r_M the radius of the micelle, the result can be cast into the following phenomenological form:

$$k_{r,esdi} = k_{T_{\pm}\to T_0,esdi} = \frac{3}{10}\hbar^2\gamma_e^2 r_0^{-3} r_M^{-3}\left(\frac{a_1\tau_1}{1+\omega_0^2\tau_1^2} + \frac{a_2\tau_2}{1+\omega_0^2\tau_2^2}\right) \qquad (20)$$

with $a_1 = 0.6$, $a_2 = 0.4$, $\tau_1 = 1.10\times10^{-16}\text{cm}^2\text{s}^{-1}D^{-1}$ and $\tau_2 = 7.70\times10^{-16}\text{cm}^2\text{s}^{-1}D^{-1}$. The symbol D denotes the sum of the diffusion coefficients of the two radicals. Later these results were corroborated analytically by Isakov et al.[30] The situation in the present linked radical pairs is very similar to the situation in a micelle. The conformational changes of the linkages modulate the distance of the two radical moieties between a separation r_0 of closest approach and a length r_M of most distant separation. The

conformational chain dynamics can be approximated by a diffusional process of the radical moieties with a phenomenological diffusion constant D (for a similar treatment of energy transfer cf. refs.[31,32]).

In order to assess the parameters of the various mechanistic contributions from the observed experimental data on k_r, we start by comparing the high-field values for the DQ-PSZ pair with the results for the EPR line width of the Me-PSZ cation radical (cf. Table 5.1). This line width exceeds the values for Me-POZ and Me-PTZ by about 0.25 Gauss. This suggests assigning the difference to the effect of spin-rotational interaction.[33] A Lorentzian width contribution of 0.25 Gauss corresponds to a value of $1/T_2$ of 7.4×10^6 s^{-1}. If we assume that the same mechanism is operative in the PSZ-moiety of the DQ-PSZ radical pair, a $k_{r,sri}$ value of 3.7×10^6 s^{-1} would be expected on the basis of equation (16). Allowing for the uncertainty of the EPR line width, a $k_{r,\,sri}$ value in the range of 2-4 $\times$ 10^6 s^{-1} should be acceptable. This is in good agreement with the limiting high-field value for the DQ-PSZ radical pair of about 3.5-4 $\times$ 10^6 s^{-1} which thus may be largely assigned to the *sri* mechanism (For a discussion of the weak field dependence of k_r at high fields cf. below). A contribution of k_T, however, on the order of 1×10^6 s^{-1} cannot be ruled out.

From the isotropic g-factor of 2.015 for the Me-PSZ radical cation we obtain $\overline{\delta g^2}$ = 7.26×10^{-4}. Assuming $k_{r,sri} = 3.5 \times 10^6$ and using equation (16) yields an orientational correlation time τ_c of 11.5 ps. We may convert this value into an effective hydrodynamic radius r of the linked PSZ radical by resorting to the Debye equation[34]

$$\tau_c = \frac{4\pi\eta r^3}{3kT} = 10^{-12}\frac{\eta}{cP}\frac{r^3}{\mathring{A}^3}s \quad (21)$$

Based on a value of η = 0.62 cP for the viscosity of nitromethane at room temperature we obtain r = 2.65 Å, which is a reasonable order of magnitude for the size of the donor and the acceptor moieties. On the other hand, this result, which is based on the bulk viscosity of the solvent indicates that the rotational mobility of the linked PSZ species does not seem to be severely impeded by the tetramethylene linker.

We now turn to the interpretation of the low-field limits of k_r for which, in the case with the POZ-moiety, only the *ahfi* mechanism and the *esdi* mechanism can be invoked. The anisotropic hyperfine coupling of the nitrogen nucleus may be estimated by analogy with the stable TEMPO radical.[35] Here the isotropic hyperfine coupling constant of nitrogen is A_N = 16.6 G and ΔA_N = 29.5 G. We assume that the ratio of 1.77 between ΔA_N and A_N can be also applied to other nitrogen centered radicals. For the DQ radical cation the two isotropic nitrogen couplings are A_N = 4.0 G[36] leading to an estimation of ΔA_N = 7.1 G, and for POZ the nitrogen coupling is taken as A_N = 9.2 G as listed in Table 5.1, leading to an estimated ΔA_N = 15.9 G. Employing these values together with the value of the orientational correlation time τ_r obtained above from the contribution of the spin-rotational mechanism, we obtain $k_{r,a}^{POZ} = 3.0 \times 10^5$ s^{-1} at 10 mT, the lowest field, for which the experimental value of k_r has been unambiguously determined. The experimental value of 5.4×10^6 s^{-1} is more than 10 times larger than the theoretical value from the *ahfi* mechanism. Also, as a consequence of the used correlation time of 11.5 ps, $k_{r,a}^{POZ}$ is constant up to about 100 mT which is at variance with the experimental behaviour.

Thus it is clear, that the *ahfi* mechanism cannot account for the behaviour of k_r in the low field region up to about 100 mT. Electron spin dipolar interaction is a promising

candidate to fill this gap. In order to apply equation (20) we need to fix the parameters r_0, the distance of closest approach of the two radicals; r_M the maximum distance, and D, the effective relative diffusion constant of the two radicals. For r_0 we chose the value of $2r$, i.e. twice the value of the hydrodynamic radius of the individual radicals, for r_M a value of 20 Å can be estimated from a molecular model. It already has been pointed out, that the conformational chain dynamics of the linkers, which determines the modulation of the distance between the two radicals, can be simulated by a diffusion model. It should, however, not be expected that this diffusion is as fast as for unbound molecules in homogeneous solution. Nevertheless, we may estimate an upper limit of the corresponding diffusion constant using the Einstein-Stokes relation:

$$D = D_{DQ} + D_{PXZ} = \frac{2kT}{6\pi r\eta} = 4.37\times10^{-5}\left(\frac{r\eta}{\text{Å cP}}\right)^{-1}\frac{\text{cm}^2}{\text{s}} \qquad (22)$$

yielding D = 2.3 × 10^{-5} cm^2s^{-1}. The expected field dependence of $k_{r,esdi}$ obtained with these parameters is shown in Figure 5.10. It is evident that the $k_{r,esdi}$ values obtained for $D > 10^{-5}$ cm^2s^{-1} are much too small. However, by decreasing the effective value of D and keeping all the other parameters as given, the field dependence of $k_{r,esdi}$ nicely approaches the observed behaviour. For D = 9.0 × 10^{-7} cm^2s^{-1}, not only the low-field values for POZ and for PSZ are well approximated but also the field dependence up to 100 mT. It has been noted earlier by Steinberg and coworkers[31,32] in the theoretical study of energy transfer in linked donor-acceptor systems that the effective relative diffusion constant for two chain ends attached to an oligopeptide linker is much slower than for the unbound donor and acceptor molecule. Values in the range between 0.9×10^{-7} cm^2s^{-1} and 6.4 × 10^{-7} cm^2s^{-1} for the diffusion constant were found to appropriately describe the behaviour of 4-

9 amino acid oligopeptides in ethanol as solvent. In the light of these findings the present observation of an effective diffusion constant of 9.0×10^{-7} $cm^2 s^{-1}$ seems quite reasonable and strongly supports the leading role of the *esdi* spin relaxation mechanism in linked radical pairs at low fields.

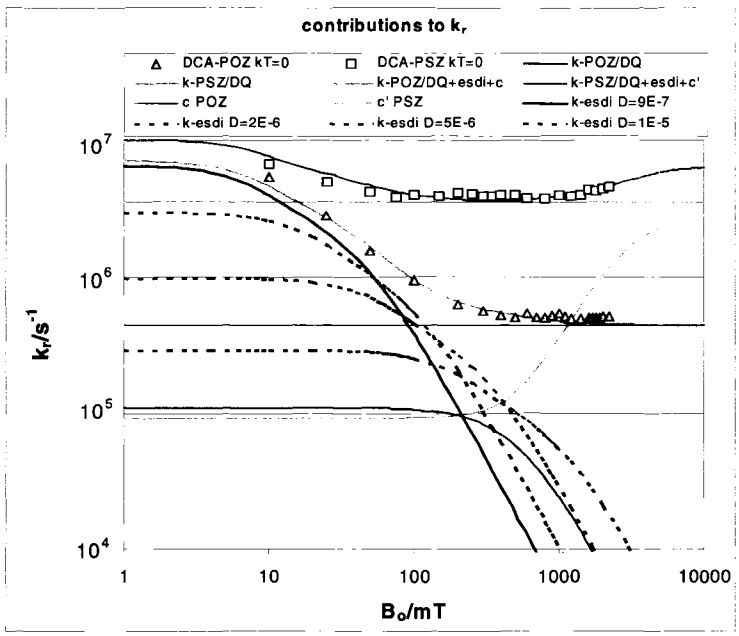

Figure 5.10 Contributions to k_r in the theoretical simulation of spin relaxation in the radical pairs from DCA-POZ and DCA-PSZ evaluated under the assumption of $k_T = 0$ (cf. data points). The full simulations are represented by the curves denoted k-POZ/DQ+esdi+c and k-PSZ/DQ+esdi+c', respectively. The contributions from the *esdi* mechanism (k-esdi D=...) are given for various values of the effective diffusion constant D. The best fit is for $D = 9 \times 10^{-7}$ $cm^2 s^{-1}$. The curves indicated as k-POZ/DQ and k-PSZ/DQ, respectively, represent the sum of the contributions of the *ahfi* and *gta* mechanisms. The constant values c POZ and c' PSZ represent the field-independent contributions to k_r. For details of the calculation cf. text.

At high fields, the k_r contribution of the *esdi* mechanism drops below the experimental values which approach a magnetic field independent limit. If this limiting value is added as a constant contribution (4.5×10^5 s^{-1} in the case of DCA-POZ) to the *esdi* contribution, the full field dependence is quite well reproduced. The $k_{r,esdi}$ contribution as adapted to

the field dependence of the DCA-POZ data yields, at the same time, an excellent description of the field dependence of the DCA-PSZ data if the appropriate constant value of $k_{r,\,sri}$, as discussed above, is added.

Now we consider the role of the *ahfi* mechamism at higher fields. As can be seen in Figure 5.10 for the case of DCA-POZ, up to about 75 mT the *ahfi* contribution is much below the *esdi* contribution. At 150 mT the order of these two mechanisms is reversed and at fields above 500 mT the *ahfi* contribution is about two orders of magnitude larger than the *esdi* contribution. Nevertheless, at all fields the *ahfi* contribution is much smaller than the observed k_r. If it is assumed that the limiting high field value of k_r is constantly contributing at all fields, then in the field region between 50 and 600 mT, the overall sum including *ahfi* results in up to 50% too high values for k_r, indicating an overestimation of the *ahfi* contribution. A good fit is obtained (cf. Figure 5.10) if the anisotropy ΔA is taken only to be a factor of 1.1 times the isotropic hyperfine constant of the nitrogen atoms.

None of the mechanisms discussed so far can account for the limiting high-field value of about 5×10^5 s^{-1} in the DCA-POZ case. While in the case of DCA-PSZ the magnetic field independent contribution to k_r is explicitly accounted for by the spin-rotational mechanism, this mechanism has only a negligible contribution (about 10^3 s^{-1}) to the field independent part of k_r in the case of POZ. At present we cannot assign an explicit mechanism for it. After consideration of all rotational and translational contributions to the stochastic modulation of magnetic interactions as possible sources of spin relaxation, there remain only local inner vibrational motions as have been invoked for contributions to radical spin relaxation occasionally.[37] In the case of DCA-PTZ, the high field limit of

k_r is similar to POZ. However, here the theoretical contribution of the *sri* mechanism (3.5×10^5 s^{-1}) is considerable and accounts for the largest part if not all of k_r.

In the case of the DCA-PSZ radical pair, a slight but significant decrease of k_r at high fields is observed. Similar high-field reversions of magnetic field effects with radical pairs have been observed by Hayashi and coworkers.[15,38,39] In principle, two g-tensor dependent mechanistic explanations can account for such observations:

i. the Zeeman mechanism (or "Δg-mechanism")[40] which is due to a magnetic field dependent enhancement of the coherent T_0-S process, due to different g-factors of the two radicals and

ii. the *gta*-mechanism which is due to a magnetic field dependent enhancement of spin relaxation in the individual radicals.

The former mechanism only becomes apparent if the frequency of T_0-S mixing due to the coherent action of isotropic hyperfine interaction is not sufficient to establish T_0-S spin equilibrium between two radical pair encounters. The latter mechanism is slower than or comparable with the frequency of reencounters. If the effect of a magnetic field is observed through a time-integrated observable, e.g. as the radical escape yield in case of unlinked radical pairs, a decision as to whether mechanism (i) or (ii) is operating may be found by using a paramagnetic quencher which, at not too high concentration, can only affect the *gta*-relaxation mechanism.[15] The TEMPO effect on τ_{slow} shown in Figure 5.7 is a clear indication that it is the *gta*-mechanism which is working here; what we see is that not only the value of τ_{slow} in general becomes shorter by the addition of TEMPO, but also that the high-field reversion of the magnetic field effect disappears at higher TEMPO concentration.

Another criterion against the Zeeman mechanism as an explanation of the observed high-field reversion of the magnetic field effect in the DCA-PSZ system, is the observed validity of the kinetic model. If this model is correct, effects according to the Zeeman mechanism cannot show up in the kinetics since the model assumes establishment of the T_0-S equilibrium at any stage of the recombination. That the model is indeed correct, is borne out in the amplitude ratio of the slow and fast decay components which is not a free parameter in the fitting of the kinetic curves but a function of the adopted rate constants (cf. equation (4)).

The effect of the *gta*-relaxation mechanism can be assessed by equation (15). At high fields, the quadratic term in Δg dominates. It leads to a contribution to k_r which increases quadratically with the magnetic field B_0. At high fields, however, it approaches a constant limit. The half field value $B_{1/2,\,gta}$ for the saturation occurs at

$$B_{1/2,gta} = \frac{1}{\gamma_e \tau_{c,gta}} \qquad (23)$$

For a simulation (cf. Figures 5.6 and 5.10), all parameters except for $\tau_{c,gta}$ are known. An optimum fit is achieved for $\tau_{c,gta} \approx 2$ ps. This value is about one order of magnitude shorter than reasonably expected for rotational tumbling (cf. equation (21)) of the PSZ radical moiety. A stochastic motion modulating the *g*-tensor might be sought in a modulation of the butterfly like central ring deformation in the PSZ molecule. Due to the non-planar hybridization of the methylated ring nitrogen,[41] this species (and its radical) is bent along the axis connecting the two central heteroatoms. By Raman spectroscopy as well as by DFT calculations, several thermally easily excitable vibrational modes of the central ring deformation have been assessed in the range of 50–500 cm^{-1}.[42] Variations of vibrational excitation of these modes will affect the *g*-tensor. Vibrational correlation

times on the order of some picoseconds (corresponding to vibrational linewidths of several cm^{-1}) appear reasonable and could account for the observation of a correlation time $\tau_{c,gta}$ as short as observed.

Paramagnetic quenching of the magnetic field effect by TEMPO.

Several studies of the effects of paramagnetic species on spin chemical magnetic field effects have been reported in the literature. Among the species that have figured prominently as paramagnetic perturbers are Ln^{3+} ions[43-46] and transition metal ions,[43,47] nitroxyl radicals (in particular TEMPO)[48-52] and molecular oxygen.[53] In some cases, the paramagnetic perturber is covalently linked to either the biradical species[51,52] or to one of the radicals in the radical pair.[49] In these cases the total spin system is strongly coupled. It is the situation of a triplet-doublet pair wherein the coupled spin states of a quartet and a doublet that are energetically separated by considerable exchange splitting, are kinetically relevant. In our experiment with unlinked TEMPO, this perturber interacts with the rather weakly coupled radicals of the CS state. Formally, it enhances the transitions between $T_{\pm}$ and T_0/S, or the transitions between T_0 and S. In a magnetic field, the latter occur on a much faster time scale than the former and rather high concentrations of the paramagnetic perturber would have to be used to affect the T_0 and S process. Such enhancements of T_0/S transitions have been observed with a 10^{-2} M concentration of Gd^{3+} ions.[15] With a TEMPO concentration of 0.1 M, even in zero field, a noticeable effect was observed on the recombination of a radical pair.[45] For the low TEMPO concentrations employed in our experiments only the slow $T_{\pm} \rightarrow T_0/S$ relaxation can be affected. This can occur by two mechanisms: electron spin dipolar interaction, or Heisenberg spin exchange. If the latter mechanism operates between typical organic radicals in low

viscous solvents, rate constants of 2-4 × 10^9 M^{-1} s^{-1}, i.e. close to diffusion controlled, seem to be typical.[54,55] The relaxation effect due to the electron spin dipolar interaction between a paramagnetic perturber and a radical can be estimated according to an equation derived by Rao[43,56]

$$k_{q-esdi} = \frac{8\pi N_A}{30 r_0^3} \gamma_e^2 \mu^2 \tau_c \left(1 + \frac{3}{1+\omega_0^2 \tau_c^2} + \frac{6}{1+4\omega_0^2 \tau_c^2} \right) \quad (24)$$

where μ, the magnetic moment of the perturber in case of TEMPO is equal to 1.73β (β representing Bohr's magneton) and the correlation time is given by

$$\tau_c = \frac{12\pi r_0^3}{kT} \quad (25).$$

Using a value of 5 Å for r_0, the distance of closest approach, one obtains τ_c = 710 ps. In this case, equation (24) predicts a limiting, constant value of $k_{q\text{-}esdi}$ at fields above about 50 mT. This is the region where the paramagnetic quenching effect has been investigated in our experiments. The saturation value, 2.3 × 10^8 $M^{-1}s^{-1}$, is about 10 times smaller than the value to be expected for the Heisenberg spin exchange mechanism.

From the time regime of the magnetic field dependent kinetics where the TEMPO effect is observed, as well as from the low concentrations of TEMPO employed, it is clear that in our experiments this quencher accelerates the $T_{\pm} \rightarrow T_0$, S relaxation processes. Denoting this contribution of relaxation by $k_{r,TEMPO}$, the total rate constant of relaxation can be decomposed as

$$k_r = k_{r,[0]} + k_{r,TEMPO} \quad (26)$$

where $k_{r,[0]}$ denotes the relaxation constant in the absence of TEMPO. Substituting equation (24) into equation (5) and using the result $k_T = 0$ arrived at above, we can determine $k_{r,TEMPO}$ as follows:

$$k_{r,TEMPO} = \frac{k_a(k_a - k_S/2)}{2(k_a - k_S/4)} - k_{r,[0]} \qquad (27)$$

The values of $k_{r,\ TEMPO}$ as a function of the concentration of TEMPO obtained for various magnetic fields are plotted in Figure 5.11.

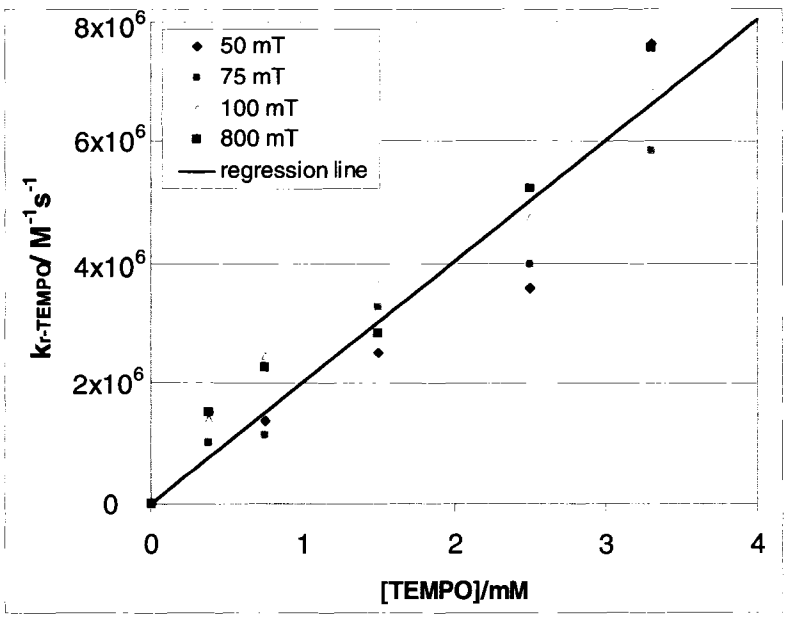

Figure 5.11 Contribution $k_{r,TEMPO}$ to spin relaxation as a function of TEMPO concentration for various magnetic fields.

In the field range from 50 mT to 800 mT where the values of $k_{r,TEMPO}$ have been determined, they exhibit no significant dependence on the magnetic field strength. The data points are well represented by a linear correlation

$$k_{r,TEMPO} = k_{q,\ TEMPO}[\text{TEMPO}] \qquad (28)$$

with $k_{q,\ TEMPO} = 2.0 \times 10^9\ M^{-1}s^{-1}$. This result indicates that the magnetic quenching by TEMPO is close to diffusion controlled and about 10 times faster than to be expected for an electron-dipolar relaxation mechanism, but it fits well to the typical range observed for Heisenberg spin exchange between organic radicals in low viscous solution (cf. above).

5.4 CONCLUSION

The conclusions from the analysis of our results may be summarized as follows:

Contributions of direct, spin-forbidden recombination of triplet RPs seem negligible, i.e. $k_T << k_r(B \rightarrow \infty)$.

Spin-rotational interaction has been explicitly confirmed as being responsible for the saturating limit of the magnetic field effect in high fields for PSZ Electron spin dipolar interaction is the dominant relaxation mechanism for the presently investigated linked radical pairs in the field range between 1 and 100 mT.

Contributions of anisotropic hyperfine interactions to spin relaxation in the present systems are minor and seem to contribute mainly in the intermediate field region around 200 mT.

The limiting high field contribution to spin relaxation in the DQ-POZ is not of rotational origin. A vibrational mechanism might be invoked.

The slight increase of k_r at high fields in the case of PSZ is most likely due to the *gta*-mechanism. The extremely short correlation time of about 2 ps for the underlying stochastic modulation of the g-tensor is tentatively assigned to a conformational flapping of the ring system about the central N-Se axis. The coherent Zeeman mechanism of T_0-S mixing can be definitely excluded as an explanation of this effect.

REFERENCES

(1) Fox, M. A.; Chandon, M., Eds. *Photoinduced Electron Transfer*; Elsevier: Amsterdam, 1988; Vol. A-D.

(2) Schanze, K. S.; Walter, K. A. Photoinduced Electron Transfer in Metal-Organic Dyads. In *Molecular and Supermolecular Photochemistry: Organic and Inorganic Photochemistry*; Ramamurthy, V., Schanze, K. S., Eds.; Marcel Dekker: New York, 1998; Vol. 2; pp 75.

(3) Kalyanasundaram, K. *Photochemistry of Polypyridine and Porphyrin Complexes*; Academic Press: San Diego, 1992.

(4) Armaroli, N. *Photochem. Photobiol. Sci.* **2003**, *2*, 73.

(5) Scandola, F.; Chiorboli, C.; Indelli, M. T.; Rampi, M. T. Covalently Linked Systems Containing Metal Complexes. In *Biological and Artificial Supermolecular Systems*; Wiley: Weinheim, 2003; Vol. 3; pp 337.

(6) Gust, D.; Moore, T. A.; Moore, A. L. *Electron Transfer in Chemistry* **2001**, *3*, 272.

(7) Gust, D.; Moore, T. A. *Porphyrin Handbook* **2000**, *8*, 153.

(8) Klumpp, T.; Linsenmann, M.; Larson, S. L.; Limoges, B. R.; Buerssner, D.; Krissinel, E. B.; Elliott, C. M.; Steiner, U. E. *J. Am. Chem. Soc.* **1999**, *121*, 1076.

(9) Danielson, E.; Elliott, C. M.; Merkert, J. W.; Meyer, T. J. *J. Am. Chem. Soc.* **1987**, *109*, 2519.

(10) Larson, S. L.; Cooley, L. F.; Elliott, C. M.; Kelley, D. F. *J. Am. Chem. Soc.* **1992**, *114*, 9504.

(11) Larson, S. L.; Elliott, C. M.; Kelley, D. F. *J. Phys. Chem.* **1995**, *99*, 6530.

(12) The inclusion of two donor moieties is simply a matter of synthetic expediency (it is easier to prepare the complex containing two donors) and is of no particular consequence in the qualitative behavior of the assemblies.

(13) Hayashi, H.; Nagakura, S. *Bull. Chem. Soc. Jap.* **1984**, *57*, 322.

(14) The rate constant of direct, *soc* assisted spin forbidden recombination is expected to vary as the square of the *soc* constant, while g-tensor related effects as *gta* and *sri* should vary linearly.

(15) Wakasa, M.; Sakaguchi, Y.; Hayashi, H. *Mol. Phys.* **1994**, *83*, 613.

(16) Linsenmann, M. Ph. D. Dissertation, University of Konstanz, 1997.

(17) Treadway, J. A.; Chen, P.; Rutherford, T. J.; Keene, F. R.; Meyer, T. J. *J. Phys. Chem. A* **1997**, *101*, 6824.

(18) The modest difference between the k_a value reported herein and those in reference 8 is likely due to trace oxygen impurities present in the samples considered in the earlier study.

(19) Weller, A.; Nolting, F.; Staerk, H. *Chem. Phys. Lett.* **1983**, *96*, 24.

(20) Steiner, U. E.; Wolff, H.-J. Magnetic field effects in photochemistsry. In *Photochemistry and Photophysics*; Rabek, J. F., Ed.; CRC Press Inc.: Boca Raton, 1991; Vol. IV; pp 1.

(21) The coefficient c_a is not very sensitive to variations in k_r and k_T compatible with a given k_a, nor is the phenomenological rate constant k_b.

(22) Steiner, U. E.; Winter, G. *Chem. Phys. Lett.* **1978**, *55*, 364.

(23) Rawls, M. T.; Kollmannsberger, G.; Elliott, C. M.; Steiner, U. E. *Manuscript in preparation.*

(24) Carrington, A.; D., M. A. *Introduction to Magnetic Resonance*; Chapman and Hall: London, 1979.

(25) Moore, C. E. Atomic Energy Levels, Vol. I (1949), Vol. II (1952), Vol.III (1953), Circular of the National Bureau of Standards No. 467 (US).

(26) Fraga, S.; Malli, G. *Many electron systems: properties and interactions*; Saunders: Philadelphia, London, Toronto, 1968.

(27) Atkins, P. W.; Kivelson, D. *J. Chem. Phys.* **1966**, *44*, 169.

(28) Steiner, U. E.; Serebrennikov, Y. A. *J. Chem. Phys.* **1994**, *100*, 7503.

(29) Steiner, U. E.; Wu, J. Q. *Chem. Phys.* **1992**, *162*, 53.

(30) Isakov, S. V.; Lukzen, N. N.; Morozov, V. A.; Sagdeev, R. Z. *Chem. Phys.* **1995**, *199*, 119.

(31) Haas, E.; Katchalski-Katzi, E.; Steinberg, I. Z. *Biopolymers* **1978**, *17*, 11.

(32) Katchalski-Katzir, E.; Haas, E.; Steinberg, I. Z. *Ann. Rev. N.Y. Acad. Sci.* **1981**, *366*, 44.

(33) At X-band, the line-width contribution of the *gta*-mechanism can be estimated to be about one order of magnitude smaller.

(34) Debye, P. *Polar Molecules*; Dover Publicatons: New York, 1945.

(35) Ottaviani, M. F.; Baglioni, P.; Martini, G. *J. Phys. Chem.* **1983**, *87*, 3146.

(36) Rieger, A. L.; Rieger, P. H. *J. Phys. Chem.* **1984**, *88*, 5845.

(37) Yong, L.; Harbridge, J.; Quine, R. W.; Rinard, G. A.; Eaton, S. S.; Eaton, G. R.; Mailer, C.; Barth, E.; Halpern, H. J. *Journal of Magnetic Resonance* **2001**, *152*, 156.

(38) Wakasa, M.; Hayashi, H.; Mikami, Y.; Takada, T. *J. Phys. Chem.* **1995**, *99*, 13181.

(39) Wakasa, M.; Igarashi, M.; Sakaguchi, Y.; Hayashi, H. *Chem. Lett.* **1994**, 1991.

(40) In this term, Δg stands for the difference of g-factors of the two radicals. Since we are already using the symbol Δg in a different meaning, i.e. as a designation of the g-tensor anisotropy, we will avoid here the term "Δg-mechanism".

(41) Clarke, D.; Gilbert, B. C.; Hanson, P.; Kirk, C. M. *J. Chem. Soc., Perkin Trans. II* **1978**, 1103.

(42) Pan, D.; Phillips, D. L. *J. Phys. Chem. A* **1999**, *103*, 4737.

(43) Kita, Y.; Tanimoto, A.; Itoh, M.; Okazaki, M.; Nakagaki, R. *Chem. Phys. Lett.* **1990**, *165* 184.

(44) Sakaguchi, Y.; Hayashi, H. *Chem. Phys. Lett.* **1984**, *106*, 420.

(45) Turro, N. J.; Lei, X.; Gould, I. R.; Zimmt, M. B. *Chem. Phys. Lett.* **1985**, *120*, 397.

(46) Basu, S.; Nath, D.; Chowdhury, M. *J. Lumin.* **1988**, *40&41*, 252.

(47) Sakaguchi, Y.; Hayashi, H. *Chem. Phys.* **1992**, *162*, 119.

(48) Chen, J.; Mori, Y.; Sakaguchi, Y.; Hayashi, H. *Mol. Phys.* **2002**, *100*, 1355.

(49) Mori, Y.; Sakaguchi, Y.; Hayashi, H. *J. Phys. Chem. A* **2000**, *104*, 4869.

(50) Step, E. N.; Buchachenko, A. L.; Turro, N. J. *J. Am. Chem. Soc.* **1994**, *116*, 5462.

(51) Mori, Y.; Sakaguchi, Y.; Hayashi, H. *J. Phys. Chem. A* **2002**, *106*, 4453.

(52) Mori, Y.; Sakaguchi, Y.; Hayashi, H. *Chem. Phys. Lett.* **1998**, *286*, 446.

(53) Levin, P. P.; Kuzmin, V. A. *Chem. Phys.* **1992**, *162*, 79.

(54) Eastman, M. P.; Kooser, R. G.; Das, M. R.; Freed, J. H. *J. Chem. Phys.* **1969**, *11*, 2690.

(55) Eastman, M. P.; Bruno, G. V.; Freed, J. H. *J. Chem. Phys.* **1970**, *52*, 2511.

(56) Hyde, H. S.; Swartz, H. M.; Antholine, W. E. The spin-probe-spin-label method. In *Spin Labeling, Vol. 2* Berliner, L. J., Ed.; Academic Press: New York, 1979; pp 71.